8-2013

Ventricular assist device and extracellular matrix combination therapy in a chronic ischemic heart failure bovine model.

Erin F. Smith
University of Louisville

VENTRICULAR ASSIST DEVICE AND EXTRACELLULAR MATRIX COMBINATION THERAPY IN A CHRONIC ISCHEMIC HEART FAILURE BOVINE MODEL

By

Erin F. Smith
B.S., University of Louisville, 2012

A Thesis
Submitted to the Faculty of the
University of Louisville
J.B. Speed School of Engineering
as Partial Fulfillment of the Requirements
for the Professional Degree

MASTER OF ENGINEERING

Department of Bioengineering

August 2013

VENTRICULAR ASSIST DEVICE AND EXTRACELLULAR MATRIX COMBINATION THERAPY IN A CHRONIC ISCHEMIC HEART FAILURE BOVINE MODEL

Submitted by:_____
Erin F. Smith, B.S.

A Thesis Approved on

_____
(Date)

By the following Reading and Examination Committee:

_____
Steven C. Koenig, Ph.D., Thesis Director

_____
Guruprasad A. Giridharan, Ph.D.

_____
Kevin Soucy, Ph.D.

_____
Gail DePuy, Ph.D

DEDICATION

This thesis is dedicated to my parents,

Donald L. Smith

and

Louise A. Smith

ACKNOWLEDGMENTS

I would like to thank Dr. Mark Slaughter and Dr. Steven Koenig of Advanced Heart Failure Research for the opportunity to take part in this exciting project. I would also like to thank Dr. Kevin Soucy and Mike Sobieski for their continuous guidance throughout the past year. I am especially grateful for the support of fellow staff and student members of the lab: Mary Anne Hauck, Cary Woolard, Laura Lott, Karen Lott, Dr. Paul Linsky, Young Choi, and Sue Weyland. My thesis project would not have been possible without your help. I would also like to thank my sister, Kathryn Allawala for her crucial editorial support. Lastly, I would like to thank all the members of my thesis committee: Dr. Steven Koenig, Dr. Kevin Soucy, Dr. Guruprasad Giridharan, and Dr. Gail DePuy. You have both supported and challenged me to achieve more than I would have ever thought possible. My experience as a master's student at the Cardiovascular Innovation Institute has been invaluable and helped and me to grow in many ways. My experiences have allowed me to intimately learn about and solidify my career aspiration of practicing medicine.

ABSTRACT

Purpose: Currently, heart transplantation and mechanical circulatory support (MCS) are the preferred treatments for end stage heart failure. However, these therapies are associated with a shortage of donor organs, a 5-yr survival rate of 80%, and adverse events associated with long-term MCS usage. To overcome these limitations, new clinical paradigm is proposed using a combination therapy of MCS and extracellular matrix (ECM) injection therapy to promote myocardial recovery.

Methods: The experimental design consisted of a control (no therapy, n=10) and 3 test groups: (1) ECM only (n=2); (2) MSC (HVAD) only (n=2); and (3) HVAD + ECM (n=2) in a 60-day chronic ischemic heart failure (IHF) bovine model. The ECM (CorMatrix®, Atlanta, GA) was injected into the ischemic region of myocardium and the HVAD (HeartWare®, Miami Lakes, FL), a centrifugal continuous flow device was implanted. Cardiovascular efficacy and function were quantified using by serial measurements of hemodynamics, echocardiogram and fluoroscopy imaging, fluorescent microsphere perfusion, and BrdU labeling (myocyte proliferation).

Results: The study demonstrated HVAD+ECM therapy may provide greatest benefits toward myocardial remodeling and recovery. The preliminary data indicates feasibility in the new treatment method and a larger sample size is needed to determine significance.

TABLE OF CONTENTS

LIST OF TABLES

LIST OF FIGURES

I. INTRODUCTION

A. Heart Failure Background

Cardiovascular disease (CVD) is among the most prevalent and costly diseases plaguing the United States. In 2010, it was reported that CVD affects more than 80 million people in the United States, and had an associated mortality of 500,000 deaths per year[2, 3]. In fact, CVD is the leading cause of morbidity and mortality in the country for both men and women[4]. Although it is estimated that more than 70% of cardiovascular disease can be prevented through avoidance of cardiovascular risk factors, such as smoking, poor diet, and insufficient exercise, only 5% of middle-age and older adults are considered to have avoided the associated risk factors to the ideal level[5].

By 2030, the prevalence of CVD is expected to increase by 25%[6] as more and more of the population is diagnosed with diabetes, metabolic syndrome, and other CVD risk factors[7]. Because of these trends, CVD will increasingly be the United States' most deadly healthcare issue. As a consequence, CVD is also one of the most economically draining diseases. The number of inpatient cardiovascular operations has increased by 30% in the last

decade[2]. The American Heart Association has estimated that the direct and indirect cost of CVD and stroke in the United States was more than $316.6 billion in 2012[2].

The term “cardiovascular disease” encompasses many diseases that involve the heart and vasculature system. These include atherosclerosis, coronary heart disease, cardiomyopathy, cardiac dysrhythmias, and valvular heart disease[8]. Heart failure (HF) is often considered a related syndrome[3] because it has a specific set of features and symptoms but multiple possible causes. CVD most often affects patients through heart failure[3]. With the emergence of a CVD precursor, such as hypertension or acute myocardial infarction, a cascade of destructive structural, functional, and biologic changes is initiated[9]. The destructive changes ultimately lead to the development of HF as the heart struggles to meet the body’s metabolic demand. Some of the underlying causes and reactive changes involved in the development of chronic HF include ischemic insult, poor myocardial perfusion, impaired cardiac function, and cardiac remodeling[10]. It is estimated that HF affects 5 million people in the Unites States, and severe class IV heart failure HF is associated with a 1-year mortality rate of 60%[11].

B. Left Ventricle (LV) Remodeling

Progressive heart failure is characterized by a pathological remodeling of myocardial muscle associated with contractile dysfunction and systolic

expansion[12]. Myocardial remodeling, thought to be the result of myocardial infarction and acute ischemia, adversely affects ventricular function[13]. During the original insult, myocytes undergo necrosis, which is followed by edema and inflammation of the myocardium. Proliferating fibroblasts then invade the necrotic tissue, and matrix metalloproteinases degrade the myocardial extracellular matrix. The fibroblasts then deposit high density collagen tissue. This process creates non-contractile scar tissue[13].

Both the infarcted and non-infarcted regions undergo a gradual lengthening process, which causes the ventricle to lose contractile power. The high-density collagen scar tissue has a greater tensile strength than healthy tissue and, as a result, the infarcted tissue begins to lengthen and lose thickness[14]. This process causes significant expansion of the infarcted region in the hours and days following the original insult. Within weeks, the entire ventricle dilates. Because of slippage between muscle fiber bundles, the number of myocytes is reduced across the region. That contributes further to the lengthening, thinning, and loss of contractility of the ventricle [15]. Figure 1 Part (A) shows the progression of myocardial expansion at the site of an apical infarction.

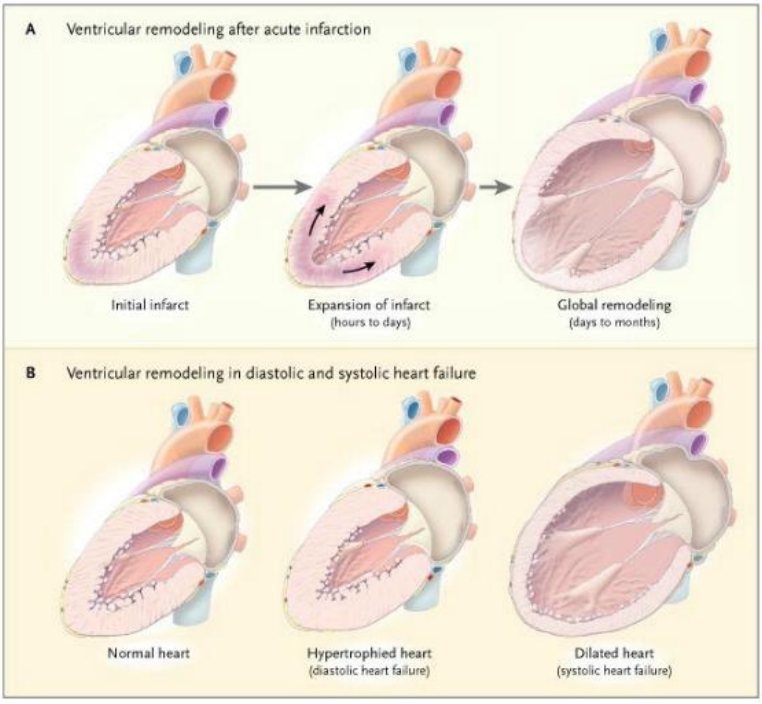

Figure 1: Part (A) Ventricular Remodeling after Infarction; Part (B) Remodeling in Diastolic and Systolic Heart Failure [3]

Ventricular remodeling in infarcted and non-infarcted regions is also thought to be a response to myocardial dysfunction. The magnitude of ventricular remodeling is positively associated with the extent of the initial damage at the time of infarct. The loss of contractility and dilation at systole, or systolic heart failure, acutely decreases the heart's stroke volume, ejection fraction, and cardiac output. In order to adapt to decreased contractility, the heart must compensate: the ventricle dilates in size to achieve a restored stroke volume and cardiac output, although total ejection fraction decreases to abnormally low values. Figure 1 Part (B), right panel, shows complete left ventricle dilation in systolic heart failure. In order to maintain cardiac function, distension of the viable myocardium, utilization of the Frank-Starling mechanism, and positive chronotropy and inotropy occur[13]. In the Frank-Starling mechanism, diastolic distension during filling increases myosin-actin interaction

and maximizes contractility. The chronotropic and inotropic activity helps compensate for poor cardiac function by increasing the frequency of beats and myocardial contractility, thereby increasing stroke volume and cardiac output.

Although this compensatory mechanism helps restore adequate function in the short term, long term dilation has been shown to increase diastolic and systolic wall stress, which stimulates further ventricular dilation[16]. That process results in the progressive nature of heart failure. The surviving myocytes have been shown to undergo hypertrophy, increasing cellular volume by up to 78%, in order to compensate for the amplified wall stress[17]. However, cellular hypertrophy is inadequate to compensate for myocardial loss and does not balance out the mounting effects of ventricular dilation[17]. Rather, the cardiomyocytes experience more stress as the ventricle enlarges to compensate for poor myocardial performance and the contractile fibers in each sarcomere are stretched to the limit and, in turn, lose more mechanical contractile power. Figure 1 Part (B), middle panel, depicts left ventricle myocardial hypertrophy. In diastolic heart failure, which is a response to hypertension rather than to infarction, the myocardium undergoes extreme hypertrophy to compensate for systemic resistance to flow[3]. Although systolic function is preserved, diastolic function is hindered. Diastolic heart failure may account for 20–50% of the heart failure population[3]; however, this paper will continue to focus on classical systolic heart failure.

As the heart undergoes remodeling, not only do the ventricular walls begin to dilate and enlarge, the heart also begins to lose its compact and conical

shape, becoming more globular. This negatively impacts the effectiveness of the mitral valve. Many heart failure patients begin to develop mitral regurgitation as the geometric relationship between the mitral valve leaflets and the papillary muscles, which are responsible for holding the valve in place, are drastically altered[18]. The regurgitation of blood during systole only adds to the ineffectiveness of cardiac function during heart failure, as blood is recirculated back into the atrium. It is readily apparent that the compensatory effects of heart failure compound and promote further structural damage, gradually worsening the patient's condition.

C. Current Therapeutic Approaches

The treatment of heart failure is a complex process that involves many levels of intervention to prevent the development and progression of ventricular remodeling and cardiac dysfunction. Figure 2 shows the standard clinical treatments required at each stage of heart failure.

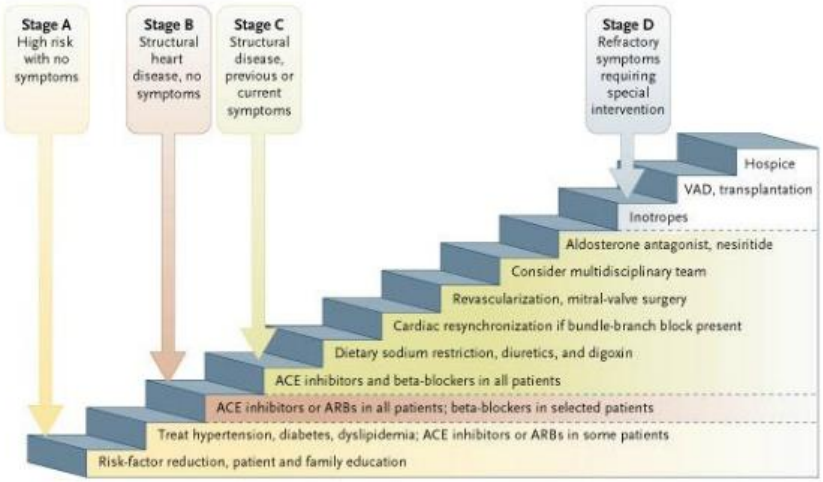

Figure 2: Stages of Heart Failure and Treatment Options for Systolic Heart Failure [3]

Stage A (stage I) is characterized by a high risk for the development of heart failure without any symptoms or structural damage. Patients at this stage are treated for hypertension or other cardiovascular disease precursors, with the intention of preventing any pathological structural remodeling. Intervention at this stage has shown to decrease the incidence of heart failure by 30–50%[19]. Stage B (stage II) involves the structural damage associated with heart failure but with no symptoms. These patients may have undergone a previous myocardial infarction but the associated structural changes have not yet physically affected their quality of life. At this stage, physicians use several objective methods to diagnose the level of heart failure including electrocardiogram to detect electrical abnormalities and cardiac imaging via echocardiography and chest x-ray to detect pulmonary congestion or an enlarged heart[20].

Stage C (stage III) patients have structural damage and physical symptoms. The symptoms commonly involve breathlessness and fatigue at rest or during moderate exercise, which result from poor cardiac function[21]. These patients receive aggressive pharmaceutical treatment and may undergo mitral valve or cardiac resynchronization therapy. Lastly, stage D (stage IV) patients experience refractory symptoms, extreme fatigue even at rest and require hospitalization. Surgical intervention and specialized care is necessary for patient survival. The following sections examine the common approaches to treating heart failure.

1. Pharmacological Treatments

Researchers have isolated and studied several important factors in heart failure as avenues for possible treatment, although the exact mechanism of action for each is not yet completely understood. It is thought that, to halt the progression and possibly reverse heart failure and the associated remodeling, there needs to be a decrease in myocardial wall stress and therefore a reduction in resistance to flow. With an increased emphasis on the relationship between altered cardiovascular dynamics and the neuro-hormonal effects of them, pharmaceutical treatments are currently being developed to alleviate the heart's increased workload.

Figure 3 diagrams the pathophysiology and neuro-hormonal relationship in progressive heart failure. During heart failure, poor cardiac function causes a drop in systemic pressures. Because of a pathologic unloading at the sites cardiovascular baroreceptors (blue circles), an afferent sensory signal (black arrow) is transmitted to the cardio-regulatory center in the central nervous system. This causes the activation of the sympathetic nervous system (green arrows) and the stimulation of a hormonal response (blue arrows) to drive up blood pressure to stimulate increased atrial filling[22]. These sympathetic signals, in turn, place more of a burden on the failing heart, adding to the cyclical nature of progressive heart failure.

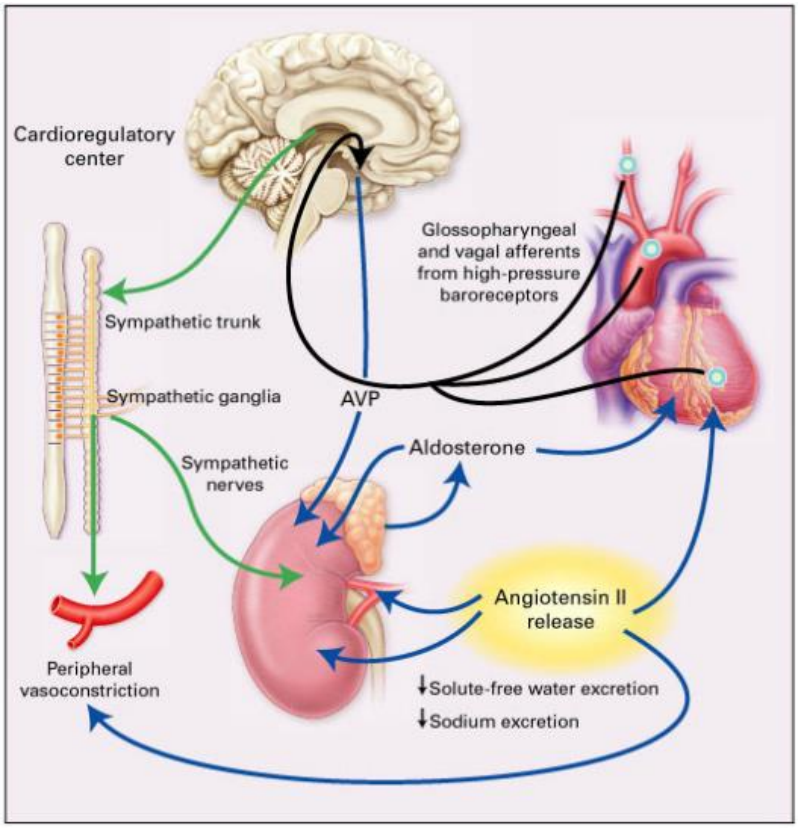

Figure 3: Pathophysiology of Heart Failure [22]

With the neuro-hormonal response in mind, several pharmaceuticals have been designed to disrupt the hormonal pathway of heart failure. For example, beta-blockers slow heart rate and decrease blood pressure by inhibiting the sympathetic β-adrenergic mechanisms[23]. Beta-blockers stop the sympathetic nervous system from promoting the release of vasoactive chemicals, such as renin, which stimulate vasoconstriction and tachycardia and only serve to exacerbate ventricular remodeling[3]. Angiotensin-converting-enzyme (ACE) inhibitors also decrease the afterload by blocking the renin-angiotensin-aldosterone system[3]. Likewise, diuretics encourage excess fluid elimination, effectively decreasing blood pressure. Aldosterone, which causes water retention and increased blood pressure, is often elevated in heart failure patients.

Aldosterone acts to increase the afterload and the stress on the myocardium. Specific inotropic agents and chemicals, such as digoxin, can be used to maintain optimum heart rate, contractility, and ventricle filling times[24]. Digoxin acts as a NA^{+}/K^{+} ATPase inhibitor that increases intracellular Ca^{2+}, which causes an increase in contractility and duration of systole, effectively decreasing the heart rate while maintaining optimum stroke volume[25]. Although the use of pharmaceuticals is generally the first course of treatment in every heart failure case, many patients' conditions progress into dangerous pathologies and require specialized care and surgical intervention.

2. Heart Transplant

Today, heart transplantation remains the ideal destination therapy for advanced and refractory heart failure. It has an associated 50% 10-year survival rate[26], which greatly exceeds the 60% 1-year survival rate for stage IV patients without transplantation. However, this treatment method has dramatic limitations that prevent its widespread use. Because of an extreme shortage of viable human donor hearts, less than 4,000 cardiac transplant surgeries are performed in the United States each year[27]. In addition, patients who receive a heart transplant must remain immunosuppressed to prevent rejection. That can leave already compromised patients susceptible to life-threatening diseases and complications[26]. Because of the scarcity of donor hearts and the associated limitations, alternative replacement hearts have been developed in the form of mechanical circulatory support.

3. Mechanical Circulatory Support

The first mechanical circulatory support (MCS) device, a cardiopulmonary bypass machine, was developed in 1953 to support patients during open heart surgery[28]. The development of artificial hearts for use in heart failure patients started in the 1960's with the National Heart Institute's establishment of the Artificial Heart Program. At this time, research was focused on producing a complete heart replacement, or total artificial heart (TAH). TAH devices were originally developed for use until such a time that a replacement donor heart became available. This method is known as bridge to transplant therapy (BTT). The TAH devices presented problems with durability and biocompatibility. The complex moving parts in the TAH devices invited the distinct possibility of premature mechanical failure. TAH devices, such as the SynCardia's CardioWest TAH (FDA BTT approved in 2004), are only designed to support a patient for a matter of months until transplantation[29]. These devices are used in cases in which the patient is at severe risk of mortality within 30 days. Although the TAH method had great success supporting patients until transplant, the devices had limitations that encouraged researchers to explore different avenues.

By the 1980s, the first generation of ventricular assist devices (VAD) was created. Instead of aiming to completely replace the heart, researchers developed a method of unloading the stressors associated with heart failure. They developed devices to divert blood flow from the ventricle to a secondary mechanical pump and return it back to the aorta. The bypass of flow essentially relieves the cardiac demands on the ventricle, and completely disrupts the

destructive signals associated with LV remodeling and dilation. The first generation of VADs were pulsatile, large, and often extracorporeal, meaning the pump remained outside the body. The devices that were fully implantable were installed in the abdomen below the diaphragm. These devices advanced in biocompatibility as new materials were developed that were inert in the body, such as Heartmate XVE's unique surface texturing that reduced the risk of stroke from emboli[30]. The HeartMate XVE, along with other first-generation VADs, were conceived as a destination therapy. However, these devices still faced durability issues and were primarily used as BTT devices[31].

With the need for smaller, implantable, and more durable VADs, researchers developed a second generation. The new generation abandoned the pulsatile pumping mechanisms of the first generation, such as pneumatic actuators. Instead, they utilized axial rotors that continuously propelled blood. With this new mechanism, researchers could miniaturize VADs and even develop pediatric pumps. These constitute the first generation of MCS that was approved for destination therapy (DT), such as the Jarvik 2000 (EU approved DT in 2005). With success in the second generation, a third and fourth generation of VADs are now being developed. These devices utilize centrifugal flow and very few moving parts. They are characterized by extremely durable pumping mechanisms. Many of the devices are seeking approval for DT.

Figure 4: The HeartWare ® HVAD (left) and the internal centrifugal rotor (right) [32]

In this study, the HeartWare® HVAD, a centrifugal continuous flow device, is being utilized as the experimental MCS device. Depicted in Figure 4 (left), it is considered a fourth generation VAD because of its small size (<150g) and the fact that it can be implanted above the diaphragm. The device received BTT FDA approval in 2012 for patients with end-stage heart failure. The pump is the first FDA approved full-support device -- it has the ability to produce up to 10L/min flow -- to be implantable in the pericardial space. The centrifugal rotor, shown in Figure 4 (right), is the device's only moving part. It is magnetically suspended and designed to maximize device durability. Globally, the HVAD has been implanted in more than 2,500 heart failure patients[33].

D. Myocardial Recovery

Although mechanical circulatory support has been increasingly reliable in treating and sustaining patients with end-stage heart failure, many questions have been raised about the possibilities of recovery. With increasing VAD miniaturization, durability, and adaptability, patients have been reported to have

undergone heart failure recovery. The unloading of the ventricles not only alleviates the symptoms of heart failure, but it has also been shown to reverse heart failure as the ventricles undergo reverse-remodeling. VAD support, allowing for hemodynamic unloading, been shown to trigger neuro-hormonal, cellular, and tissue adaptations towards the less pathologic state[34]. These adaptations imply great myocardial plasticity and the ability for the heart to heal.

These findings also reveal that mechanical overload is the primary factor in sustaining the state of heart failure. With complete cardiac unloading, the left ventricle shows an almost immediate decrease in end-diastolic volume and an increase in wall thickness[35]. As this hemodynamic change is sustained, the body shows a gradual decrease in pathologic neuro-hormonal activation[36]. Mechanically unloading the heart encourages a decrease in myocyte hypertrophy[37], increased systolic contractility, improved diastolic relaxation[38], a restoration of normal electrical activity[39], and decreased tissue fibrosis[40]. With these findings in mind, MSC is not only being used to support refractory patients, but is also being researched as a bridge to recovery device. Researchers are creating a new MCS treatment paradigm that includes mechanical rest and restoration. The heart is immediately unloaded for a period of myocardial rest and is allowed to return to its normal un-dilated state. It is then gradually be reloaded for a period of functional restoration therapy. The myocardial tissue is slowly reloaded and trained to sustain a normal cardiac output. In this study, the HVADs will be used for full-support and complete unloading, followed by a partial support restoration period.

E. Regenerative Medicine

Because of the possibilities of heart failure recovery and recent advancement in tissue engineering, many researchers have focused on cellular therapy and on the use of biomaterials to aid in heart failure recovery. Several strategies for the treatment of myocardial infarction and heart failure using biomaterials are depicted in Figure 5.

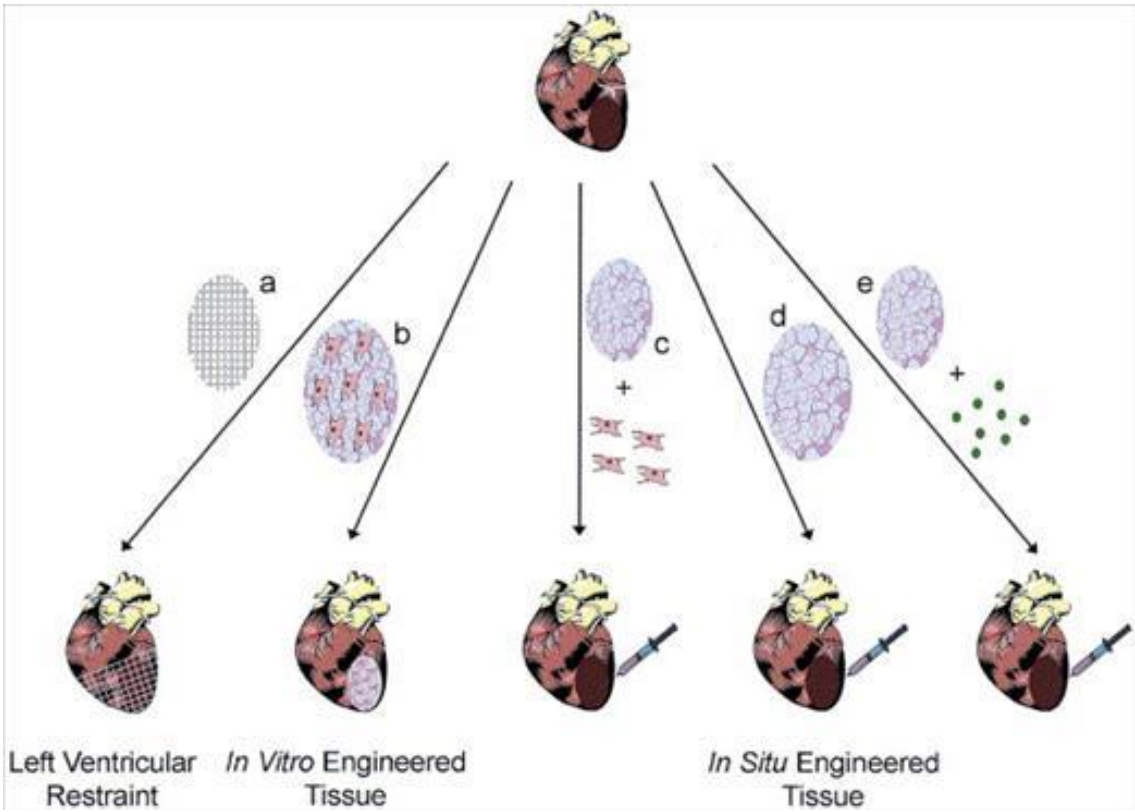

Figure 5: Biomaterial strategies for treatment of myocardial infarction. (a) polymer mesh restraints to prevent remodeling, (b) implantable scaffold seeded with cardiomyocytes *in vitro*, (e) injectable scaffold as a delivery vehicle for cells, (d) injectable decellularized scaffold, (e) injectable scaffold with therapeutic agents [41]

Researchers have developed implantable polymer meshes, Figure 5 Part (a), that act as a restraint on the expansion of the heart. It has been shown that restraining the initial infarct expansion process prevents a progressive decline in cardiac function. A polymer mesh, sutured exclusively onto the area of infarct,

helped to preserve LV geometry and to reduce instances of mitral regurgitation[42]. However, it was shown that wrapping the entire LV helped to preserve normal LV volume[43]. Cardiac support devices, which wrap both ventricles, have been shown to decrease end diastolic LV volume, myocyte hypertrophy, and fibrosis[44]. Polymer mesh restraints have shown promising results in animal studies, but initial results in the clinic have been conflicted. Researchers are also pursuing other biomaterial strategies, such as cellular and scaffold implantation to aid in tissue regeneration.

Researchers have studied cellular transplantation as a means of cardiac repair. Some of the first studies involved direct injection of viable cells to the infarcted tissue, or cellular cardiomyoplasty[41]. However, this technique is limited by poor cellular retention and transplant survival[45]. With the development of new biomaterials and tissue engineering, more recent studies have attempted to create in-vitro engineered tissue, Figure 5 Part (b). The tissue is often composed of a scaffold seeded with a cell type, via *in vitro* culturing, which is implanted into the myocardium.

Much research also is focused on the usage of decellularized biological scaffolds in the treatment of damaged and necrotic tissue, Figure 5 Part (d). These applications include esophageal and muscle reconstruction[46], aortic grafts[47], tendon rupture[48], intestinal mucosa defects[49], skin grafts[50], and now myocardium[51]. In these applications, the scaffolds are composed of naturally occurring extracellular matrix (ECM) derived from a xenogenic tissue source, such as porcine intestinal submucosa. The biologic ECM scaffolds

contain the same structural and functional proteins that are present in the native ECM and are responsive to the same ECM proteases[48]. This means that the scaffolds are easily degraded, infiltrated, and incorporated into new tissue by the native cells in a matter of 60-90 days[52]. It is hypothesized that ECM degradation and remodeling cause progenitor cell recruitment and bioactive molecule release, such as the release of growth factor, which is responsible for the construction of remodeled tissue[48]. The ECM scaffold has been shown to encourage tissue vascularization because of progenitor cell release of vascular endothelial cell growth factor[53]. The reconstruction of a normal ECM is important in the myocardial healing process because it provides a healthy cellular microenvironment that supports cellular migration, growth, differentiation, and signaling[54].

Many such biological scaffolds are created as sheets or patches, which are then sutured onto an infarcted area. In one study, a myocardial patch was shown to be populated with small regions of myocytes within 8 weeks of implantation[51]. In more recent studies, the sheet of ECM is broken down into an injectable emulsion. This process breaks down the relatively large patch into much smaller and more manageable micro-scaffolds that can be directly injected throughout the infarcted tissue rather than placed at the surface. Although the emulsion is fine enough to be injected as a therapeutic gel, the scaffold pieces remain comparatively large at the cellular level and provide matrix microenvironments for progenitor cell invasion and new tissue deposition[55]. It has been shown that ECM injections improved myocardial healing with LV wall

thickening and a preservation of cardiac systolic function[55]. In this study, an ECM emulsion (CorMatrix® Roswell, GA) will be used in combination with MCS to determine the benefit of the combination of therapies: ventricular unloading and biological scaffold support for healing.

F. Heart Failure Models

In order to accurately test possible heart failure therapies in the pre-clinical setting, relevant models of the disease must be utilized, which means conducting tests on a large animal model, closely related to human cardiovascular anatomy and physiology. The industry standard model for MCS safety, reliability, and efficacy testing is healthy calves, as they are large enough to accommodate such devices. However, there are very few large animal heart failure models utilized today. Having an accurate model of the heart failure disease is extremely important for testing the physiological response to heart failure, treatment, and recovery for both MCS and tissue engineering applications. An accurate animal model is important in examining the mechanisms and pathways of myocardial remodeling[56] and heart failure recovery during therapy[57, 58].

Previously, researchers have developed non-ischemic large animal heart failure models that utilize toxic coronary infusions of doxorubicin to induce myocardial necrosis[59]. However, non-ischemic heart failure only accounts for a third of heart failure patients. Because ischemic heart failure is the more prevalent type of heart failure in humans, this study uses a novel bovine chronic

ischemic heart failure model. This model was first described in a previous manuscript[1], in which the left coronary artery is selectively embolized using 90μm polystyrene microspheres. This procedure produces a region of myocardial infarction within the wall of the LV with acute ischemic insult. The heart failure pathology is allowed to develop for a minimum of 30 days, and the damage, such as ventricular remodeling and hemodynamic changes, is assessed using several analysis techniques including weight monitoring, imaging, hemodynamic biosensing, and regional blood flow analysis.

G. Project Aim

The overall objective of the study is to demonstrate the efficacy of a new heart failure treatment paradigm that combines the regenerative aspects of extracellular matrix therapy and the rehabilitative aspects of mechanical circulatory support. The hypothesis is that the combination of both therapies will demonstrate a better treatment strategy than each individual therapy. The rationale is that the MCS device will provide unloading and support myocardial reverse remodeling, while the ECM therapy will encourage the regeneration of healthy myocardial tissue.

II. ANALYTICAL TOOLS

A. Weight and Body Condition Score

Body weight and condition are very important indicators of health. An average healthy Jersey calf is expected to grow approximately 20 kg a month (0.6 kg/day) within the first 3–7 months[60], which is the ideal timeline for heart failure treatment studies. Deviations from this growth rate can help to confirm heart failure pathology and suggest recovery with treatment. Changes in weight are an indicator of cardiac cachexia, or body wasting. Cachexia is characterized by a loss of lean tissue, fat tissue, and bone tissue, and is thought to be governed by a neurohormonal response to heart failure[61].

The body condition score (BCS) is an indicator of the amount of stored energy reserves and good health. The score is judged on the amount of fatty tissue distributed throughout the animal. A drop in BCS could indicate severe heart failure pathology.

B. Blood Specimens

Complete blood count (CBC) is a laboratory test for measuring the number of red blood cells, white blood cells, and platelets as well as amount of hemoglobin and hematocrit percentage in a subject's blood. CBC can be used to diagnose infections, blood clotting problems, and anemia[62]. With the HVAD implant and external driveline, it is vital to test for and immediately treat infections. When using a mechanical circulatory support device, it is also important to test for plasma-free hemoglobin, an indicator of hemolysis, or destruction of red blood cells. In normal and healthy conditions, there should be no detectable plasma-free hemoglobin. A positive result is an indicator of blood trauma associated with MCS and surgery. A troponin test is used to test for levels of troponin T and troponin I in circulation, which are released with myocardial damage. The amount of troponin in the blood is proportional to the amount of damage.

C. Imaging

Cardiac imaging is a vital tool in the diagnosis and analysis of heart failure. Physicians use imaging to diagnose several types of structural damage seen in heart failure patients, such as cardiomegaly (enlarged heart) and systolic dysfunction. Echocardiogram (ECHO) is one of the most common noninvasive cardio-imaging techniques. Using ultrasound technology, cardiac function can be

assessed including systolic and diastolic LV volumes and ejection fraction. ECHO can be used to diagnose mitral regurgitation and aortic insufficiency.

Fluoroscopy is another useful, but more invasive, imaging technique. Through the use of X-ray and radio opaque dye, coronary anatomy and blood flow can be visualized. Figure 6 is an example fluoroscopy image showing a still frame of an LV gram in the left panel and the isolated left main coronary arteries in the right panel.

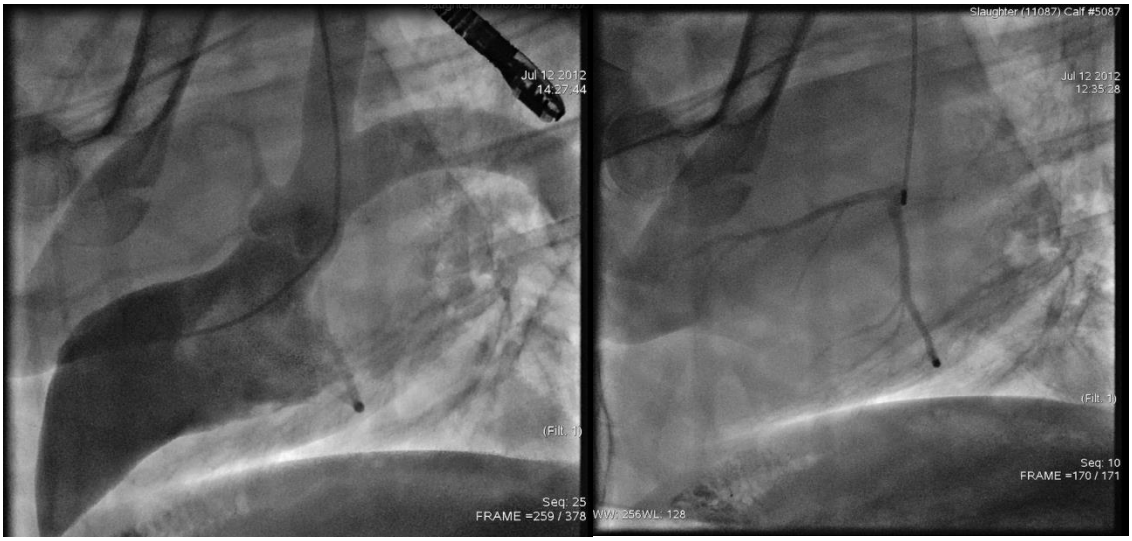

Figure 6: Pre-embolization fluoroscopy image of (left) left ventricle and aorta and (right) left main coronary arteries

D. Hemodynamics

Altered hemodynamics is a major factor in cardiovascular disease and heart failure. Hemodynamics can be measured to understand the underlying mechanical processes associated with ventricle dilation and systolic dysfunction. left ventricle pressure (LVP), aortic pressure (AoP), arterial pressure (ART), central venous pressure (CVP), left ventricular volume (LVVol), and

electrocardiogram (ECG) waveforms are collected and analyzed to reveal different disease states. During a myocardial insult, such as the coronary embolization used in this study, immediate changes in the electrocardio-activity, such as an elevation in the ST segments, occur as portrayed in Figure 7. ST elevation is an indicator of cardiac muscle damage as the contractile and electrical properties of the heart, such as neuromuscular repolarization pathways, change. Also depicted in Figure 7 are noticeable changes in the aortic and LV pressures during the progression of heart failure. Not only do peak systolic pressures drop, there are also changes in ventricle relaxation and filling during diastole. While in the normal state, the ventricle is fully relaxed for a significant fraction of the cycle, creating almost binary pressure conditions. The heart is instantaneously fully relaxed or contracted. In the heart failure state with diastolic dysfunction, the contraction and relaxation states are not as starkly defined. At the end of diastole, the low pressures of diastole gradually waver up into the high pressures of systole.

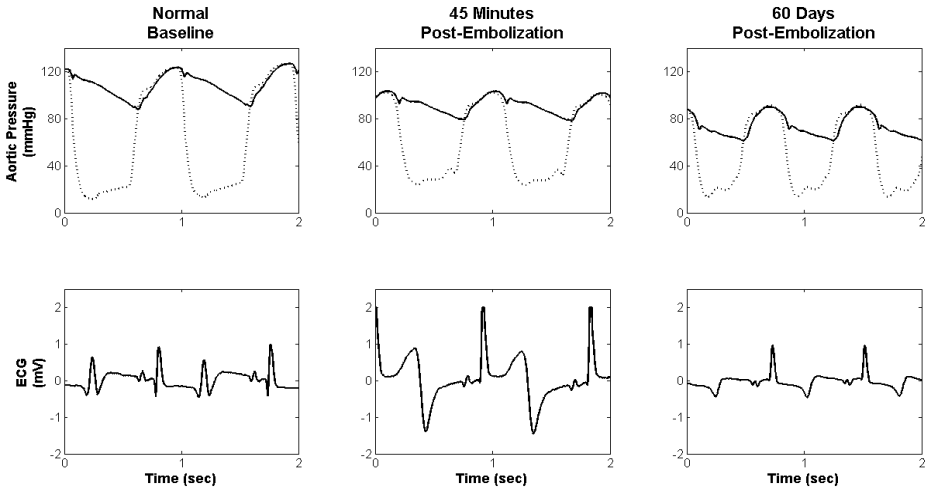

Figure 7: Hemodynamic changes during coronary embolization: (top) aortic pressure (bold line) and left ventricular pressure (dotted line), (bottom) ECG; (left) normal state, (middle) post embolization, and (right) chronic heart failure conditions

Hemodynamic waveforms can be used to visualize and assess ventricular unloading during treatment with mechanical circulatory support. Figure 8 shows the reduction in LV pressures as the continuous flow VAD unloads volume from the ventricle. As the pump speed is increased from partial to full support, LVP is minimized along with the pulsitility of AoP. At complete unloading, the aortic valve is completely bypassed and remains closed.

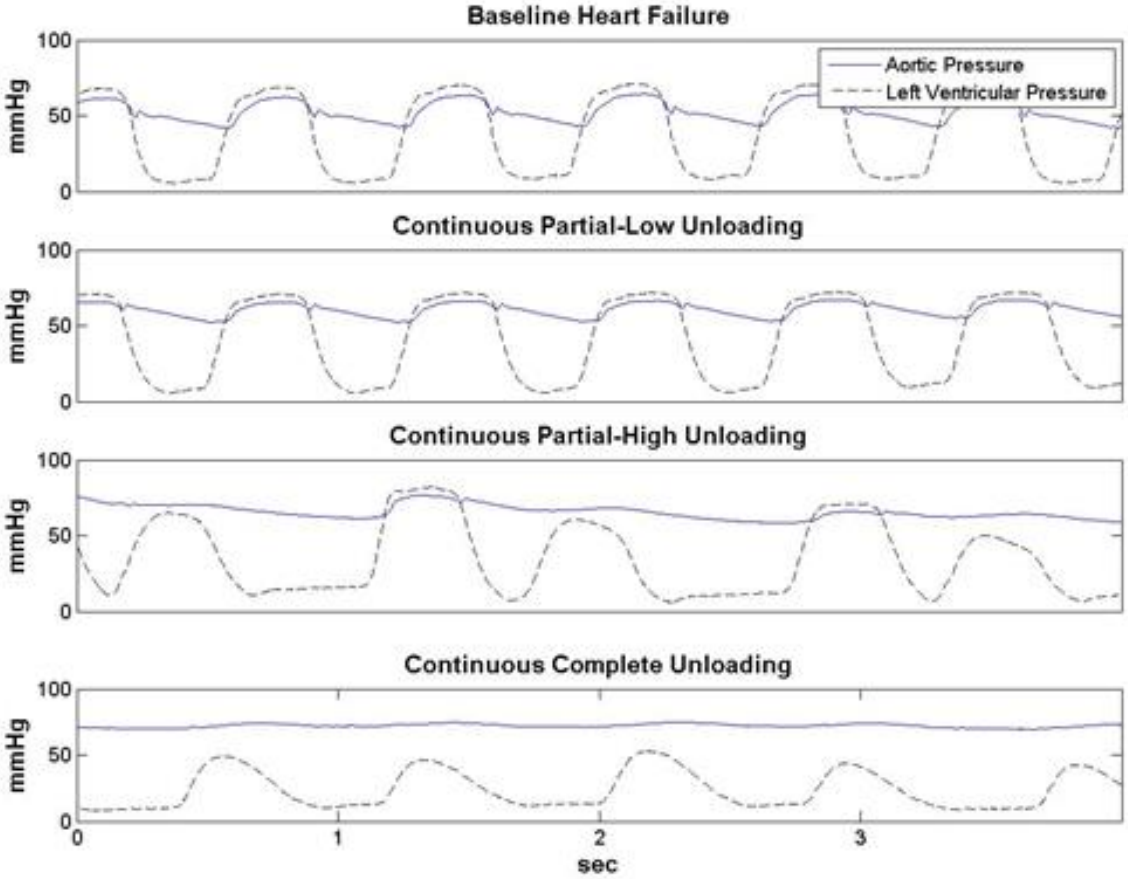

Figure 8: Hemodynamic changes associated with ventricular unloading

E. Regional Blood Flow Calculations

The measurement of regional blood flow (RBF) is extremely important for understanding cardiovascular efficacy and function, since the definitive target of

cardiac function is end organ perfusion. Microspheres have been used to study RBF for over 40 years[63]. Traditionally, microspheres were radioactively labeled, but this method had distinct disadvantages due to health and environmental hazards and relatively short radioactive isotope half-lives[64]. This made chronic experiments particularly difficult and costly. Fluorescently labeled microspheres (FM) are the ideal alternative, since they eliminate the disadvantages associated with radioactivity. FM do not have fluorescent half-lives, making chronic studies possible. Multiple colors of FM can be used in each subject to compare different experimental conditions or time points [65].

Microsphere distribution is used to accurately estimate regional blood flow depending on several assumptions. Upon injection into the arterial system, the microspheres must be well mixed and evenly distributed in the blood. That ensures that the concentration of microspheres is consistent at every arterial branch and that each organ receives a consistent dose of microspheres according to the organ's perfusion[66]. In order to ensure optimum mixing for the study of systemic flow, the initial injection must take place the farthest up-stream from the target organs. It has been shown that injection into the left atrium or LV allows for accurate systemic measurements[67]. Next, the entire dose of microspheres must be entrapped in the vascular bedding during the first circulation and remain entrapped until tissue recovery[66]. This ensures that microspheres are not recirculated to certain tissues, skewing the original pattern of blood flow. Lastly, the entrapment of microspheres must not occlude vessels or affect the hemodynamics of organ blood flow[66]. To address these

constraints, the size of the microsphere is carefully considered, as the size of capillaries and arterial anastomosis may vary between species and organ[68]. The microspheres must be large enough to ensure that a significant number of them do not pass into venous circulation. On the other hand, the microspheres must be small enough to embed in only the smallest diameter capillary beds without occluding major vessels and changing the native pattern of blood flow.

At each time of FM injection, a reference blood sample is taken at a known rate of withdrawal. This blood sample is used in the final RBF calculation. In order to quantify the amount of FM in each sample, the microspheres are extracted from the tissue and analyzed through flow cytometery. A specific amount of control FM are added to each sample. The remaining microspheres can be quantified in relation to the control. A fluorescent dot plot is created, separating the FM into regions according to the intensity of red and yellow in each FM color as shown in Figure 9. The clusters are then isolated into elliptical regions-of-interest and counted.

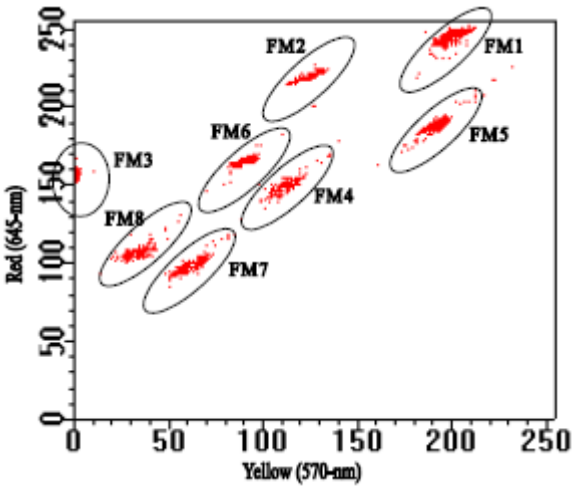

Figure 9: Example fluorescent microsphere dot plot [69]

RBF is calculated based on the ratio of microspheres per gram of tissue to the amount of microspheres per reference blood sample according to the following equation:

$$Q_i = Q_r \left(\frac{C_i}{C_r}\right)$$

Where Q_i is the regional blood flow per gram (ml min^{-1} g^{-1}) of the sample, C_i is the microsphere count per gram of tissue in the sample, Q_r is the reference blood sample withdrawal rate (ml min^{-1}), and C_r is the microsphere count in the reference blood sample[69]. Once Q_i is calculated, it can be used to investigate RBF and end-organ perfusion for the different states of heart failure, heart failure recovery, and even HVAD motor settings.

F. BrdU Cellular Proliferation Assay

5-bromo-2'-deoxyuridine (BrdU) is a synthetic nucleoside, uridine derivative, used in the detection of proliferating cells in live tissue. Researchers first developed it as a way to determine the proliferative index of certain tumors[70] without the use of hazardous radiolabeled substrates and time consuming methods, such as [3H]-thymidine autoradiography[71]. BrdU usage is also advantageous because it allows for the detection of labeled cells in relatively thick tissue samples[72]. It can be used in both cell culture and living tissue applications. BrdU can be administered to animals either shortly before euthanasia or as a chronic treatment. Because of these advantages, BrdU is used widely in neurogenesis and myogenesis studies.

Cardiomyogenesis is a controversial topic in biomedical research. In the field of cardiovascular research, it is deeply engrained that the heart is a postmitotic organ. The number of parenchymal cells is established at birth, and cardiomyocytes cannot be replaced when lost to cardiovascular disease[73]. However, with the discovery of native cardiac stem cells in developing, postnatal, and adult hearts, the traditional view has been challenged and it has been confirmed that cardiomyocyte turnover naturally occurs[74]. The cardiovascular research field is increasing incorporating BrdU to study cardiomyocyte turn over and heart failure recovery.

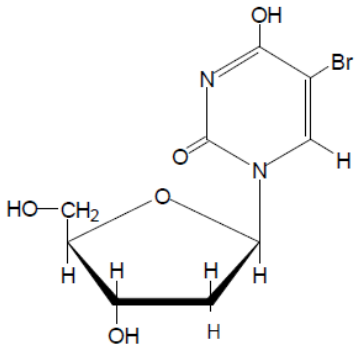

Figure 10: Structure of 5-bromo-2'-deoxyuridine (BrdU) [75]

As an analogue of thymidine, BrdU is spontaneously incorporated into newly formed DNA as cells undergo the synthesis phase of the cell cycle. The chemical structure of BrdU is depicted in Figure 10. BrdU is detected through the use of immunohistochemistry. A monoclonal antibody, directed against single-stranded DNA containing BrdU, is added to the sample[76]. In order to bind to the DNA, it must first be denatured into the single-stranded form. This may involve treatment with HCl or with DNase 1[77]. A secondary antibody, labeled with a specific marker, is added and it binds to the original antibody. The sample

is then imaged and BrdU positive cells are counted. A secondary label can also be used to isolate a specific cell type or cellular component, such as the nucleus, within the tissue sample.

One disadvantage of BrdU labeling is that it only labels cells at a specific time point in the cell cycle, during the synthesis of DNA. In order to fully label cells that are actively proliferating, BrdU must be administered multiple times throughout the desired period of study[78]. The literature suggests that BrdU is available for DNA incorporation for only a few hours after administration[71]. The half-life of BrdU is extremely short (2 hours), since it is rapidly metabolized by dehalogenationin in the plasma[79]. The body quickly eliminates it. Even with multiple injections at dosages of 25-100mg/kg of body weight, BrdU may only label a portion (60%) of the proliferating cellular population[80].

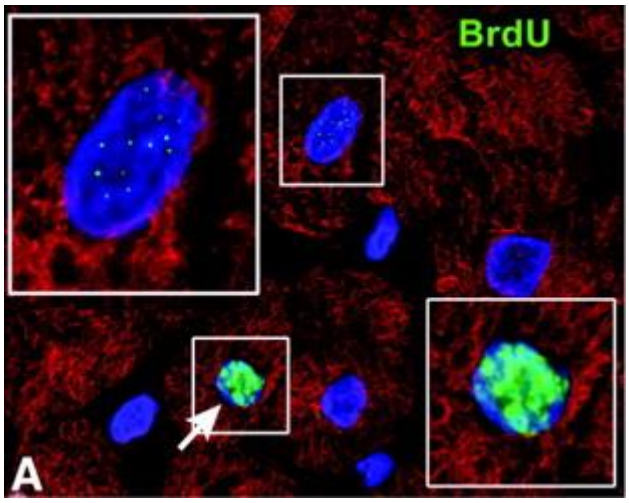

Figure 11: BrdU labeled human myocardium comparing the difference between partial BrdU labeling in cases of cells undergoing DNA repair and full incorporation of BrdU in proliferating cells (arrow) [74]

Another important consideration in labeling DNA synthesis as a marker for cellular proliferation is that mature cells often undergo DNA repair. DNA repair is

performed by cellular enzymes in order to ensure genomic stability[81]. However, DNA repair occurs at only discrete sites and is labeled in a punctuated pattern. These myocyte nuclei can be distinguished from nuclei undergoing DNA synthesis because the BrdU is incorporated evenly across the entire strand. Figure 11 demonstrates the difference between punctuated incorporation of BrdU in myocyte undergoing DNA repair (white box) and total incorporation of BrdU in proliferating myocyte (white box with arrow).

G. Histopathology

Histopathology is an important tool in determining disease states on the cellular level. It involves the examination of tissue specimens, using microscopy, by a medically qualified pathologist. The tissue is fixed, sectioned, and stained to visualize cellular components. The pathologist is able to identify certain indicators of disease, in the case of myocardial infarction: necrosis of myocardiocytes, cellular granulation, and collagen deposition. The amount of scar tissue and fibrosis is able to be quantified as an indicator of myocardial damage[82].

III. METHODS

A. Experimental Design

Figure 12 shows the project organization for the ECM and MCS study, outlining the experimental groups, measurements, and timeline. This project presents the results for the 60-day group, with the goal of producing preliminary data that demonstrates the efficacy of combination ECM and MCS therapy.

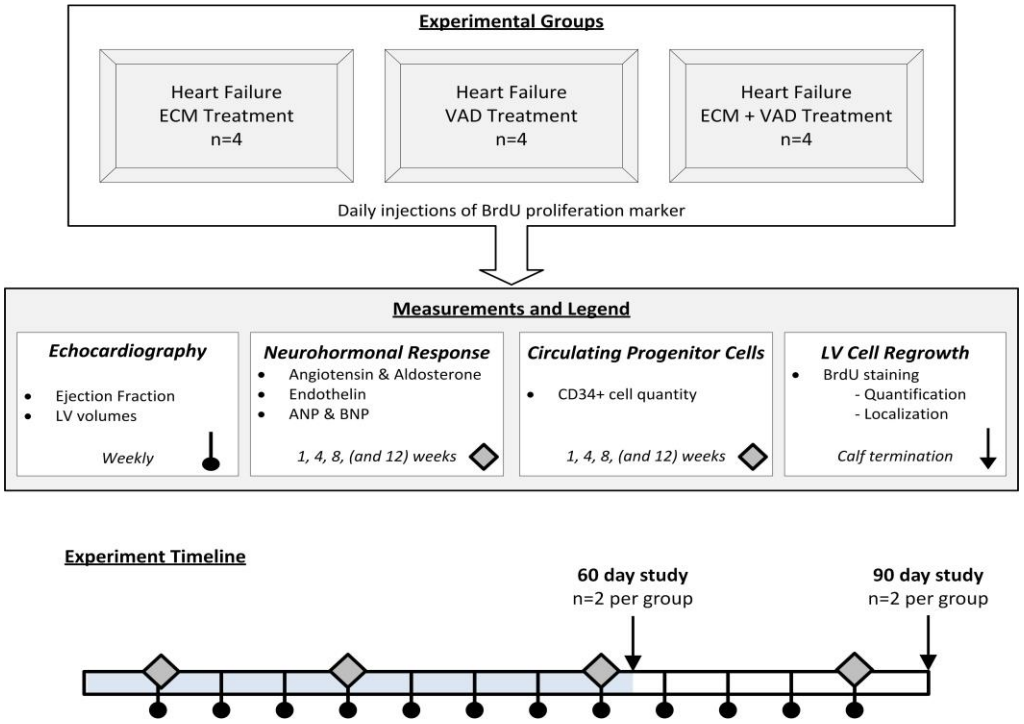

Figure 12: Experimental design to investigate the efficacy of ECM (CorMartix®), HVAD (Heartware®), and HVAD+ECM to promote myocardial remodeling and recovery

Male jersey calves (n=2) were used in each experimental group. The animals had a desired initial weight of 75±10kg. The animals were quarantined for a minimum of 14 days, given prophylactic antibiotic treatments, and were inspected by the veterinarian faculty. Once out of quarantine, each animal underwent a coronary embolization procedure in order to produce a model of LV failure. The heart failure pathology was allowed to develop over 30–60 days to produce chronic ischemic heart failure conditions.

Due to the small sample size, the 6 animals were then semi-randomly divided into 3 study groups based on severity of heart failure. The average heart failure ejection fraction was kept relatively similar across each group. Each group received one heart failure treatment method: HVAD only, ECM only, and combination HVAD+ECM. An animal terminal study was performed 60 days after each treatment and the animal was euthanized accordingly. The animals were handled in accordance with the National Institutes of Health, and all experimental procedures were approved by the University of Louisville Institutional Animal Care and Usage Committee (IACUC).

B. Surgical Procedures

Throughout the study, the animal underwent a total of 3 different surgical procedures: 1) heart failure induction via coronary embolization, 2) treatment initiation (ECM injection, HVAD implant, and combination HVAD+ECM), and 3) terminal study.

1. General Surgical Preparations

In each of the aforementioned surgical procedures, the following practices were consistently used. On the day prior to surgery, a Fentanyl 25 or 50 µg/hr transdermal patch was applied to the animal's flank in order to decrease overall pain. The animal was weighed to obtain its normal weight. The animal was then fasted 18–22 hours before surgery. Water was withheld for a minimum of 12 hours before surgery.

On the day of surgery, the calf was weighed to obtain the reduced NPO (nothing-by-mouth) weight. An intravenous catheter was placed in a marginal ear vein. For embolization procedures, anesthesia was induced via intravenous administration of Valium and Ketamine. For treatment and end study procedures, Propofol was used. Once lightly anesthetized, the calf was intubated and anesthesia was maintained via Isoflurane (3–5%) with oxygen saturation maintained above 90%.

In the operating room, strict aseptic technique was used for all surgical procedures, with exception of the terminal study procedure. The animal was administered Cefazolin (prophylactic) and Fluxinin Maglumine (analgesic). ECG clips and a pulse oximeter were attached for intra-operative monitoring. Magnesium and heparin were given via intravenous infusion to support cardiac function and prevent coagulation. In order to monitor arterial pressure (ART) and central venous pressures (CVP), temporary partially-veloured catheters were placed in the carotid artery and jugular vein and secured to the skin. Once

patency was achieved, the catheter was connected to a pressure transducer line for pressure monitoring.

2. Coronary Embolization

Prophylactic Atenolol (beta blocker) was given 12 hours prior to surgery in order to decrease embolization mortality. In the fluoroscopy operating room, the calf was placed in a lateral recumbency position. An Access™ Vascular Access Port (VAP) was implanted prior to embolization. The VAP catheter was inserted into the jugular vein opposite to the CVP line, and the remaining length was tunneled under the skin toward a second incision near the topline of the neck. The access port was then connected to the catheter, the patency was checked, and then it was locked with TCS solution. Additional heparin was given to prevent coagulation, and a Cordis sheath was placed into the carotid artery using a modified Seldinger technique. A unit of Lidocane was given and Amiodarone drips were started to prevent arrhythmias.

Coronary embolization was achieved by injecting polystyrene beads into coronary circulation. The embolization solution consisted of polystyrene beads (Polybead® Polystyrene 90.0 µm microspheres, 2.64% Solids-Latex, Polysciences, Warrington, PA), bacteriostatic saline, and radio-opaque dye (Conray 43, Iothalamate Megumine 43%, Mallinckrodt Inc., St. Louis, MO) in a 2:1:1 ratio. A target dose of the mixed embolization solution was calculated per animal (0.17 mL solution/kg normal calf weight). A J coronary catheter was positioned in the left main coronary artery and position was confirmed by coronary angiography with radio-opaque dye. A preconditioning dose of

microsphere solution (3ml) was administered into the left main coronary artery. The animal was then monitored over the course of 20 minutes.

Using the calculated target dose as a guide, the remaining volume of microsphere solution was given in alternating doses (1–3ml) between the left anterior descending and circumflex coronary artery, allowing for a minimum of 10 minutes between each dose. The actual dosage used was adjusted based on the animal's response to each injection. The animal was monitored for severe and sustained electrocardiographic changes (ST segment changes) and impaired cardiac function (assessed via echocardiogram). The embolization was considered successful with a minimum of a 1mV ST change and a sustained 40–50% decrease in ejection fraction (EF). Upon completion of the embolization procedure, the actual volume of administered microsphere solution was recorded.

60 minutes after the initial embolization preconditioning dose, a bolus of Furosemide was administered to promote diuresis, mitigate pulmonary effects associated with elevated LV filling pressures involved in heart failure, and promote post-operative recovery and survival. The cordis sheath was removed and the incision was closed. The animal was then allowed to recover in post-op care.

3. Heart Failure Therapy Initiation Procedures

Once the animal had sustained symptomatic heart failure (lowered EF) for approximately 60 days, a treatment (HVAD, ECM, or HVAD+ECM) could be initiated. The same general surgical procedures were used for animal

preparation, anesthesia induction, and patient monitoring. In the operating room, the animal was positioned in a right lateral recumbency position. A thoracotomy was performed. Succinylcholine (neuromuscular blocking agent) and heparin were administered prior to chest incision. A 14cm incision was made, and the 5th rib was removed. The heart was exposed and pericardium was opened to allow for each heart failure treatment procedure.

After the treatment was complete, the pericardium was closed. A chest tube was inserted into the pericardial space and secured. Bupivacaine and epinephrine was injected into the intercostal margins to reduce post-operative pain. The chest incision was closed and the animal was moved to post-op recovery for monitoring and pharmaceutical treatment.

a. HVAD Implant. Mechanical circulatory support was achieved through implantation of the clinically-used HVAD (HeartWare, Miami Lakes, FL). The HVAD device was prepared by assembling the graft outlet and bend relief rings. The pump was then filled with saline and its motor was initially run for a minimum of 5 minutes to ensure proper function. The HVAD driveline was tunneled under the skin to the dorsal aspect next to the spine. Heparin (10,000 units) was administered to maintain the desired ACT (>480 seconds), which prevented coagulation during device implantation. The HVAD graft was cut to proper length. The aorta was clamped and the graft was anastomosed to the aorta.

The apex of the heart was elevated and a sewing ring was sutured, circumferentially, to the apex. Using a scalpel, the tip of the apex was removed and an incision was cut into it for insertion of the coring device. The coring

device was used to create a circular hole within the sewing ring at the apex of the heart. The inlet of HVAD device was then inserted through the sewing ring and secured. The HVAD was activated and the motor speed was initially adjusted to achieve maximum heart unloading. That involved a complete unloading of LV pressure to allow the cardiac muscle to “rest” and the dilated LV volume to return to more normal values. Complete unloading was assessed by the following parameters: sustained closure of aortic valve, absence of mitral regurgitation, and septum return to midline.

Once the device implantation was complete, the incision was closed and the HVAD driveline was secured to the skin. In post-op recovery, the pump speed was maintained and adjusted throughout the 60-day treatment. Around day 40, the HVAD speed was reduced by 30% in order to initiate a weaning process. By day 50, the pump speed was reduced by 75% in order to restore optimal cardiac function.

b. ECM Injection. The ECM therapy was achieved by injection of a proprietary ECM emulsion (CorMatrix® Cardiovascular, Inc, Roswell, GA) into the infarcted regions of the LV. Prior to ECM injection, the aorta was temporarily clamped as if preparing for graft anastomosis. This mimics the HVAD implantation protocol as a control. The infarcted areas of the left ventricle were identified and a 3x3 matrix was drawn covering a selected region. An echocardiogram (ECHO) at each matrix square (approximately 1 in^2) was taken using a small surgical ECHO probe on the surface of the heart. LV wall thickness was measured at each square to determine the depth safety limit for

the ECM injections to prevent ECM from entering the LV chamber and potentially acting as emboli. The ECM emulsion was then injected into the LV muscle (1mL/square) using a pneumatically driven injection device (CorMatrix® Cardiovascular, Inc, Roswell, GA) at each matrix square as shown in Figure 13.

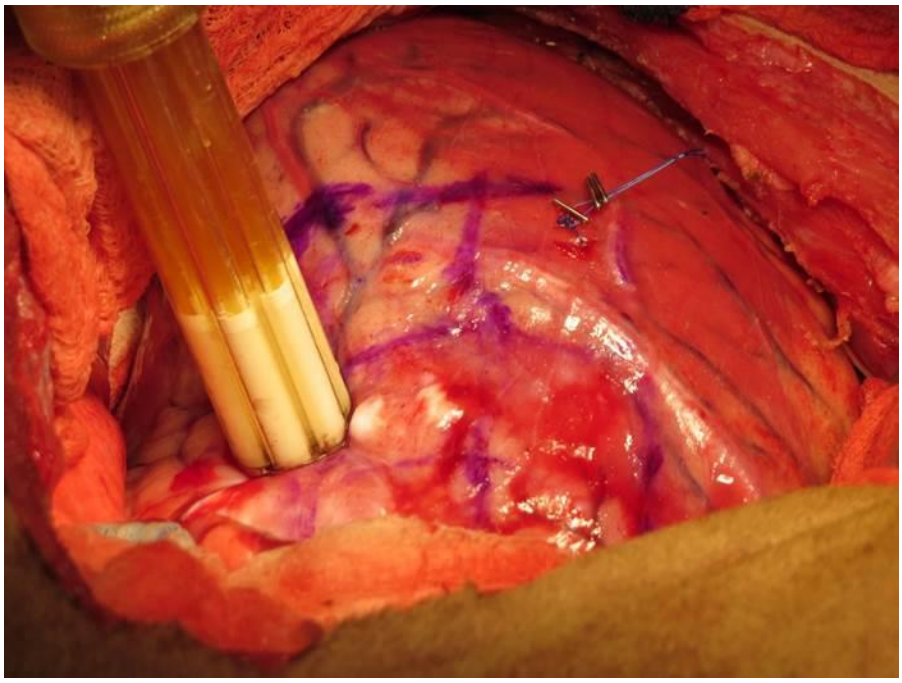

Figure 13: Photograph of CorMatrix® ECM injection into an infarcted region of the left ventricle

An echocardiogram was then retaken at each square to visualize the injected ECM collagen spots. Additional injections were performed if the ECM spot density was minimal. Suture was used to outline the corners of the injected area for reference during necropsy. Once the procedure was complete, the incision was closed and the animal was moved to post-op recovery.

c. HVAD+ECM Combination Procedure. The combination therapy procedure follows both the previous HVAD implant and ECM injection procedures. The ECM injections were performed first. Once the ECM injections

were complete and animal's conditions stabilized, the HVAD implant procedure took place, starting with HVAD preparation and graft anastomosis. Once the HVAD was implanted, the chest incision was closed and the animal was moved to post-op recovery.

4. Pharmacological Treatment Techniques

During each of the surgical procedures, close attention was paid to cardiac function and animal stability. The following drugs and fluids were used to provide intraoperative support:

1. Antiarrhythmics:
    a. Amiodarone (1.8mg/ml) 17-25ml/hr
    b. Lidocaine (100mg boluses)
2. Inotrope infusions
    a. Phenylepinephrine (100mg/ml) 1-6ml/hr
    b. Dobutamine (0.5mg/ml) 1-6ml/hr
    c. Epinephrine (25mg/ml) 1-2ml/hr
1. Lactated Ringers Solution
3. Vitamin B Complex Solution
4. Magnesium Sulfate infusion (2g)
5. KCl (2mEq/ml) 5ml/hr

During post-operative care, the animal was monitored 24 hours a day by trained attendants. Animal care was overseen by a Dr. of Veterinary Medicine. Post-operative and treatment care involved monitoring for arrhythmias and managing blood pressure. Care attendants also treated the animals for several

conditions associated with HF and cardiothoracic surgery. The following fluids and pharmacological agents were used in post-operative care to provide support to the animal.

1. Antiarrhythmics
    a. Amiodarone (1.8mg/ml) 17-25ml/hr
    b. Lidocane (1 amp boluses)
2. Inotrope infusions
    a. Phenylepinephrine (100mg/ml) 1-6ml/hr
    b. Dobutamine (0.5mg/ml) 1-6ml/hr
3. Vasodilator (Nitropress) – maintain a mean arterial pressure of 60-80 mmHg
4. Beta blocker (Atenolol) – maintain a resting heart rate below 100 bpm.
5. Diuretic (Furosemide) – prevent pulmonary edema and prevent right heart failure.
6. Lactate Ringer Solution – maintain fluid volume and IV drip medication carrier.
7. Antibiotics
    a. Cefazolin
    b. BioMycin
8. Probios® – prevent rumen dysbiosis

Depending on the severity of the animal's condition, the arterial and venous lines were maintained for 7–10 days, which allowed for constant arterial and venous pressure monitoring. The lines were removed once the animal no

longer required IV drips and medication. The venous access port (VAP) was maintained throughout the duration of the study. Arterial blood gases and electrolytes were continuously monitored throughout the study to screen for abnormalities and to guide pharmaceutical care.

5. Necropsy/Euthanasia

After the 60-day course of treatment was complete, a terminal study was performed. The procedure was consistent with recommended practices of the 2007 American Veterinary Medical Association Guidelines on Euthanasia and involved minimal distress to the animal. The animal was prepared for surgery in the usual method. It was placed in a lateral recumbancy position. 30,000 units of heparin were given to maintain a high ACT (>480 seconds) to prevent coagulation during the procedure. A cordis sheath was placed into the carotid artery. End study measurements were taken including: Echocardiogram (ECHO), LV Gram, Hemodynamics, and Fluorescent Microsphere circulation studies. An in-depth description of each technique is discussed in Part C: Analytical Techniques.

Upon completion of the end-study procedure, the calf was euthanized with an IV bolus of Beuthanasia. The animal was then exsanguinated. The veterinarian completed a gross examination. Complete photographic documentation of the procedure was performed, and tissue samples from all major end-organs and multiple regions of the heart were collected for RBF, BrdU assay, and histopathology. If present, the HVAD was retrieved.

C. Analytical Techniques

1. Clinical Evaluation

Animal weight was measured on a weekly schedule and at important time points using a bovine-specific scale (SPX scale systems, GSE model 350, Novi, MI). From this information, the rate of growth can be established in normal, heart failure, and treatment conditions. The care attended noted the animal's body condition score, or BCS, on a daily basis.

2. Blood Specimens

Complete Blood Count was analyzed weekly at each important time point using HEMAVET 950 (Drew-Scientific, Oxford, CT). Troponin was tested at baseline and 72 hours post embolization. Plasma free hemoglobin was analyzed at heart failure condition baseline and weekly after initiation of treatment. Both blood tests were analyzed by a CLEA-certified laboratory (Jewish Hospital, Louisville, KY). All results were recorded in the subject logs.

3. Echocardiography

Echocardiograms (ECHO) were taken on a weekly basis throughout the study and during each surgical procedure and time point using a Phillips iE-33 machine. Transthoracic ECHOs (TTE) were taken using a S8-3 ultrasound probe, and transesophageal ECHOs (TEE) were taken using the X7-2t probe. Weekly ECHOs, performed with the animal in the awake state, were always taken using the TTE probe. Once an animal was anesthetized, TEE ECHOs were taken to supplement the transthoracic recordings. The TEE probe was

inserted into the animal's stomach via the esophagus, and the probe tip was angled to obtain an apical four-chamber view of the heart. Using either probe, a beat-by-beat 2-D recording was collected. Using a modified Simpson's summation technique, LV length, area, and volume at both end-systole and end-diastole were calculated. Using the TEE probe, a 3-D ECHO recording could be collected and 3-D left ventricle volumes could be calculated using a modeling software add-in (QLAB). The LV is modeled as a volumetric shape once the reviewer identifies key land marks, including the inferior wall, lateral wall, septum, and apex. Both 2-D and 3-D data was collected during surgical procedures. Figure 14 shows an example 2-D and 3-D TEE ECHO of the left ventricle with end diastolic LV volume analysis.

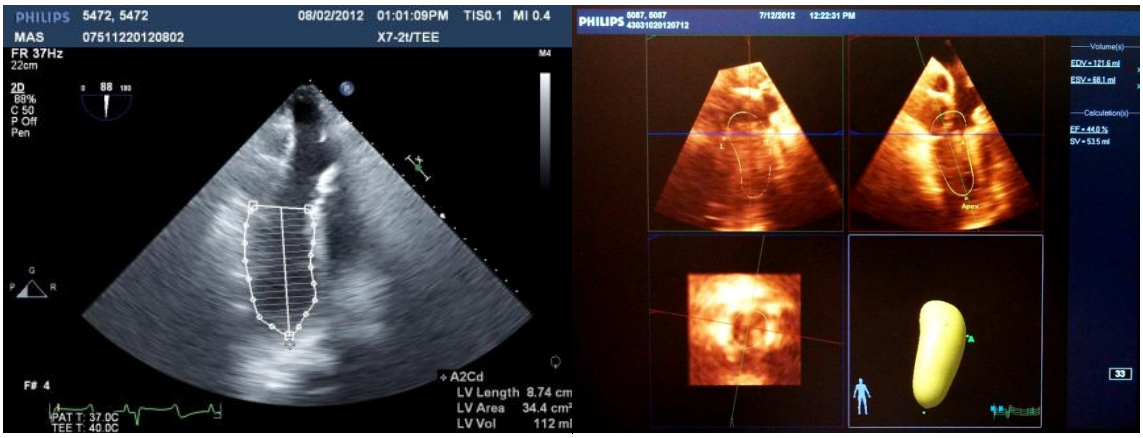

Figure 14: A comparison of the left ventricular volume analysis techniques (left) 2D TEE ECHO (right) 3D TEE ECHO

Using the end-systole and end-diastole LV volumes, cardiac ejection fraction could be calculated. The recordings could also be reviewed for instances of aortic insufficiency (AI) and mitral regurgitation (MR). When these abnormalities were observed, they was recorded in the animal's echo log along with the ejection fraction.

During the heart failure induction surgery, ECHOs were taken at baseline and various time points to closely monitor the progress of embolization and cardiac function impairment. Typically, baseline ECHOs were taken with the animal awake and again after anesthesia. A third baseline ECHO was measured after inotropes were initiated to support the animal during the surgical procedure. This third baseline condition (anesthetized and on inotropic drips) served as the reference for cardiac function impairment during the embolization. The target for successful heart failure induction was a > 40% reduction of EF with respect to the last baseline EF.

ECHO measurements were recorded after the injection of 10 mL of microsphere solution to review the embolization progress. Ejection fraction was then titrated down to the desired point (>40% reduction) by injecting 1–3 mL at a time, with an ECHO measurement after each dose. Once the heart failure induction criteria was achieved, a final ECHO was measured 10–15 minutes after the final microsphere dose to verify that EF reduction was sustained. The final ECHOs were taken using both TTE and TEE probes.

During both the treatment procedure and necropsy, when the animal was anesthetized and placed on cardiac supporting drugs, similar pre-surgical baselines and end-points were taken using the TTE and TEE probes.

4. Fluoroscopy and LV Gram

Through the use of fluoroscopy (GE Innova 3100), LV Grams were taken at key time points during the study: pre-embolization baseline, post-embolization, and end-study. Due to concerns for animal well-being, fluoroscopy was not

performed during the treatment procedure for the chronic heart failure and post-treatment condition.

During embolization and end-study surgical procedures, a pig-tail catheter was advanced through the cordis sheath and positioned at the base of the left ventricle. The catheter was connected to an angiographic injector (Mark V Plus, Medrad, Warrendale, PA). Using radio-opaque dye (Conray 43, Mallinckrodt, St. Louis MO) and a set injection speed of 50mL/sec, the left ventricular flow field and coronary circulation were visualized and recorded as the catheter was slowly withdrawn from the left ventricle chamber into the aortic space.

5. Hemodynamics

Hemodynamic measurements were taken during embolization and end-study procedures. The following signals were recorded:

1. Arterial Pressure (ART) - mmHg
2. Central Venous Pressure (CVP) -mmHg
3. Electrocardiogram (ECG) - mV
4. Aortic Pressure (AoP) - mmHg
5. Left Ventricle Pressure (LVP) - mmHg
6. Left Ventricle Volume (LVVol) - mL

ART and CVP were acquired using the monitoring system from the jugular vein and carotid artery catheters. The ECG signal was also acquired from the patient monitoring system using the ECG clips. AoP, LVP, and LVVol were acquired through the use of a 6-French dual-tip pressure-volume conductance catheter (Millar, Houston TX). The conductance catheter was first opened to air

and zeroed. The catheter was advanced through the cordis sheath and, using fluoroscopic guidance, was placed in optimum position at the base of the left ventricle. The data was then acquired at a sampling frequency of 400 Hz for a set duration of 30 seconds at a time. After each surgical procedure, the conductance catheter was calibrated for post-surgical data analysis. The conductance catheter was placed in a hydrostatic pressure chamber, introduced to multiple pressures, and the catheter's response (AoP and LVP) was collected.

Figure 15: Example hemodynamic waveform collection (top to bottom) AoP, CVP, LVVol, ART, ECG, and LVP

During embolization, hemodynamic measurements were taken at the following time points: pre-embolization baseline, 2-min after the pre-conditioning embolization dose, 20 minutes after the pre-conditioning embolization dose, and post-embolization. The conductance catheter was used at only the pre- and post-embolization time points. During the end-study procedure, hemodynamics were measured to assess the three HF treatments. For the ECM-only animals, a final 60-day hemodynamic measurement was taken. If an HVAD was present, hemodynamics were taken for the following conditions: VAD off, 1800 RPM

(neutral flow), 2200 RPM, 2600RPM, 3200RPM, 3300RPM, 3600 RPM (maximum unloading), chronic support RPM with no inotropic drips, and chronic support with inotropic drips.

6. Fluorescent Microsphere

Blood flow and organ perfusion were measured using 15 μm fluorescent-labeled polystyrene microspheres (5.25 million NuFlow Microspheres, Interactive Medical Technology, Irvine, CA). The fluorescent microspheres were administered during the embolization and the end-study procedure. During heart failure induction, a pre- and post-embolization dose of microspheres were given. During the end-study procedure with ECM-only calves, a final dose was given. During HVAD only and HVAD+ECM end-study procedures, two doses were given with chronic support and VAD failure settings. Each test condition corresponded to a unique fluorescent color within the animal.

The fluorescent microspheres were administered to the LV via cardiac catheter. As the microspheres were injected, a reference arterial blood sample was withdrawn at a rate of 15mL/min for 100 seconds using a calibrated syringe pump (Harvard Apparatus, Holliston, MA). The 100-second withdrawal was initiated, followed by a 10-second count. At 10 seconds, the fluorescent microspheres were injected as a bolus, followed by a 5 mL saline flush. At 100 seconds, the withdrawal was terminated.

During the animal necropsy a ~5 gram sample of each tissue was collected and stored at 4°C.

1. *Heart*: aorta (distal to graft anastomosis), pulmonary artery, LV (2 core samples), right ventricle (RV) (1 core sample), and septum (1 core sample)
2. *Liver*: left lobe
3. *Spleen*: right pole
4. *Lung*: right caudal
5. *Brain*: brain stem, frontal lobe, and cerebellum
6. *Kidney*: left
7. *Small Intestines*
8. *Skin*: subcutaneous layer
9. *Skeletal Muscle*: Left hind thigh

After animal necropsy, each tissue sample was processed. The samples were cut down to slightly less than 3g. One of the LV core samples was further dissected into three layers: the outermost layer closest to the pericardium (M1), the middle layer (M2), and the innermost layer closest to the LV chamber (M3). The fluorescent microspheres for the reference blood samples and all tissue samples were quantified using flow cytometry (IMT/Stason Laboratories, Irvine, CA). Regional blood flow (mL/min/mg tissue weight) was calculated for each condition (microsphere color) per tissue sample, based on the ratio of spheres in tissue, spheres in blood reference, known blood withdraw rate, and tissue sample mass.

7. BrdU Administration

Bromodeoxyuridine (BrdU, Sigma-Aldrich®, St. Louis, MO) was administered intravenously at a dosage of 5 mg/kg of normal weight at a concentration of 20mg BrdU/ml. BrdU was given every other day, starting on treatment post-op day 15 and continuing until day 60. At necropsy, tissue samples were taken from the RV, anterior left ventricle (LV ant), and lateral left ventricle (LV lat). Samples were fixed in formalin, cryosectioned, and stained for nuclei, sarcomeric actin (SA) and BrdU. BrdU+ cells and BrdU+/SA+ cells were counted in each tissue sample.

8. Histopathology

At necropsy, the following tissue specimens (3–6mm thickness) were collected and fixed in 10% formalin solution.

1. *Heart:* LV apex, aortic valve, pulmonary valve, aortic annulus, right atrium, left atrium, LV free wall, RV free wall, IV septum, papillary muscles, and pulmonary artery
2. *Liver*: left and right lobe
3. *Spleen*: left and right lobe
4. *Lung*: left and right cranial, left and right caudal,
5. *Brain*: left and right cerebrum, left and right thalamus, cerebellum, brain stem,
6. *Kidney*: left and right
7. *Adrenal Gland*: left and right
8. *GI*: abomasum, jejunum, colon

Tissue sample slides were prepared using hematoxylin and eosin (HE) staining (Mass Histology Service, Worcester, MA) and the percentage of fibrotic tissue was determined for each tissue. The slides were examined by a board-certified veterinary pathologist, and the major findings for each subject were compiled in a final report.

D. Analysis Methods

Using the previously reported results for the 60-day chronic heart failure group with aggressive medical management (n=10) as a control [1], the results for each treatment group are presented below. An analysis of variance (ANOVA) was conducted to compare the different measurement indices between each treatment group to determine statistical significance ($p \leq 0.05$). All data presented as mean±standard deviation.

IV. RESULTS

The mortality rate of the embolization procedure for each group was an overall reported value of 10%, which was consistent with the previous coronary embolism heart failure model study[18]. Mortality during embolization was caused by atrial fibrillation. Baseline troponin levels, an indicator of myocardial damage, were within normal range. Following embolization, peak troponin levels for all animals peaked over 100ng/ml, indicating severe myocardial infarction. The average plasma free hemoglobin (PFHb) was around 5-6mg/dL following treatment for all experimental groups. Ideally, plasma contains no PFHb, indicating a level of hemolysis in all of the subjects. One HVAD+ECM animal, number 5088, had a peak PFHb of 30mg/dL on post-op day 40. The other animals had similar levels of PFHb peaking at 20mg/dL.

The only reportable adverse event during post-operative care was an incident involving animal number 5086, an ECM-only treatment subject. On post-op day 8 following ECM therapy, the animal chewed through the arterial line and lost an estimated 50-100mL of blood. The arterial line was replaced and the animal did not appear to be adversely affected. Three animals were treated for

bacterial infections. One HVAD-only animal was treated for infection in quarantine and a recurring infection during HVAD implant. The other HVAD-only animal and one ECM-only animal were treated for infection after treatment.

A. Animal Weight Analysis

The animals had a reported baseline weight gain rate consistent with previous studies. For all groups, the baseline rate was 0.78±0.10 kg/day and the heart failure rate dropped to 0.64±0.11 kg/day. The rates for each treatment group are depicted in Figure 16. The values for the control group include a 0.75±0.3 kg/day baseline. The values for the control (60-day chronic heart failure) were used to compare to the heart failure time point and the 60 day treatment time point.

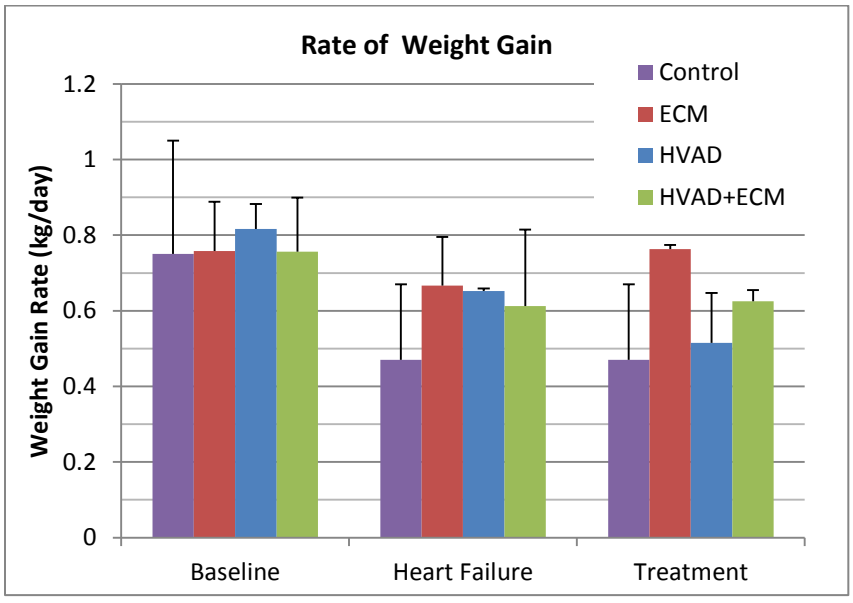

Figure 16: Comparison of baseline, heart failure, and 60 day treatment weight gain per day demonstrating a reduction in weight gain in heart failure for all groups and a recovery of weight gain in the ECM group

There were no reported significant ($p \leq 0.05$) differences between treatment groups, time points, or interactions. For all groups, the value of heart failure weight gain per day drops 17±17%. The treatment groups had varying recovery of weight gain, according to Table 1.

Table 9: Comparison of the values of weight gain per day for the control and treatment groups

(kg/day)	Control	ECM	HVAD	HVAD+ECM
Baseline	0.75±0.3	0.76±0.13	0.82±0.07	0.76±0.14
Heart Failure	0.47±0.2	0.67±0.13	0.65±0.01	0.61±0.2
Treatment	---	0.76±0.01	0.52±0.13	0.63±0.3

The values for heart failure and 60-day treatment were normalized to baseline in Figure 17 to visualize any trends in decreasing or increasing weight gain rates. The ECM-only group had a recovery rate of 102±16% of the baseline, the HVAD-only group had a further reduction of the rate to 62.7±11% of the baseline, and the HVAD+ECM group had a recovery rate of 83.8±12% of the baseline.

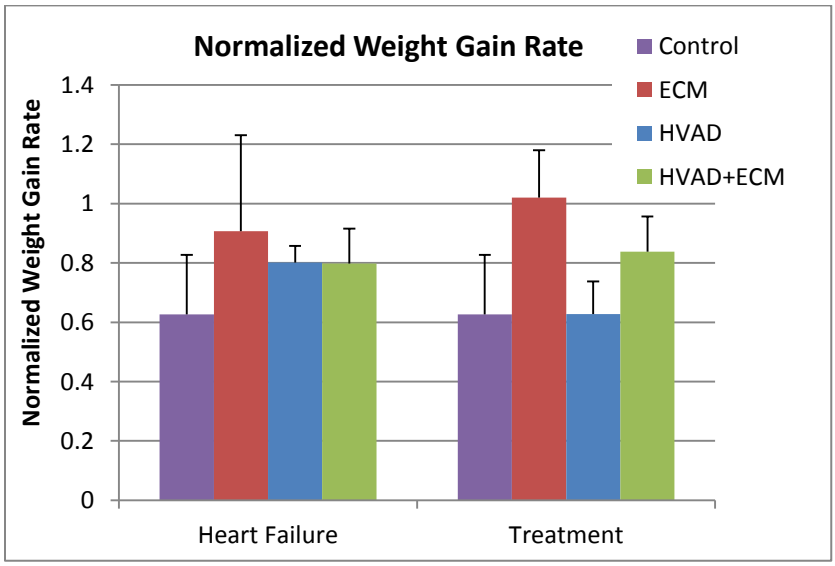

Figure 17: Comparison of heart failure and treatment weight gain per day normalized to baseline weight gain per day

B. Ejection Fraction and Left Ventricular Volume

In order to maintain consistency, the ECHOs used in analysis were taken with the TTE ECHO probe when the animal was in the awake condition with no inotropic agents present. The following values were calculated using only the 2D volume analysis technique shown in Figure 18.

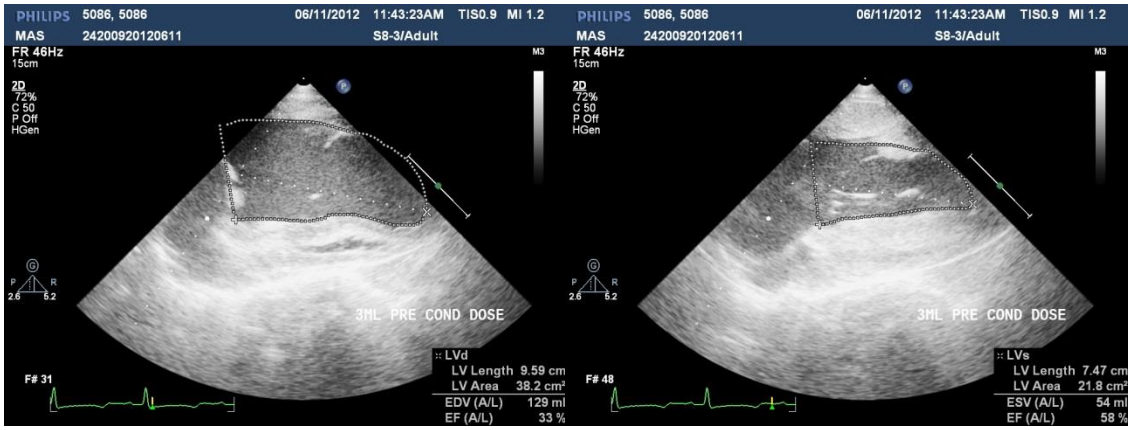

Figure 18: Example 2D TEE ECHO showing (left) end diastolic and (right) end systolic LV volume and ejection fraction analysis (Animal #5086, embolization)

The ejection fraction (EF) is analyzed as an indicator of cardiac function and myocardial contractility. The overall baseline EF was found to be 74.8±6.8%. The overall heart failure EF was found to be 36.4±9.5%. The ejection fractions for each treatment group are listed in Table 2. Blank values for standard deviation indicates that a comparable ECHO (awake/no inotropes) was not performed at the specific time point for an animal, leaving an n=1 for the treatment group timepoint.

Table 10: Comparison of ejection fraction for the control and treatment groups

Treatment	Control	ECM	HVAD	HVAD+ECM
Baseline	72 ± 8	69 ± 2.8	80	81
Heart Failure	31 ± 8	27 ± 0	41.5 ± 7.8	45
Treatment	---	66.5 ± 4.9	69.5 ± 2.1	75 ± 4.2

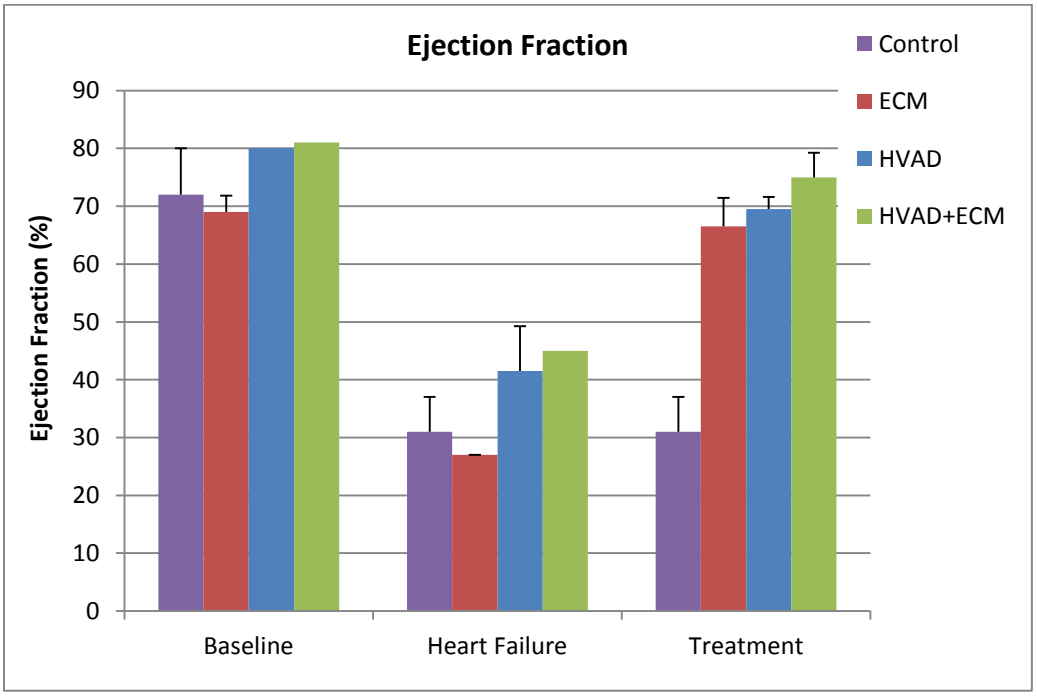

Figure 19: Comparison of baseline, heart failure, and 60 day treatment EF demonstrating a reduction in EF at heart failure for all groups and a recovery of EF for all groups excluding the no treatment control group

Figure 19 compares the ejection fraction at all three time points. All treatment groups demonstrated a 55.3±7.8% decrease in EF. The decrease is comparable to the New York Heart Association (NYHA) class-IV HF patients who have 40% lower EF compared to normal values (65±10%). Table 3 shows the normalized EF values for heart failure and treatment as compared to the baseline. The ECM group saw a 96.6±11.1% restoration of the baseline EF, the HVAD and HVAD+ECM group saw an 89% restoration of the baseline EF.

Table 11: Comparison of the values of normalized EF to the baseline value for the control and treatment groups indicating a significant (p=0.002) decrease for heart failure, and significant increase with recovery with treatment for all study groups.

Normalized EF (%)	Control	ECM	HVAD	HVAD+ECM
Heart Failure	43.1	39.1 ± 1.6	45	55.6
Treatment		96.6 ± 11.1	88.8	88.9

The results of the ANOVA indicated that the time point significantly affected the normalized ejection fraction (p = 0.002) as the 55% decrease in EF with heart failure was significant. However, the interaction of treatment and time point was not significant.

End diastolic (ED) and end systolic (ES) LVVols were recorded under the same conditions as the EF calculations and are analyzed as indicators of LV remodeling and systolic and diastolic function. Figure 20 shows both ED and ES LVVol for the control and treatment groups at each time point.

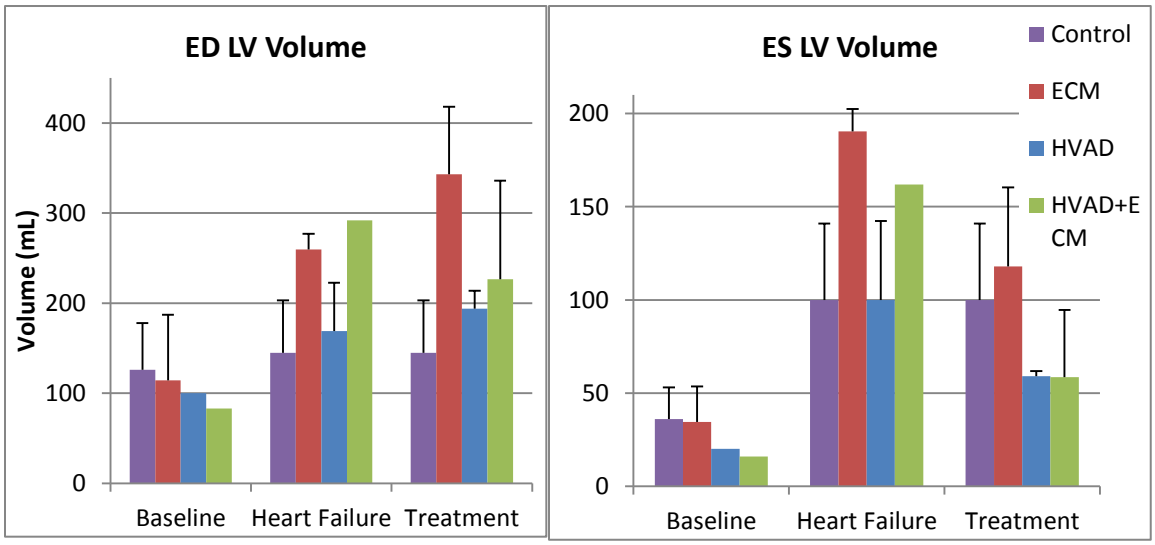

Figure 20: Comparison of baseline, heart failure, and 60 day treatment ED and ES LVVol demonstrating an increase in diastolic volume in all groups for both heart failure and treatment. And an increase in systolic volume at heart failure for all groups and reduction in systolic volume with treatment for all groups excluding the no treatment control group

The groups had an overall baseline ED LVVol of 103±44mL and ES LVVol of 26±14mL. The HF condition volumes increased to 230±64mL and 149±51mL respectively. The values for each treatment group are listed in Table 4.

Table 12: Comparison of baseline, heart failure, and 60 day treatment ED and ES LVVol

	Control		ECM		HVAD		HVAD+ECM	
LVVol (mL)	**ED**	**ES**	**ED**	**ES**	**ED**	**ES**	**ED**	**ES**
Baseline	126 ± 52	36 ± 17	115 ± 73	35 ± 19	100	20	83	16
Heart Failure	145 ± 58	100 ± 41	260 ± 18	191 ± 12	169 ± 54	100 ± 42	292	162
Treatment			343 ± 75	118 ±42	194 ± 20	59 ± 2.8	227 ± 110	59 ± 36

It is thought that rate of overall growth will affect the size of the animal's heart and therefore ventricular volume. Because there was a large range of animal weights among the calves, the ventricular volume was normalized to the weight of the calf at the time point of measurement. These values were then plotted in Figure 21.

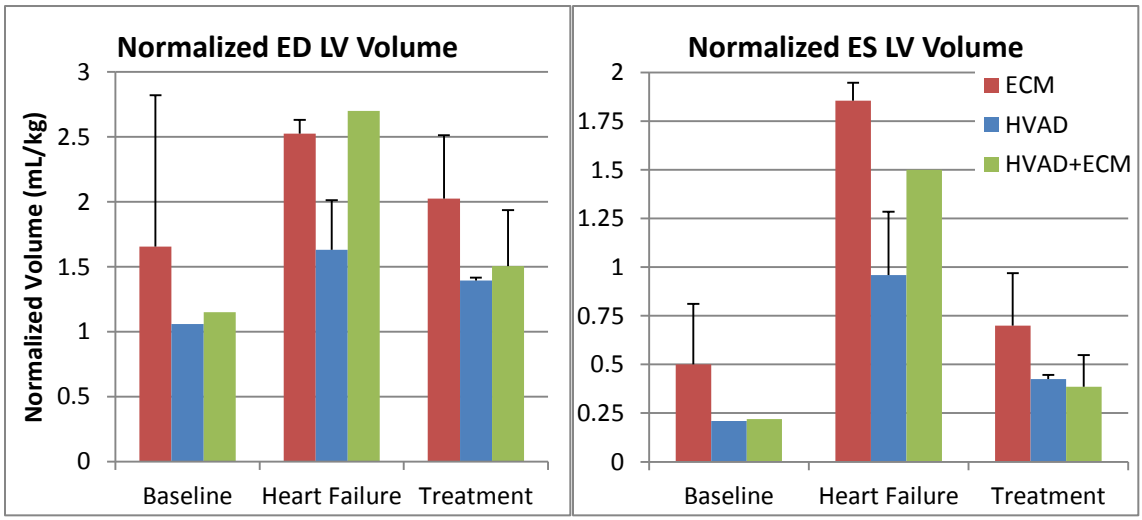

Figure 21: Comparison of baseline, heart failure, and 60 day treatment for normalized ED and ES LVVol demonstrating an increase in diastolic and systolic volume in all groups for heart failure, and a decrease in diastolic and systolic volume with treatment for all groups

The normalized plot shows a correlation consistent with the previous trend. The analysis of variance for LVVol revealed that the time point was significant for both ED ($p = 0.029$) and ES LVVol ($p = 0.003$), which indicates that

the increase in volumes during heart failure and the subsequent decrease in systolic volume was significant. However, there were no significant differences among treatment groups. When the volumes were normalized to calf weight, the time point was not significant for diastolic volume. When normalized, both the treatment ($p = 0.035$) and the time point ($p = 0.001$) were significant for systolic volume, but not the interaction of the two ($p = 0.363$). The normalized values for ED and ES LVVol are listed in Table 5.

Table 13: Comparison of baseline, heart failure, and 60 day treatment normalized ED and ES LVVol demonstrating an increase in systolic volume in all groups for heart failure and a decrease in systolic volume for 60 day treatment

Normalized LVVol (mL/kg)	ECM		HVAD		HVAD+ECM	
	ED	ES	ED	ES	ED	ES
Baseline	1.66 ± 1.17	0.5 ± 0.31	1.06	0.21	1.15	0.22
Heart Failure	2.53 ± 0.11	1.86 ± 0.09	1.63 ± 0.38	0.96 ± 0.33	2.7	1.5
Treatment	2.03 ± 0.49	0.7 ± 0.27	1.4 ±0.02	0.43 ± 0.02	1.51 ± 0.43	0.39 ± 0.16

C. Hemodynamics

The hemodynamic waveforms were first plotted then analyzed. Only LVP and AoP sensors were calibrated, so only their values were used in post-operative analysis. Because hemodynamics were not recorded at the time of implant, the chronic heart failure time point is not included. Post-embolization is used as the reference for heart failure. In order to visualize the electrocardio-changes associated with each time point, sample ECGs were plotted in Figure 22. The waveforms for animals with HVAD implants were taken at neutral HVAD flow settings (1800 RPM).

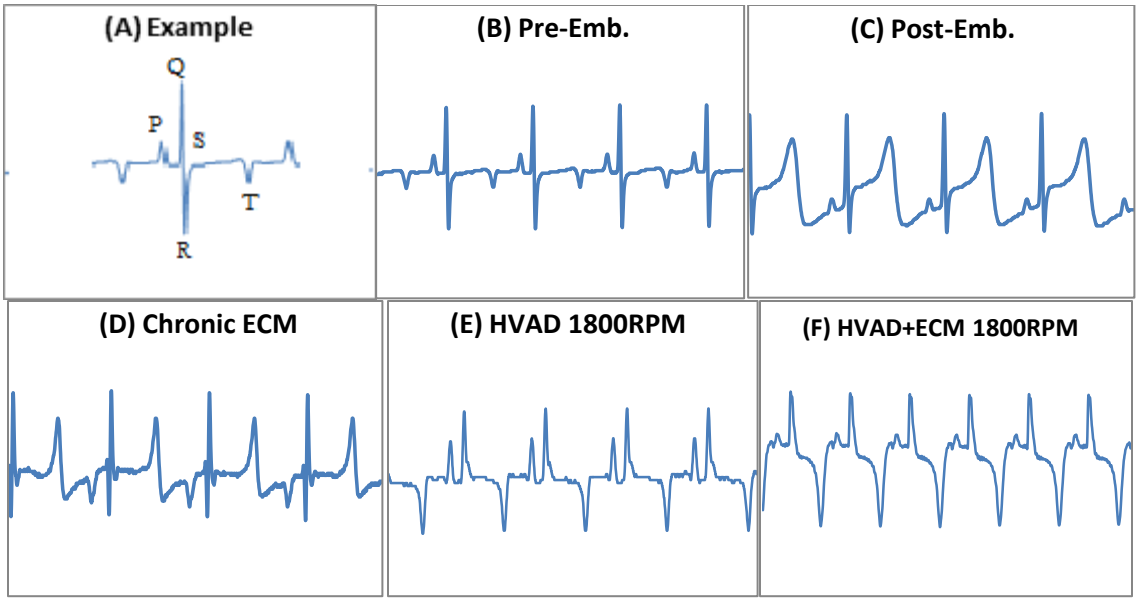

Figure 22: (A) An example waveform with labeled landmarks and a comparison of electrocardiogram waveforms for (B) pre-embolization baseline, (B) post-embolization, and 60 day treatment with (C) ECM, (D) HVAD, and (E) HVAD+ECM

The sample ECG waveforms show general patterns and abnormalities in the electro-cardiac functioning of the heart. Immediately after embolization, the animal shows tombstone patterning, or extreme ST segment elevation, and T-wave inversion. In all the chronic treatment ECGs, the patterns return to more normal shapes, but there is still evidence of dysfunction in repolarization. The repolarization segment (ST) in Part E appears to be completely reversed. However, the patient monitor might have been recording a signal from a different lead.

Next, sample LVP-AoP waveforms were plotted as an indicator of contractile functioning. Sample pressure waveforms for pre- and post-embolization and for chronic treatment are shown in Figure 23. The waveforms show changes in peak pressures with embolization, chronic treatment, and the different support levels of the VAD. There is also a difference in the shape of

diastole and systole for both LVP and AoP. Diastole and systole are less defined than in the baseline. The LV contraction pressures are more gradually sloping than the sharp contraction of the baseline waveform. Using the HEART v2.1 Program (Bill Perreult ©2000), LVP and AoP were analyzed for heart rate, peak pressures, pulse pressure, and peak pressure changes. The results are plotted in Figures 24-27. Table 6, showing the previously reported values for the control study, is included as a comparison to the 60 chronic treatment groups.

Table 14: Hemodynamic parameters for the normal control and heart failure baseline [1]

	Normal Control (n=9)†	Heart Failure (n=10)	p-value
HR (bpm)	78±4	93±7	0.08
$LVP_{end\text{-}diastolic}$ (mmHg)	16±2	18±2	0.40
$LVP_{peak\text{-}systolic}$ (mmHg)	103±3	85±5	<0.01
+dP/dt (mmHg/s)	1,252±136	1,125±157	0.55
-dP/dt (mmHg/s)	-2,528±289	-1,018±78	<0.0001
AoP_{mean} (mmHg)	90±4	66±6	<0.01
$AoP_{systolic}$ (mmHg)	105±3	81±6	<0.01
$AoP_{diastolic}$ (mmHg)	73±4	55±6	<0.05
AoP_{pulse} (mmHg)	32±2	26±3	0.09
CO/Weight (ml/min/kg)	105±5	64±8	<0.001

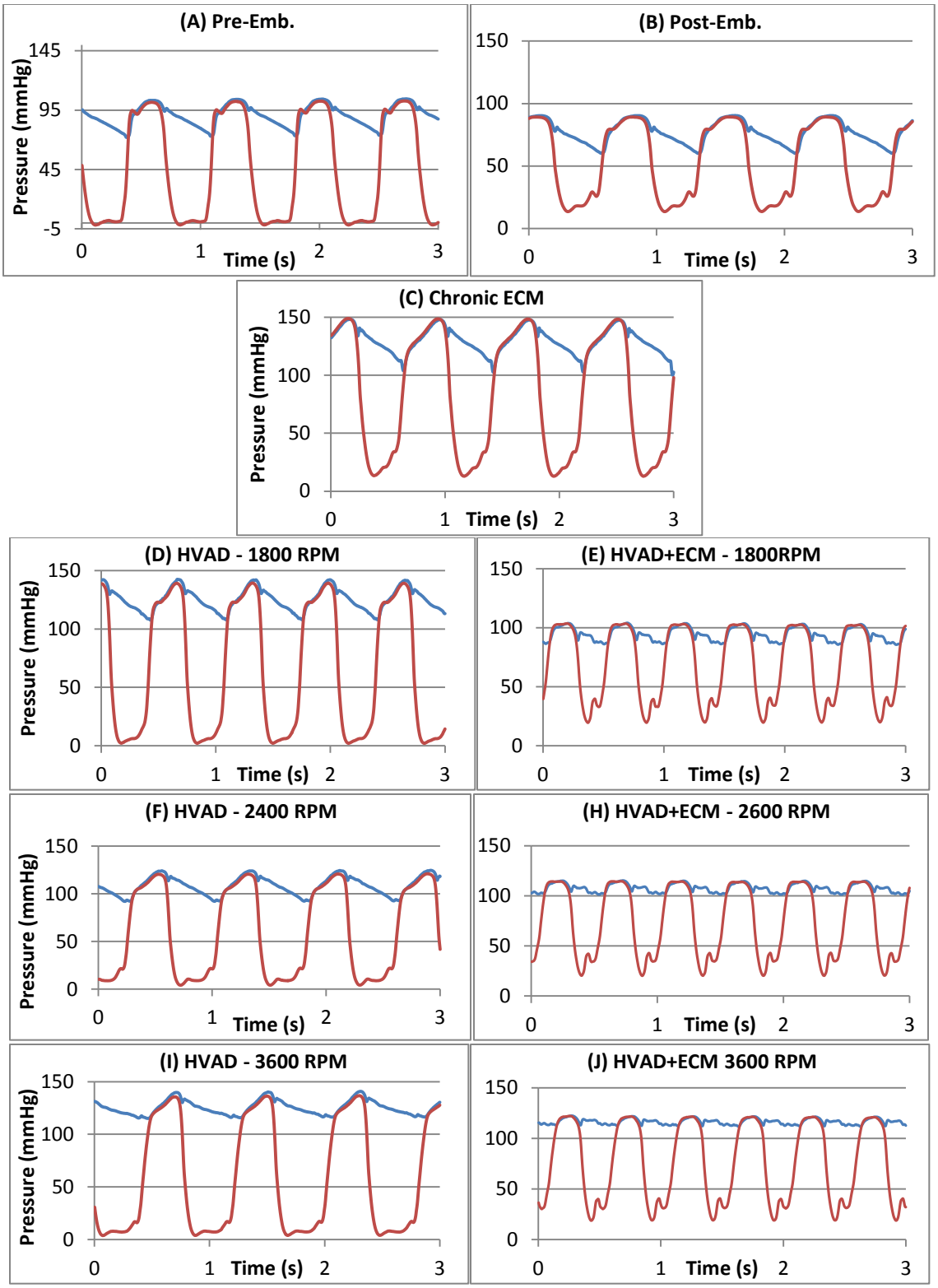

Figure 23: A comparison of LVP (red) and AoP (blue) waveforms for (A) pre-embolization baseline, (B) post-embolization, (C) 60 day chronic ECM treatment, 60 day chronic HVAD treatment at (D) neutral flow – 1800 RPM, (F) partial support – 2400 RPM, (I) maximum support – 3600 RPM, and 60 day chronic HVAD+ECM treatment

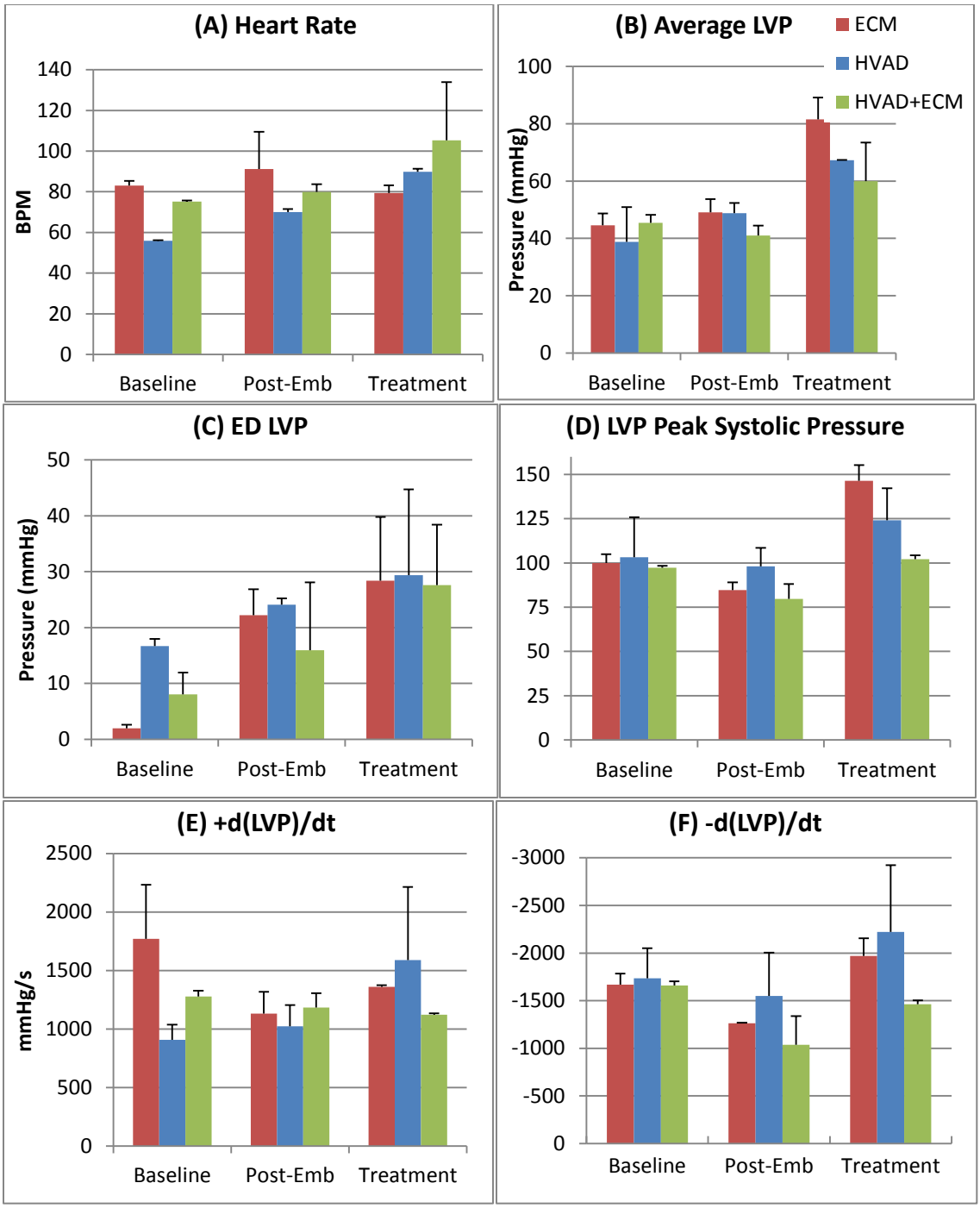

Figure 24: A comparison of LVP qualities for each time point including (A) heart rate, (B) Average LVP, (C) end diastolic LVP, (D) peak systolic LVP, and maximum LVP (E) positive rate of change, and (F) negative rate of change

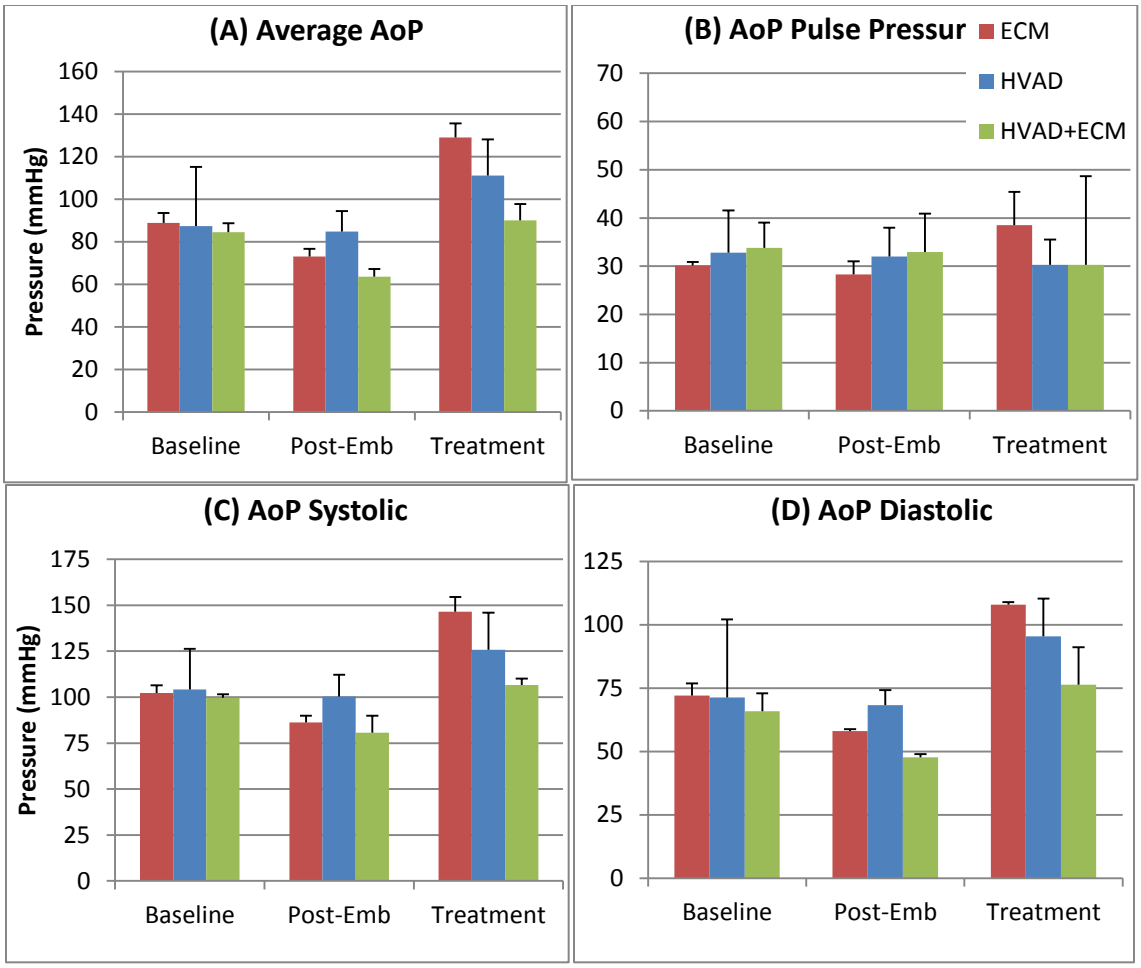

Figure 25: A comparison of AoP qualities for each time point including (A) average pressure, (B) pulse pressure, (C) systolic pressure, and (D) diastolic pressure

In Figure 24 and Figure 25, the values for the treatment time point were calculated using data recorded with the HVAD set to neutral flow (1800 RPM). The results show an increase in ED and ES LVP, (+/-) dP/dt, ED and ES AoP, and AoP pulse pressure for all 60 day treatment groups in comparison to the heart failure control group. The ECM only group had the greatest average and ES LVP and ED and ES AoP and the HVAD only group had the largest (+/-) dP/dt at the treatment time point. In the following figures, Figure 26 and Figure 27, the qualities of LVP and AoP were plotted with respect to HVAD motor speed

to determine the effects that MCS has on hemodynamics. These figures include the HVAD and HVAD+ECM 60 day chronic treatment groups.

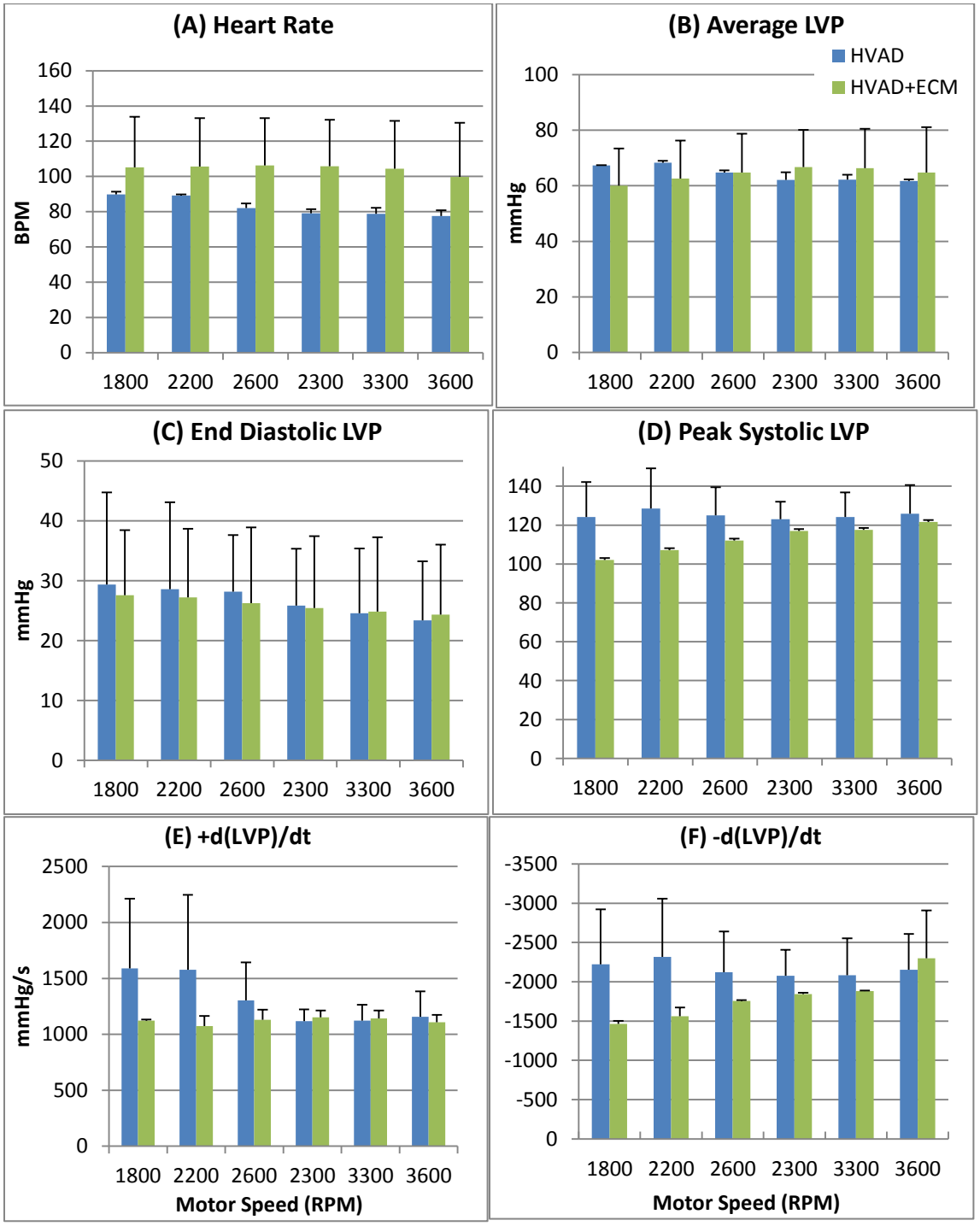

Figure 26: A comparison of LVP qualities for varying motor speed including (A) heart rate, (B) Average LVP, (C) end diastolic LVP, (D) peak systolic LVP, and maximum LVP (E) positive rate of change, and (F) negative rate of change

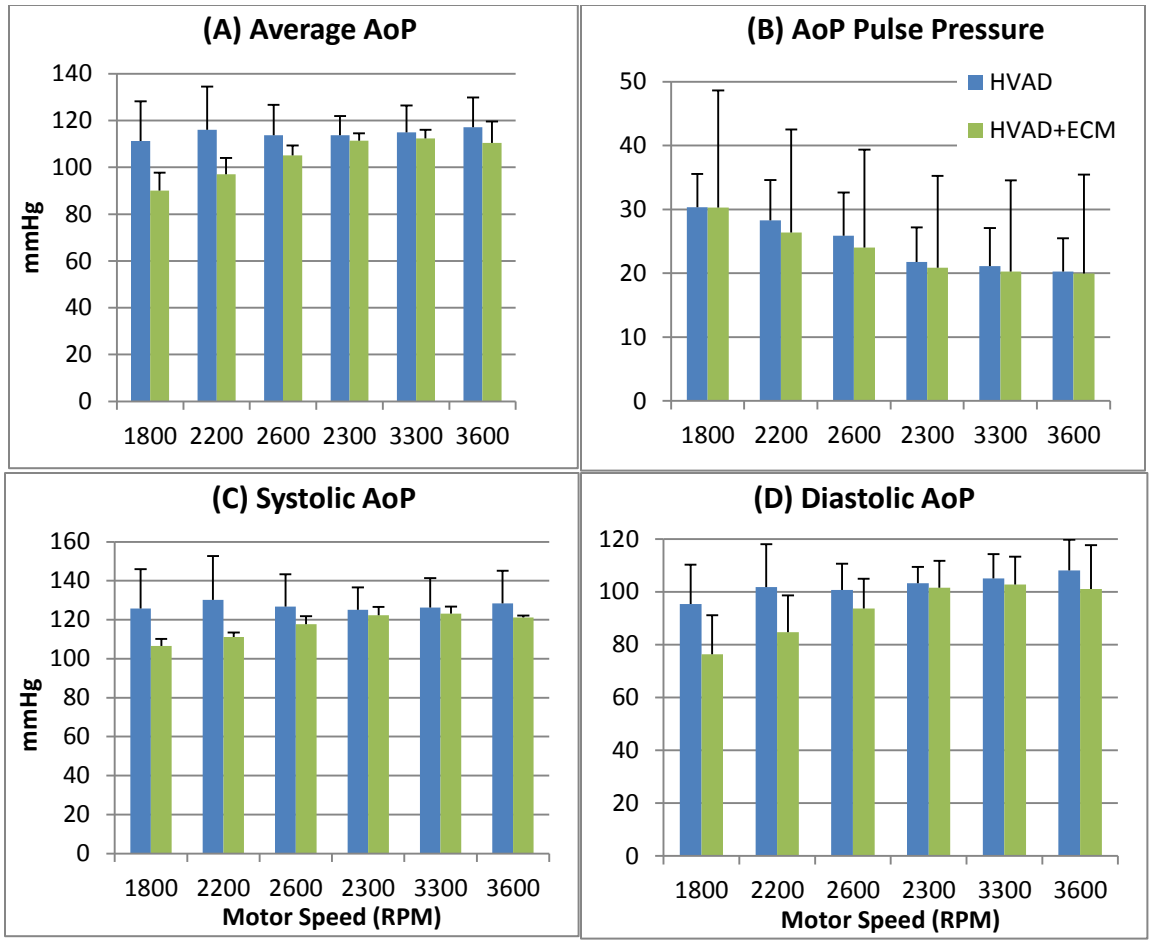

Figure 27: A comparison of LVP qualities for varying motor speed including (A) average pressure, (B) pulse pressure, (C) systolic pressure, and (D) diastolic pressure

The HVAD+ECM group had a larger heart rate than the HVAD only group. Increased VAD support increased peak systolic LVP for the HVAD+ECM treatment group, reduced end diastolic LVP for both groups, and did not affect average LVP for both groups. Increased HVAD support increased AoP and reduced pulse pressure for both groups.

D. Regional Blood Flow

Regional flood flow in each tissue sample was calculated according to the previous equation. Because of low yield, possibility the result of a bad microsphere lot or photo bleaching, one data set was omitted for HVAD only at post-embolization. Data for each time point are plotted in Figure 28 and 29. The error bars may be truncated in order for visualization of the low perfusion tissue types. Figure 30, is representative of the 60 day heart failure control group.

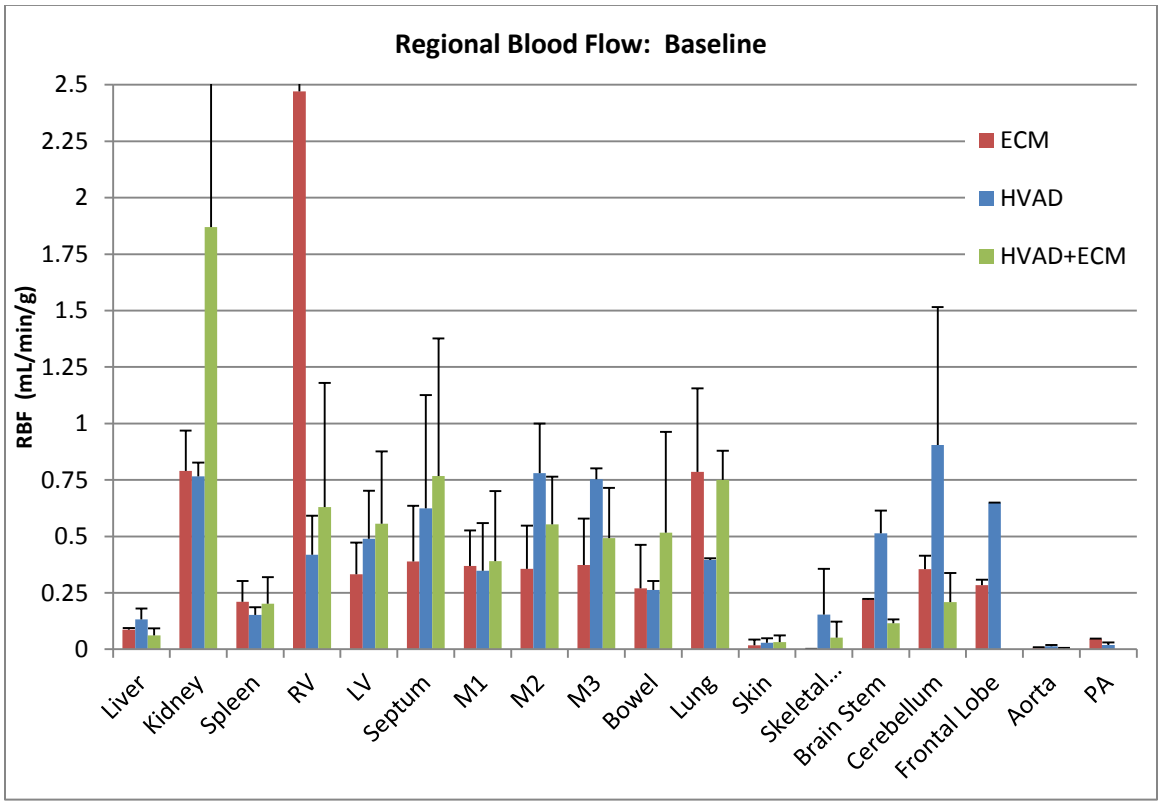

Figure 28: A comparison of regional blood flow in each tissue type for ECM, HVAD, and HVAD+ECM experimental treatment groups at baseline (pre-embolization) conditions

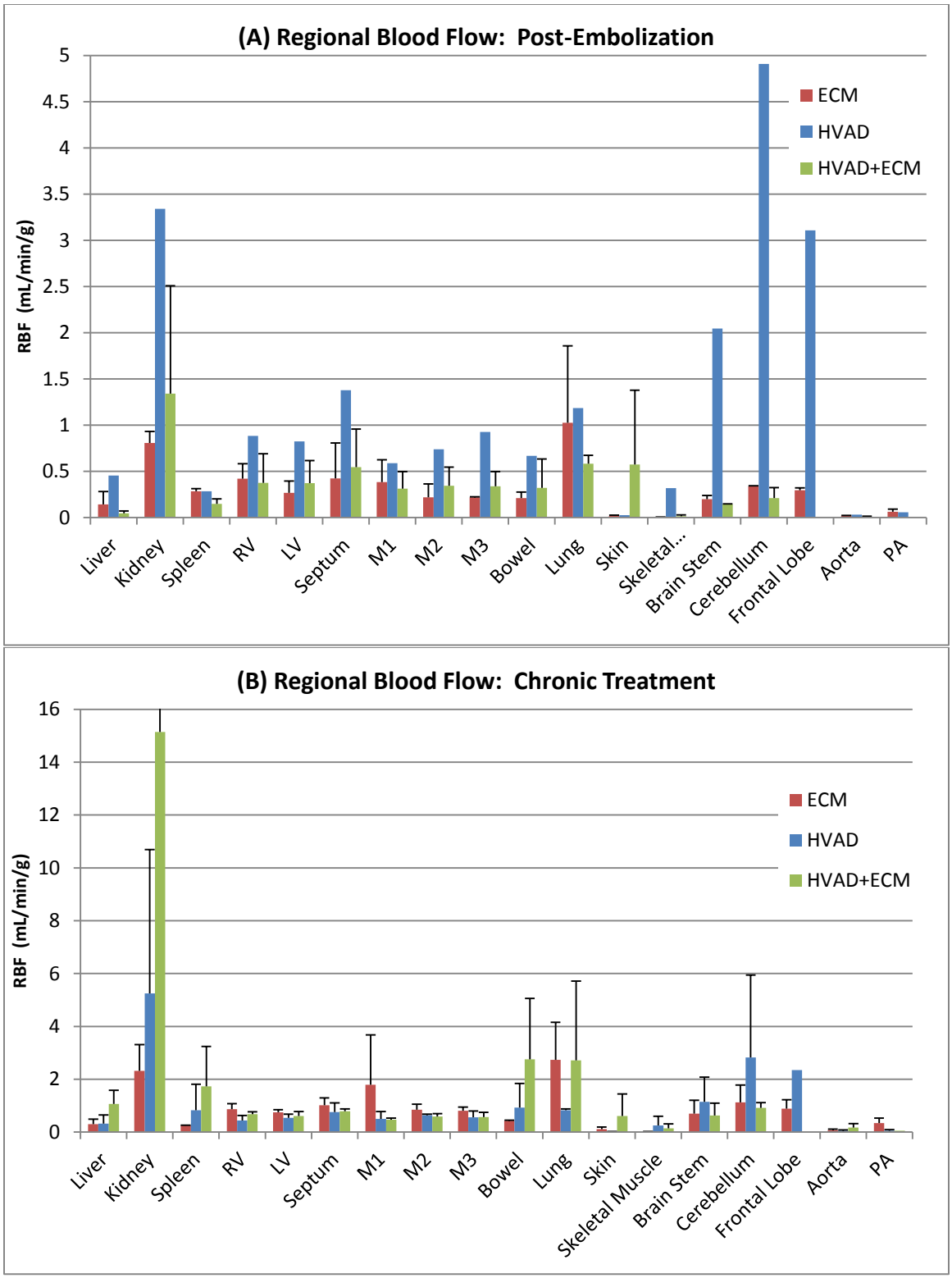

Figure 29: A comparison of regional blood flow in each tissue type for ECM, HVAD, and HVAD+ECM experimental treatment groups at (A) post-embolization (HVAD: n=1) and (B) 60 day chronic treatment

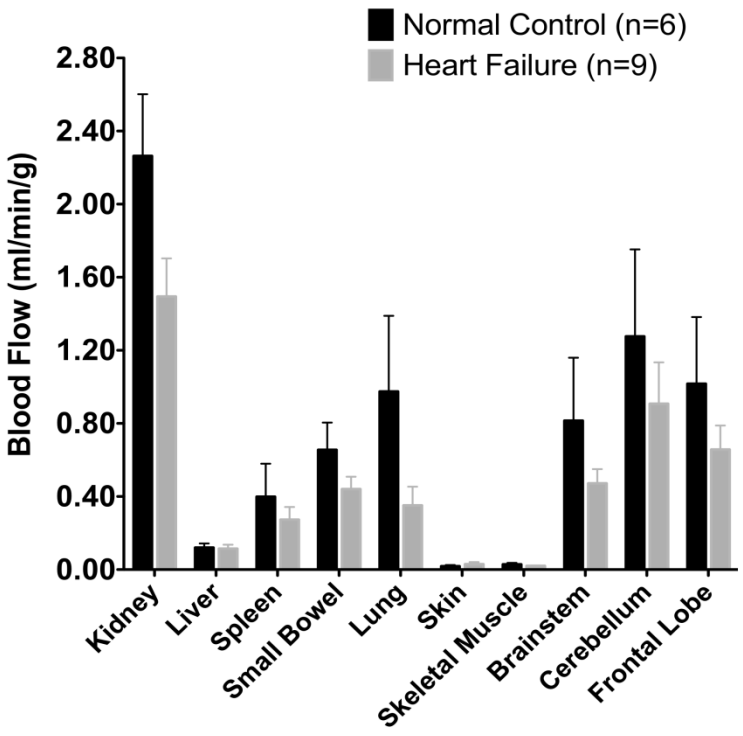

Figure 30: A comparison of regional blood flow in normal conditions and in 60 day chronic heart failure conditions [18]

At the 60-day treatment time point, it was observed that HVAD+ECM produced the greatest absolute regional blood flows than the single therapies. In comparison to the control heart failure group, the 60 day treatment groups demonstrated much greater organ perfusion. Next, in Figure 31, regional blood flow was compared at partial support and VAD failure conditions at the 60 day chronic treatment time point. It is shown that partial support HVAD+ECM had the greatest end-organ perfusion in the liver, kidney, bowel, lung, and skin, While VAD failure HVAD only had the greatest organ perfusion in the myocardial tissues and brain. In Figure 32, the 60 day chronic treatment time point was normalized to the pre-embolization baseline.

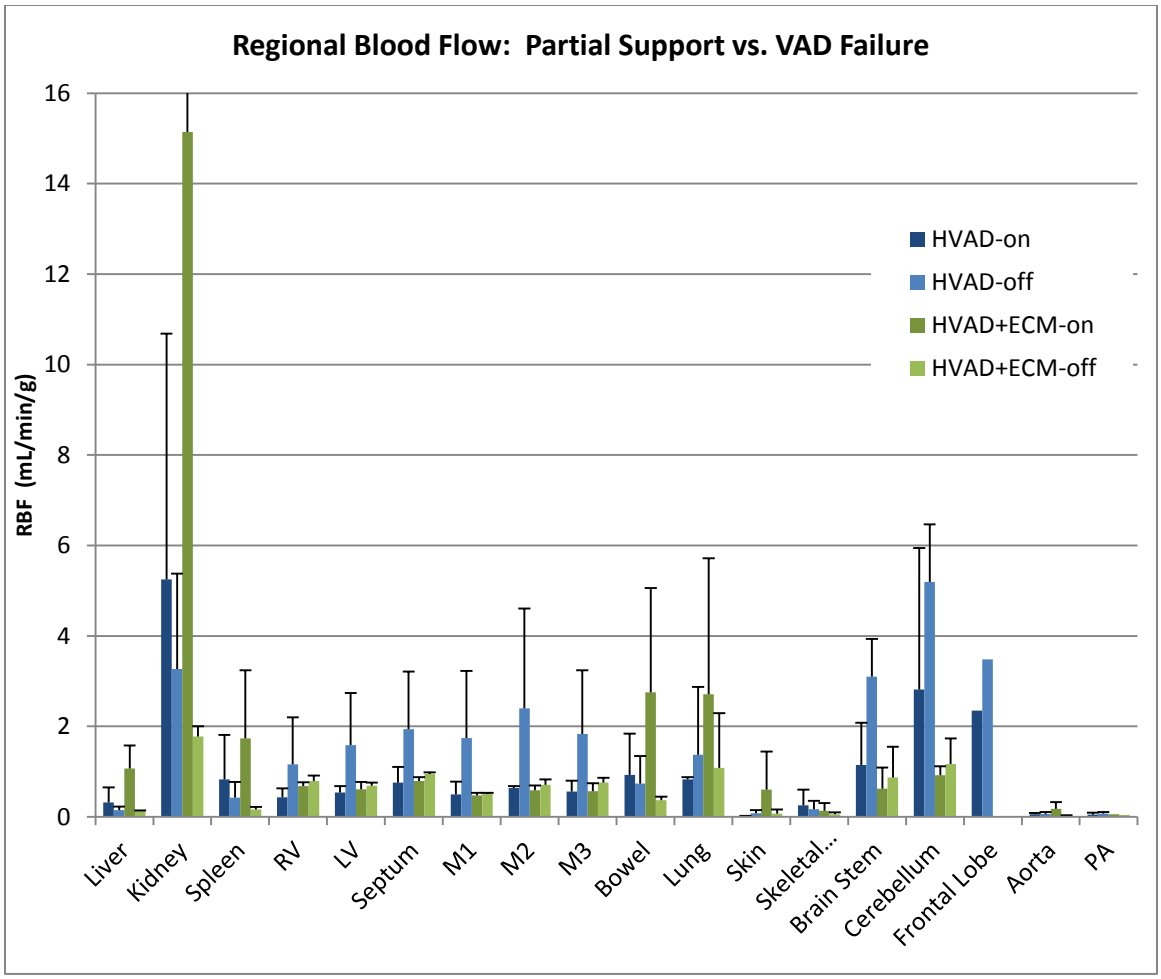

Figure 31: A comparison of regional blood flow in each tissue type for HVAD and HVAD+ECM experimental treatment groups at partial support settings and device failure at 60 day chronic treatment

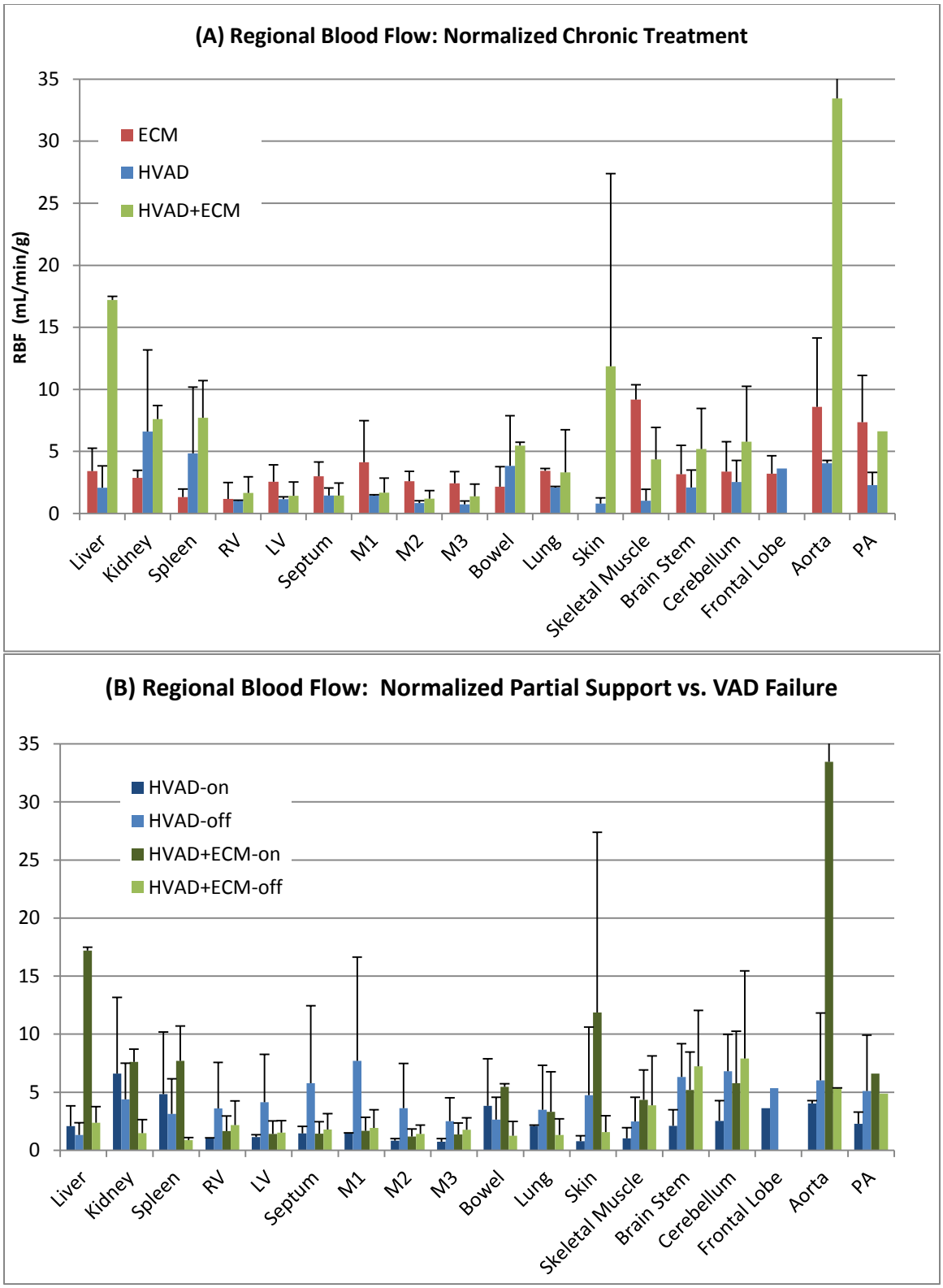

Figure 32: A comparison of regional blood flow, normalized to pre-embolization values, in each tissue type for (A) 60 day chronic treatment groups and (B) HVAD and HVAD+ECM treatment groups at partial support settings and device failure

When normalized, the trend indicated that the HVAD+ECM treatment group produced greater end-organ perfusion in the liver, kidney, spleen, skin, brain stem, cerebellum and aorta. The ECM only group had greater perfusion in the myocardial tissue (ventricular septum, M1, M2, M3, and overall LV) and skeletal muscle. HVAD-only produced the lowest relative regional blood flows.

E. BrdU - Cell Proliferation

Each myocardial specimen was stained for BrdU, cellular nuclei, and sarcomeric actin (SA), an indicator of mature myocytes. Total BrdU+ and BrdU+ cells were counted in LV and RV tissue samples. Figure 33 is an example of a resulting fluorescent image. The resulting cellular counts are plotted in Figure 34.

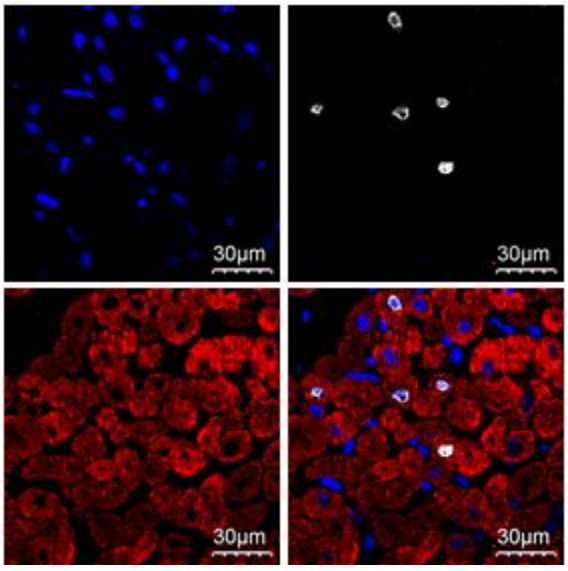

Figure 33: Fluorescently labeled myocardium (top left) nuclei, (top right) BrdU, (bottom left) sarcomeric actin, and (bottom right) overlay

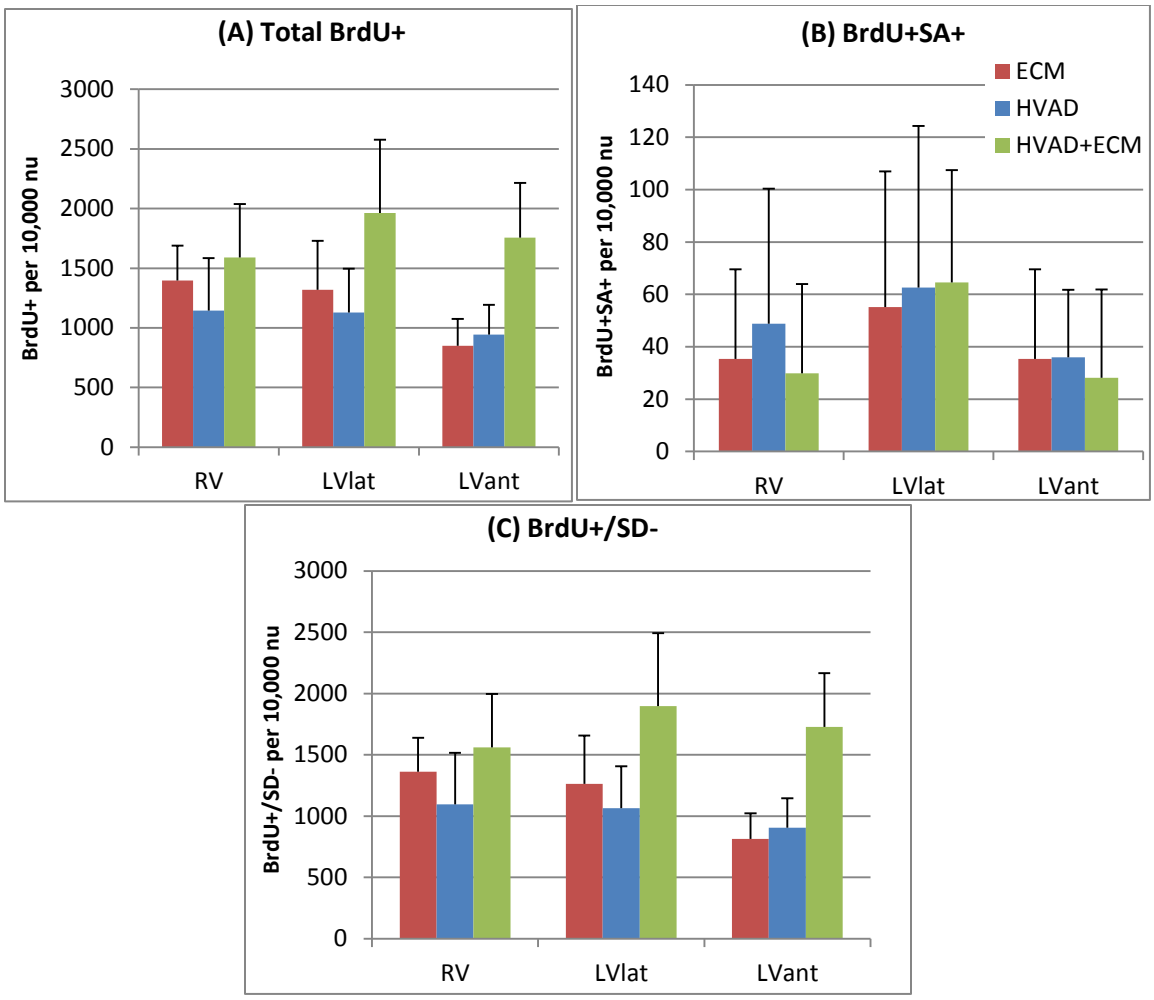

Figure 34: Cellular counts in right ventricle, left ventricle lateral, and left ventricle anterior for (A) total BrdU positive cells, (B) both BrdU and sarcomeric actin positive cells, and (C) BrdU positive and sarcomeric actin negative cells

The results show that the HVAD+ECM group had the greatest total number of BrdU+ cell in all three tissue types. There was not a significant difference for BrdU+/SA+ among the treatment groups. LV lateral appears to have the greatest number of BrdU+/SA+ cells

F. Histopathology

A histological review was performed by a licensed veterinary pathologist and the results are summarized below. Shown in Figure 35, fibrotic regions in the tissue samples were determined by HE staining. Fibrotic regions were marked and percent tissue fibrosis was calculated. The results of the HE stain are summarized in Table 7 and plotted in Figure 36 and 37.

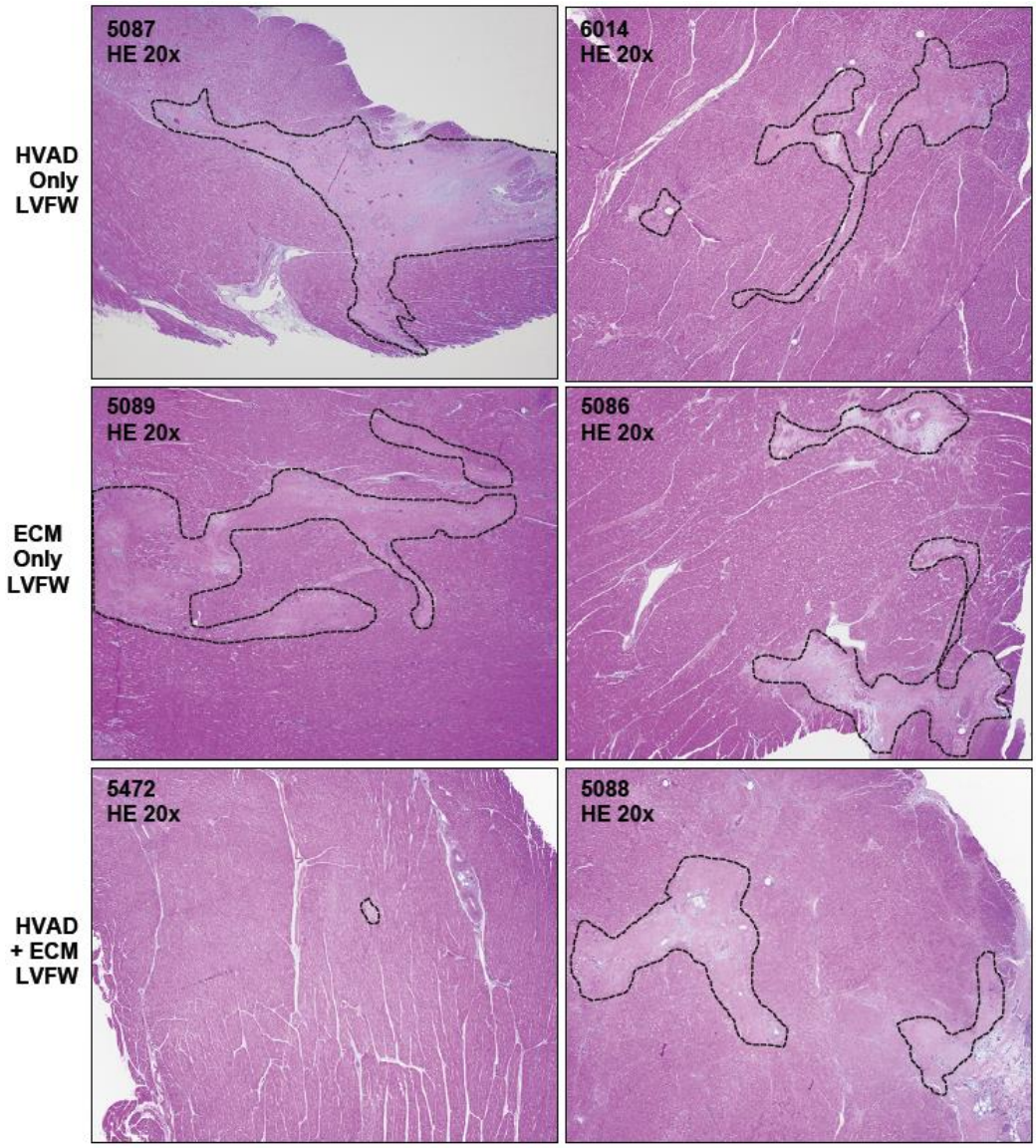

Figure 35: Sample histopathology photomicrographs for left ventricular free wall, (top) HVAD, (middle) ECM, and (bottom) HVAD+ECM; outlined regions mark areas of fibrosis

Table 15: Percent fibrosis in each tissue sample for each of the 60 day treatment groups

Fibrosis (%)	ECM	HVAD	HVAD+ECM
LV Free Wall	20 ± 7.1	35 ± 21	15 ± 14
RV Free Wall	10 ± 0	5 ± 0	7.5 ± 3.5
L Atrium	13 ± 3.5	18 ± 18	7.5 ±3.5
R Atrium	20 ± 0	28 ± 32	38 ± 18
IV Septum	5 ± 7.5	10 ± 7.1	7.5 ± 3.5
Papillary Muscle	13 ± 18	35 ± 21	10 ± 0

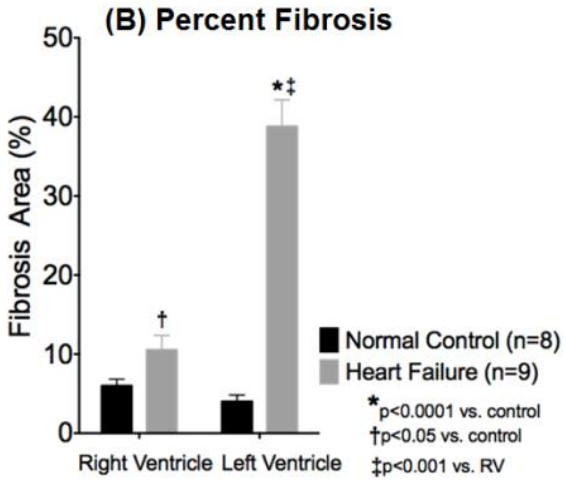

Figure 36: A comparison of the percent fibrosis in the left and right ventricle for the normal control and heart failure control group

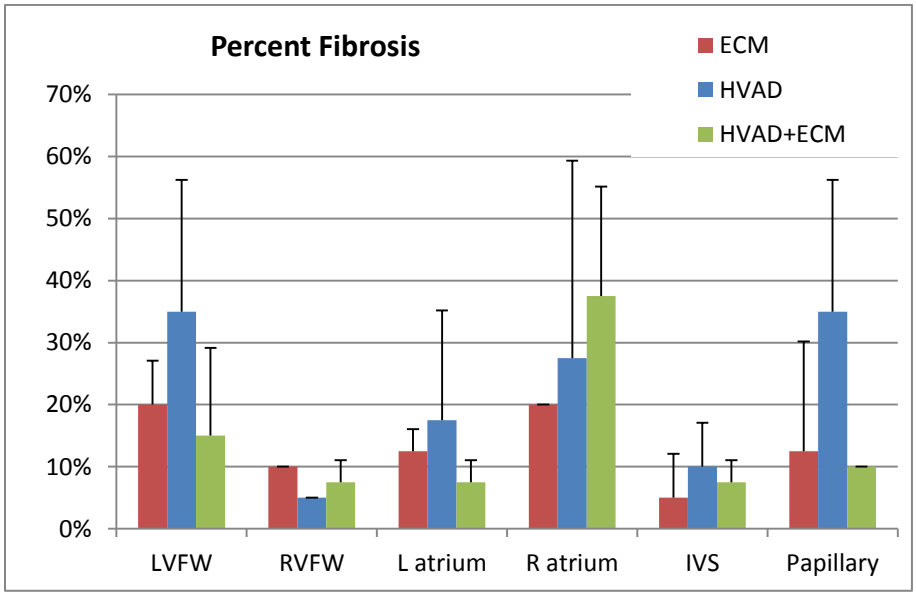

Figure 37: A comparison of the percent fibrosis in each 60 day chronic therapy treatment group for LV free wall, RV free wall, left atrium, right atrium, interventricular septum, and papillary muscle

The results of the fibrosis study are comparable to the results of the control study. The treatment group ventricles had decreased levels of fibrosis in the ventricles as compared to the heart failure control. Overall, the HVAD+ECM group had the least percentage of fibrosis in each tissue sample except for the right atrium. The major histopathologic findings for each animal are summarized in Table 8. The ECM only group had the fewest pathological changes.

Table 16: Histopathologic findings for individual animals (X indicates the presence of a lesion)

	HVAD Only		ECM Only		HVAD + ECM	
	5087	6014	5089	5086	5472	5088
Myocardial Fibrosis	X	X	X	X	X	X
Epicarditis	X	X	X (mild)		X	X
Renal Infarction	X	X			X	X
Multifocal Hepatitis	X	X	X	X	X	
Thrombosis	X	X	X (mild)		X	X
Pleuritis	X	X	X (mild)	X (mild)	X	X
Bronchitis		X			X	
Enterocolitis	X	X	X	X	X	X
Aortic Wall Hemorrhage						X
Pulmonary Edema		X	X	X	X (Mild)	
Perivascular dermatitis	X	X	X	X	X	X

V. DISCUSSION

With regards to weight analysis, the heart failure animals saw a minimal reduction in weight (17±17%) as compared to the baseline and control groups. This reduction has a large variance indicating that weight gain per day was diverse and the sample size was not large enough to demonstrate significant values. However at the 60 day treatment time point, the ECM only group regained the original rate of growth while the HVAD and HVAD+ECM group remained in the cachexic state.

Although, the HVAD+ECM group did not regain the normal rate of growth, analysis of EF indicates that HVAD+ECM group demonstrated the greatest EF with 60 day chronic treatment (75 ± 4.2%). However, when normalized to the baseline EF, ECM only had the greatest restoration of EF (96.6±11.1%). The limitations of the normalized data is that the HVAD only and HVAD+ECM group had a baseline n=1 because of missing values. Therefore, there is significant uncertainty in the normalized values. All three experimental groups at the treatment time had significantly larger EF than the heart failure time point and the 60 day heart failure control group, indicating that all three treatments feasibly

treat HF and encourage greater ventricular contractility than in the heart failure control. Using a the Tukey Test (95% confidence), it was found that EF at heart failure was significantly different from baseline and treatment, but treatment was not significantly different from baseline. The HVAD and HVAD+ECM were not significantly different from each other, but were different from the ECM group. With a larger sample size, subtle differences between treatment groups are expected to be more apparent.

Along with EF analysis, the LVVol analysis yield similar results. When normalized to animal weight ES LVVol was significant for both treatment and time point. The ECM only group had a larger normalized ES LVVol than the HVAD only group, and the heart failure time point was significantly different than the baseline and 60 day treatment. HVAD only and HVAD+ECM had the smallest normalized ES LVVol indicting that the MCS may have helped to reduce LV dilation and systolic dysfunction over the ECM only group. A larger sample size is needed to demonstrate significance for the interaction of treatment type and time point.

The results of the hemodynamic tests show an increase in ED and ES LVP, (+/-) dP/dt, ED and ES AoP, and AoP pulse pressure for all 60 day treatment groups in comparison to the heart failure control group. The ECM only group showed the largest increase in LVP average and peak pressures. This is consistent with what is expected because MCS is used to unload the ventricle, reduce pressure, and reduce wall stress. Without MCS, the ECM only group experienced higher LVP pressures. The HVAD only group demonstrated the

greatest rate of pressure changes during diastole and systole indicating greater contractile function. When comparing the HVAD support settings, there is an apparent drop in AoP pulse pressure and an increase in average AoP with increasing HVAD motor speed. This trend is expected. With increasing support from a continuous flow device, there is less pulse from native ventricular contraction.

However it is interesting to note the associated pressure waveforms in Figure 23. The maximum support level studied, 3600 RPM, reduced aortic pulse pressure, but is not considered full support. The pressure waveforms in indicate that even though AoP pulsitility is minimized at 3600 RPM, peak LVP reaches AoP, meaning that the pressure equilibrium is reached and surpassed. This causes the aortic valve to open with each ventricle contraction. Therefore, the HVAD support at 3600 RPMs is considered only partial support. Full support (continuous complete unloading) waveforms are shown previously in Figure 8.

In terms of cardiac function, the RBF results showed interesting trends as to how each treatment group aided in organ perfusion. The HVAD+ECM group was shown to produce the greatest overall RBF than the single therapies, suggesting that the combination therapy provided the greatest end-organ perfusion. It is shown that partial support HVAD+ECM had the greatest end-organ perfusion in the liver, kidney, blood, lung, and skin. When the 60 day treatment data is normalized to the pre-embolization baseline, the HVAD+ECM treatment group produced greater end-organ perfusion in the liver, kidney, spleen, skin, brain stem, cerebellum and aorta. The ECM only group had greater

perfusion in the myocardial tissue (ventricular septum, M1, M2, M3, and overall LV) and skeletal muscle. The fact that the ECM group had the greatest myocardial profusion may support the previous findings that suggest that ECM encourages revascularization of tissue[53]. The ECM group is also expected to have greater myocardial perfusion because the ECM only treatment does not allow for mechanical unloading. Rather the myocardial tissue is experiencing more stress and as a result more blood flow is diverted to the region to meet metabolic demand.

Significant findings in the analysis of BrdU staining are limited. The lab reported a low labeling yield for BrdU in all three tissue types, suggesting that the administration technique was not allowing for full saturation of proliferating cells. However, with the cells that were labeled, promising trends emerged. The results show that the HVAD+ECM group had the greatest total number of BrdU+ cell in all three tissue types. However, there was not a significant difference for BrdU+/SA+ (proliferating myocytes) among the treatment groups. Therefore, there was a significant amount of BrdU+/SA- cells labeled.

This could indicate a few things. Firstly, the SA- cells could be of a different cell type such as a proliferative fibroblast that has invaded the damaged myocardium and is actively depositing scar tissue. Secondly, in accordance with previous ECM scaffold studies, the ECM scaffold had attracted circulating progenitor cells. Because SA is an indicator of a mature myocycte, these progenitor cells would not be labeled. In order to meaningfully interpret the BrdU findings more studies have to be performed. If there was a significant

proliferative cardiomyocyte progenitor cell population, administering BrdU on a later time scale (90 days) would allow for further cellular differentiation and myocyte turn over. Also in future studies, it would be practical to stain for other cell types, including fibroblasts, to determine if relative cellular proliferation is due to the inflammation response involved in heart failure rather than myocardial regeneration.

While the BrdU cellular proliferation analysis allowed room for significant uncertainty, the histopathology results were an accurate measurement of fibrosis and scar tissue formation. According to the data, the HVAD+ECM treatment group had the lowest instance of fibrosis in LV free wall, left atrium, and papillary muscle. The HVAD group had the lowest percent of fibrosis for the RV free wall. Overall HVAD+ECM and ECM groups had less fibrosis than the HVAD only group suggests the ECM scaffold helped to rebuild fibrotic scar tissue. This finding has extremely exciting regenerative implications. With a 90 day study, further reduction in fibrosis can indicate scar tissue remodeling.

According to the summary of the histopathologic findings, shown in Table 8, the ECM only group had the fewest/mild instances of lesions. According to the pathology report, HVAD implant was associated with pericarditis and myocarditis as a reaction to a foreign body (implant and suture material), moderate pleuritis, and thrombosis in the cardiac or pulmonary arteries. The ECM injection was associated with early evidence of heart failure in the lung with accumulation of heart failure cells. Overall the vessel walls and heart valves were relatively unchanged in each group. The ECM only group had fewer histopathic changes

than those with an HVAD implant. All treatment groups had moderate myocardial fibrosis and mild pulmonary edema, a sign of early right HF. It is unclear if the right HF was in the process of developing or healing. A second 90 day treatment study will be useful in determining if right HF further progresses or recovers with treatment.

While very few of the results are significant to a 95% degree of confidence, the aim of the study was met. Overall, the results indicated the feasibility of successful combination MCS and regenerative heart failure therapy. The rational of the study is to gather sufficient preliminary data to demonstrate the possible benefits of combination therapy. These results will be incorporated into a larger study that will aim to support the hypothesis with significant confidence. The associated 90 day study, Figure 12, has been initiated, allowing for the collection of vital information on an extended timeline. The results of this 60 day study will be used in conjunction with the 90 day study to further analyze the timeline of myocardial recovery and regeneration. The expected results have significant clinical implications in the development of new heart failure treatment strategies. With the expected increase in patients with CVD and HF, it is more important than ever to develop methods to, not only treat and sustain patients with end stage HF, but to develop methods for possible HF recovery.

REFERENCES

1. Carlo Bartoli, L.S., Guruprasad Giriharan, Mark Slaughter, William Wead, Sumanth Prabhu, Steven Koenig, *Bovine Model of Chronic Ischemic Cardiomyopathy: Implications for Ventricular Assist Device Research.* 2013.

2. Go, A.S., et al., *Executive Summary: Heart Disease and Stroke Statistics—2013 Update A Report From the American Heart Association.* Circulation, 2013. **127**(1): p. 143-152.

3. Jessup, M. and S. Brozena, *Heart Failure.* New England Journal of Medicine, 2003. **348**(20): p. 2007-2018.

4. Lloyd-Jones, D., et al., *Heart disease and stroke statistics—2010 update A report from the American Heart Association.* Circulation, 2010. **121**(7): p. e46-e215.

5. Lloyd-Jones, D.M., et al., *Defining and Setting National Goals for Cardiovascular Health Promotion and Disease Reduction The American Heart Association's Strategic Impact Goal Through 2020 and Beyond.* Circulation, 2010. **121**(4): p. 586-613.

6. Roger, V.L., et al., *Executive summary: heart disease and stroke statistics--2012 update: a report from the American Heart Association.* Circulation, 2012. **125**(1): p. 188.

7. Prevention, C.f.D.C.a., *Declining prevalence of no known major risk factors for heart disease and stroke among adults--United States, 1991-2001.* MMWR Morb Mortal Wkly Rep., 2004. **16;53(1):4-7**.

8. Fuster, V. and B.B. Kelly, *Promoting cardiovascular health in the developing world: a critical challenge to achieve global health*2010: National Academies Press.

9. McMurray, J. and M.A. Pfeffer, *New therapeutic options in congestive heart failure: part I.* Circulation, 2002. **105**(17): p. 2099-2106.

10. Gretel Monreal, L.S., Michael Sobieski, Mark Slaughter, Steven Koenig, *Review Article: Large Animal Models for Left Ventricular Assist Device (LVAD) Research and Development.*

11. Cleland, J.G., et al., *Is the prognosis of heart failure improving?* European Journal of Heart Failure, 1999. **1**(3): p. 229-241.

12. Tennant, R. and C.J. Wiggers, *The effect of coronary occlusion on myocardial contraction.* American Journal of Physiology--Legacy Content, 1935. **112**(2): p. 351-361.

13. Sharpe, N., *Ventricular remodeling following myocardial infarction.* The American journal of cardiology, 1992. **70**(10): p. 20-26.

14. Hutchins, G.M. and B.H. Bulkley, *Infarct expansion versus extension: two different complications of acute myocardial infarction.* The American journal of cardiology, 1978. **41**(7): p. 1127-1132.

15. Weisman, H., et al., *Cellular mechanisms of myocardial infarct expansion.* Circulation, 1988. **78**(1): p. 186-201.

16. Grossman, W., D. Jones, and L. McLaurin, *Wall stress and patterns of hypertrophy in the human left ventricle.* Journal of Clinical Investigation, 1975. **56**(1): p. 56.

17. Anversa, P., et al., *Left ventricular failure induced by myocardial infarction. I. Myocyte hypertrophy.* American Journal of Physiology-Heart and Circulatory Physiology, 1985. **248**(6): p. H876-H882.

18. Van Dantzig, J.M., et al., *Pathogenesis of mitral regurgitation in acute myocardial infarction: importance of changes in left ventricular shape and regional function.* American heart journal, 1996. **131**(5): p. 865-871.

19. Deedwania, P.C., *Hypertension and diabetes: new therapeutic options.* Archives of Internal Medicine, 2000. **160**(11): p. 1585.

20. Budaj, A., et al., *Guidelines for the diagnosis and treatment of chronic heart failure: executive summary (update 2005).* Methodology, 2005. **11**: p. 16.

21. Committee, N.Y.H.A.C. and N.Y.H. Association, *Nomenclature and criteria for diagnosis of diseases of the heart and great vessels*1979: Little, Brown Medical Division.

22. Schrier, R.W. and W.T. Abraham, *Hormones and Hemodynamics in Heart Failure.* New England Journal of Medicine, 1999. **341**(8): p. 577-585.

23. Bristow, M. and R. Michael, *Mechanism of action of beta-blocking agents in heart failure.* The American journal of cardiology, 1997. **80**(11): p. 26L-40L.

24. Leier, C.V., *Regional blood flow responses to vasodilators and inotropes in congestive heart failure.* The American journal of cardiology, 1988. **62**(8): p. 86E-93E.

25. Hunt, S.A., et al., *ACC/AHA 2005 guideline update for the diagnosis and management of chronic heart failure in the adult a report of the American College of Cardiology/American Heart Association Task Force on Practice Guidelines (Writing Committee to Update the 2001 Guidelines for the Evaluation and Management of Heart Failure): developed in collaboration with the American College of Chest Physicians and the International Society for Heart and Lung Transplantation: endorsed by the Heart Rhythm Society.* Circulation, 2005. **112**(12): p. e154-e235.

26. Fisher, D.C., et al., *Changes in health-related quality of life and depression in heart transplant recipients.* The Journal of heart and lung transplantation: the official publication of the International Society for Heart Transplantation, 1994. **14**(2): p. 373-381.

27. Taylor, D.O., et al., *Registry of the International Society for Heart and Lung Transplantation: twenty-fifth official adult heart transplant report—2008.* The Journal of heart and lung transplantation, 2008. **27**(9): p. 943-956.

28. GIBBON Jr, J.H., *Application of a mechanical heart and lung apparatus to cardiac surgery.* Minnesota medicine, 1954. **37**(3): p. 171-85; passim.

29. *Summary of Safety and Effectiveness Data: CardioWest temporary Total Artificial Heart, SynCardia Systems, Inc. P030011*, U.F.a.D. Administration, Editor 2004.

30. Pagani, F.D., et al., *Improved Mechanical Reliability of the HeartMate XVE Left Ventricular Assist System.* The Annals of Thoracic Surgery, 2006. **82**(4): p. 1413-1418.

31. Frazier, O., T.J. Myers, and B. Radovancević, *The HeartMate left ventricular assist system. Overview and 12-year experience.* Texas Heart Institute Journal, 1998. **25**(4): p. 265.

32. HeartWare Internaltional, I. Pump Design: "Contactless" Suspension Mechanism Copyright (C) 2013.

33. HeartWare Internaltional, I., *HeartWare Receives FDA Approval for HeartWare® Ventricular Assist System as a Bridge to Heart Transplantation for Patients with Advanced Heart Failure*, N. Release, Editor 2012: PRNewswire.

34. Margulies, K.B., *Reversal mechanisms of left ventricular remodeling: lessons from left ventricular assist device experiments.* Journal of cardiac failure, 2002. **8**(6): p. S500-S505.

35. Nakatani, S., et al., *Left ventricular echocardiographic and histologic changes: impact of chronic unloading by an implantable ventricular assist device.* Journal of the American College of Cardiology, 1996. **27**(4): p. 894-901.

36. James, K.B., et al., *Effect of the implantable left ventricular assist device on neuroendocrine activation in heart failure.* Circulation, 1995. **92**(9): p. 191-195.

37. Zafeiridis, A., et al., *Regression of cellular hypertrophy after left ventricular assist device support.* Circulation, 1998. **98**(7): p. 656-662.

38. Dipla, K., et al., *Myocyte recovery after mechanical circulatory support in humans with end-stage heart failure.* Circulation, 1998. **97**(23): p. 2316-2322.

39. Harding, J.D., et al., *Electrophysiological alterations after mechanical circulatory support in patients with advanced cardiac failure.* Circulation, 2001. **104**(11): p. 1241-1247.

40. Li, Y.Y., et al., *Downregulation of matrix metalloproteinases and reduction in collagen damage in the failing human heart after support with left ventricular assist devices.* Circulation, 2001. **104**(10): p. 1147-1152.

41. Christman, K.L. and R.J. Lee, *Biomaterials for the treatment of myocardial infarction.* Journal of the American College of Cardiology, 2006. **48**(5): p. 907-913.

42. Kelley, S.T., et al., *Restraining infarct expansion preserves left ventricular geometry and function after acute anteroapical infarction.* Circulation, 1999. **99**(1): p. 135-142.

43. Enomoto, Y., et al., *Early ventricular restraint after myocardial infarction: extent of the wrap determines the outcome of remodeling.* The Annals of Thoracic Surgery, 2005. **79**(3): p. 881-887.

44. Chaudhry, P.A., et al., *Passive epicardial containment prevents ventricular remodeling in heart failure.* The Annals of Thoracic Surgery, 2000. **70**(4): p. 1275-1280.

45. Zhang, M., et al., *Cardiomyocyte grafting for cardiac repair: graft cell death and anti-death strategies.* Journal of molecular and cellular cardiology, 2001. **33**(5): p. 907-921.

46. Badylak, S.F., et al., *Esophageal reconstruction with ECM and muscle tissue in a dog model.* Journal of Surgical Research, 2005. **128**(1): p. 87-97.

47. Hiles, M., et al., *Mechanical properties of xenogeneic small-intestinal submucosa when used as an aortic graft in the dog.* Journal of biomedical materials research, 1995. **29**(7): p. 883-891.

48. Beattie, A.J., et al., *Chemoattraction of progenitor cells by remodeling extracellular matrix scaffolds.* Tissue Engineering Part A, 2008. **15**(5): p. 1119-1125.

49. De Ugarte, D.A., et al., *Mucosal regeneration of a duodenal defect using small intestine submucosa.* The American surgeon, 2004. **70**(1): p. 49-51.

50. MacLeod, T., et al., *Evaluation of a porcine origin acellular dermal matrix and small intestinal submucosa as dermal replacements in preventing secondary skin graft contraction.* Burns, 2004. **30**(5): p. 431-437.

51. Badylak, S.F., et al., *The use of extracellular matrix as an inductive scaffold for the partial replacement of functional myocardium.* Cell transplantation, 2006. **15**(Supplement 1): p. 29-40.

52. Gilbert, T.W., et al., *Degradation and remodeling of small intestinal submucosa in canine Achilles tendon repair.* The Journal of Bone & Joint Surgery, 2007. **89**(3): p. 621-630.

53. Voytik-Harbin, S.L., et al., *Identification of extractable growth factors from small intestinal submucosa.* Journal of cellular biochemistry, 1997. **67**(4): p. 478-491.

54. Spinale, F.G., et al., *Extracellular degradative pathways in myocardial remodeling and progression to heart failure.* Journal of cardiac failure, 2002. **8**(6): p. S332-S338.

55. Zhao, Z.-Q., et al., *Improvement in cardiac function with small intestine extracellular matrix is associated with recruitment of C-kit cells, myofibroblasts, and macrophages after myocardial infarction.* Journal of the American College of Cardiology, 2010. **55**(12): p. 1250-1261.

56. Burkhoff, D., S. Klotz, and D.M. Mancini, *LVAD-induced reverse remodeling: basic and clinical implications for myocardial recovery.* J Card Fail, 2006. **12**(3): p. 227-39.

57. Birks, E.J., et al., *Left ventricular assist device and drug therapy for the reversal of heart failure.* N Engl J Med, 2006. **355**(18): p. 1873-84.

58. Birks, E.J., et al., *Reversal of severe heart failure with a continuous-flow left ventricular assist device and pharmacological therapy: a prospective study.* Circulation, 2011. **123**(4): p. 381-90.

59. Psaltis, P.J., et al., *An Ovine Model of Toxic, Nonischemic Cardiomyopathy—Assessment by Cardiac Magnetic Resonance Imaging.* Journal of cardiac failure, 2008. **14**(9): p. 785-795.

60. Jud Heinrichs, B.L., *Monitoring Dairy Heifer: Growth*, P.S.C.o.A. Science, Editor 1998.

61. Anker SD, S.R., *The Syndrome of Cardiac Cachexia.* Int J Cardiol, 2002. **85**(1): p. 51-66.

62. David C. Dugdale, I., MD. *CBC*. 2012; Available from: http://www.nlm.nih.gov/medlineplus/ency/article/003642.htm.

63. Rudolph, A.M. and M.A. Heymann, *The circulation of the fetus in utero methods for studying distribution of blood flow, cardiac output and organ blood flow.* Circulation research, 1967. **21**(2): p. 163-184.

64. Raab, S., et al., *A new sample-processing unit for the fluorescent microsphere method.* American Journal of Physiology-Heart and Circulatory Physiology, 1999. **276**(5): p. H1801-H1806.

65. Schimmel, C., D. Frazer, and R.W. Glenny, *Extending fluorescent microsphere methods for regional organ blood flow to 13 simultaneous colors.* American Journal of Physiology-Heart and Circulatory Physiology, 2001. **280**(6): p. H2496-H2506.

66. Heymann, M.A., et al., *Blood flow measurements with radionuclide-labeled particles.* Progress in cardiovascular diseases, 1977. **20**(1): p. 55-79.

67. Buckberg, G.D., et al., *Some sources of error in measuring regional blood flow with radioactive microspheres.* Journal of Applied Physiology, 1971. **31**(4): p. 598-604.

68. Gordon, D.B., J. Flasher, and D.R. Drury, *Size of the largest arterio-venous vessels in various organs.* American Journal of Physiology--Legacy Content, 1953. **173**(2): p. 275-281.

69. *NuFLOW Fluorescent Microsphere Extraction Protocol for Regional Blood Flow Measurement*, N. (TM), Editor 2001, Interactive Medical Technologies, Ltd.

70. Hoshino, T., et al., *Variability in the proliferative potential of human gliomas.* Journal of neuro-oncology, 1989. **7**(2): p. 137-143.

71. Taupin, P., *BrdU immunohistochemistry for studying adult neurogenesis: paradigms, pitfalls, limitations, and validation.* Brain research reviews, 2007. **53**(1): p. 198-214.

72. West, M., L. Slomianka, and H.J.G. Gundersen, *Unbiased stereological estimation of the total number of neurons in the subdivisions of the rat hippocampus using the optical fractionator.* The Anatomical Record, 1991. **231**(4): p. 482-497.

73. Kajstura, J., et al., *Cardiomyogenesis in the adult human heart.* Circulation research, 2010. **107**(2): p. 305-315.

74. Anversa, P., et al., *Life and death of cardiac stem cells a paradigm shift in cardiac biology.* Circulation, 2006. **113**(11): p. 1451-1463.

75. *Product Information: 5-BROMO-2'-DEOXYURIDINE, Prod. No. B5002 and B9285*, in *Sigma-Aldrich Inc.*

76. Gratzner, H.G., *Monoclonal antibody to 5-bromo-and 5-iododeoxyuridine: a new reagent for detection of DNA replication.* Science, 1982. **218**(4571): p. 474-475.

77. Sekerková, G., E. Ilijic, and E. Mugnaini, *Bromodeoxyuridine administered during neurogenesis of the projection neurons causes cerebellar defects in rat.* Journal of Comparative Neurology, 2004. **470**(3): p. 221-239.

78. Hayes, N.L. and R.S. Nowakowski, *Exploiting the Dynamics of S-Phase Tracers in Developing Brain: Interkinetic Nuclear Migration for Cells Entering versus Leavingthe S-Phase.* Developmental neuroscience, 2000. **22**(1-2): p. 44-55.

79. Allen, J.W., *BrdU-dye characterization of late replication and meiotic recombination in Armenian hamster germ cells.* Chromosoma, 1979. **74**(2): p. 189-207.

80. Cameron, H.A. and R.D. Mckay, *Adult neurogenesis produces a large pool of new granule cells in the dentate gyrus.* Journal of Comparative Neurology, 2001. **435**(4): p. 406-417.

81. Friedberg, E.C., *DNA damage and repair.* Nature, 2003. **421**(6921): p. 436-440.

82. Mitchell, R.S.K., Vinay; Abbas, Abul K.; Fausto, Nelson, *Chapter 11.* Robbins Basic Pathology, Philadelphia: Saunders. **8th edition**.

APPENDIX I: INDIVIDUAL DATA

Table 17: Rate of Weight Gain Calculations

		ECM		HVAD		HVAD+ECM	
		5086	**5089**	**5087**	**6014**	**5088**	**5472**
Time (days)	Arrival – HF embol.	20	15	51	13	14	29
	HF - Treatment	106	103	35	34	90	32
	Treatment + 14 d	14	14	14	14	14	14
	15d - 60d	48	49	46	45	48	48
Weight (kg)	Arrival	50	66	50	72	62	51
	Embol	67	76	94	82	74	70
	Pre-treatment	128	154	117	104	142	85
	Post-treatment - 14d	130	157	122	111	139	94
	Final	167	194	150	130	170	123
Weight Gain (kg)	Pre-Emboli	17	10	44	10	12	19
	Heart Failure	61	78	23	22	68	15
	14 day recovery	2	3	5	7	-3	9
	Treatment	37	37	28	19	31	29
Rate (kg/day)	Pre-Emboli	0.850	0.667	0.863	0.769	0.857	0.655
	Heart Failure	0.575	0.757	0.657	0.647	0.756	0.469
	14 day recovery	0.143	0.214	0.357	0.500	-0.214	0.643
	Treatment	0.771	0.755	0.609	0.422	0.646	0.604

Table 18: BCS Scores at multiple time points compared with post-op day (POD)

	ECM				HVAD				HVAD+ECM			
	5086		5089		5087		6014		5088		7472	
Time Point	**POD**	**BCS**	**POD**	**BCS**	**POD**	**BCS**	**POD**	**BCS**	**POD**	**BCS**	**POD**	**BCS**
Baseline	0	2.5	0	2	0	2.5	0	2.5	0	2	0	2
1	17	2.5	18	2.5	7	2.5	5	2.5	15	2	6	2
2	35	2.5	36	2.5	13	2.5	11	2.5	31	2.5	11	2
3	53	2.5	55	2.5	20	2.5	17	2.5	46	2.5	17	2.5
4	70	2.5	73	2.5	26	2.5	22	2.5	62	2.5	23	2
5	88	2.5	92	3	33	2.5	28	2.5	77	2.5	29	2
Chronic HF	106	2	110	3	39	2.5	34	2.5	92	3	35	2
7	116	2	120	2.5	49	2.5	44	2.5	102	3	45	2.5
8	127	2	131	2.5	59	2.5	54	2.5	112	3	56	2.5
9	137	2	141	2.5	69	2.5	64	2.5	122	3	66	2.5
10	148	2	152	2.5	79	2.5	74	2.5	133	3	77	2.5
11	158	2.5	162	3	89	2.5	84	2.5	143	3	87	2.5
60 day treat	169	2.5	173	3	99	2.5	94	2.75	153	3	98	2.5

Table 19: (top) Ejection fraction and (bottom) left ventricle volume (end diastolic and end systolic) at various time points and animal conditions

	ECM 5086 EF (%)			ECM 5089 EF (%)			HVAD 5087 EF (%)			HVAD 6014 EF (%)			HVAD+ECM 5088 EF (%)				HVAD+ECM 7472 EF (%)		
	POD	Awake	Anest	Inotr	POD	Awake	Anest	Inotr	POD	Awake	Anest	Inotr	POD	Awake	Anest	Ino	POD	Awake	Anest	Inotr
Quarintine Baseline	-4	71			-1	67			-2	80			-1	81						
Pre-Embol	0		41	58	0			70	0		60		0		33	57	0			42
Post-Embol	0			25	0			32	0			28	0			37	0			28
HF-Mid Point	15	25			20	46			13	36			21	47						
	22	33			34	46														
	44	27			49	27														
Pre-Treat	106		25	21.4	110		29	32	39			28	34			35	92		29		35		34	34
Post-Treat	106			28.4	110				39			32	34			40	92				35			
Treat (mid)	119	53			124	40			43	44			51	74			101	48			43	44		
	126	30			131	68			50	50							125	64			67	71		
	141	64			146	70			64	52							132	74			74	77		
									88	40							147	72			89	84		
									95	65														
Final	169	63			173	52	23.7	62.6	99	71			94	68	34	68	153		64		98	78		50.8

	ECM 5086 LV Vol (ml) (ED/ES)				ECM 5089 LV Vol (ml) (ED/ES)				HVAD 5087 LV Vol (ml) (ED/ES)				HVAD 6014 LV Vol (ml) (ED/ES)				HVAD+ECM 5088 LV Vol (ml) (ED/ES)				HVAD+ECM 7472 LV Vol (ml) (ED/ES)			
	Awake		Anest	Inotr	Awake		Anest	Inotr	Awake		Anest	Inotr	Awake		Anest	Inotr	Awake		Anest	Inotr	Awake		Anest	Inotr
Baseline	166	48			63	21			100	20			83	16										
Pre-Embol			147	86							113	45					115	77	135	57			88	25
Post-Embol			92	31					64	19	151	103					184	78	230	168			97	70
Heart Fail	155	116			137	74			207	130			131	70			190	148	133	43				
	205	138			208	113											160	68						
	247	182			272	199											124	72						
																	292	162						
Pre-Treat			311	234			233	166	282	189			126	91			132	85			111	79		
													164	112			73	19					161	107
Post-Treat	331	154			154	92			248	138					73	19	172	90			126	71	195	123
Recovery	322	226			257	83			262	130							139	50			170	49		
	293	106			290	88			217	105							234	77			174	39		
									220	132							304	84			184	29		
									242	85														
Final	396	148			277	133	184	140	208	61									291	102			156	77
									432	161	436	203	180	57	155	102	136	43			149	33		

Table 20: Hemodynamic parameters for individual test subjects

5086-ECM			
	Baseline	Post-Emb 60d	Treat
LVHR	81.413	104.1	82.092
LVPavg	41.601	45.745	76.197
LVPed	2.4056	18.898	20.278
LVPpksys	96.503	81.58	139.99
LVppdPdt	1441.4	1263.3	1369.7
LVpndPdt	-1750.6	-1261	-1837.1
AoPavg	85.459	70.515	124.44
AoPpulse	30.698	26.326	33.588
AoPsys	99.326	83.783	140.74
AoPdia	68.628	57.457	107.15
ArtPavg	86.582	71.72	120.23
ArtPpulse	20.815	22.899	23.184
ArtPsys	102.58	87.46	140.21
ArtPdia	81.766	64.561	117.03
LVVed	120.64	131.95	32.605
LVVes	98.597	122.89	31.283
LVVSV	22.044	9.0594	1.3218
CVPavg	0.042866	1.8575	9.8982
CVPsys	3.5077	5.0802	10.214
CVPdia	-2.69	-1.3794	9.6553

5089-ECM			
	Baseline	Post-Emb 60d	Treat
LVHR	84.646	78.318	76.61
LVPavg	47.461	52.343	86.938
LVPed	1.5402	25.51	36.446
LVPpksys	103.47	87.688	152.62
LVppdPdt	2096.9	996.74	1348.8
LVpndPdt	-1585.6	-1266.5	-2101.6
AoPavg	92.194	75.615	133.82
AoPpulse	29.645	30.234	43.395
AoPsys	105.14	88.834	152.09
AoPdia	75.5	58.6	108.69
ArtPavg	92.451	74.934	124.13
ArtPpulse	26.499	23.838	23.153
ArtPsys	112.15	89.508	142.73
ArtPdia	85.649	65.67	119.58
LVVed	125.11	133.47	24.77
LVVes	98.15	125.75	22.899
LVVSV	26.958	7.7281	1.8708
CVPavg	-1.1563	7.2285	1.3071
CVPsys	2.3823	12.369	3.5564
CVPdia	-4.3251	2.62	-0.81194

5087-HVAD						
	Baseline	Post-Emb 60d	Treat	1800 RPM	2200 RPM	2600 RPM
LVHR	55.693	71.072	88.646	88.646	88.75	83.884
LVPavg	47.359	46.251	67.378	67.378	67.898	65.337
LVPed	15.771	24.873	40.247	40.247	38.828	34.863
LVPpksys	119.16	90.738	111.44	111.44	113.91	114.74
LVppdPdt	998.75	895.27	1147	1147	1105.7	1065.2
LVpndPdt	-1958.3	-1228.6	-1724.9	-1724.9	-1795.6	-1755.1
AoPavg	107.12	78.021	99.105	99.105	102.98	104.58
AoPpulse	26.587	27.813	35.252	26.622	23.841	21.067
AoPsys	119.72	91.907	111.42	111.42	114.17	114.94
AoPdia	93.131	64.094	84.8	84.8	90.325	93.87
ArtPavg	107.35	77.426	96.576	96.576	100.22	101.35
ArtPpulse	25.364	28.18	28.007	28.007	23.948	22.163
ArtPsys	123.14	96.967	116.31	116.31	117.82	117.85
ArtPdia	97.779	68.787	88.304	88.304	93.877	95.689
LVVed	130.93	131.38	36.112	36.112	35.783	35.818
LVVes	107.77	126.58	34.362	34.362	33.325	33.314
LVVSV	23.164	4.7985	1.7502	1.7502	2.4586	2.504
CVPavg	2.9991	4.793	6.9135	6.9135	7.1225	6.5595
CVPsys	4.2432	5.8091	8.3795	8.3795	8.7268	7.8133
CVPdia	1.9788	4.5333	5.871	5.871	5.9396	5.5925

5088-HVAD+ECM						
	Baseline	Post-Emb 60d	Treat	1800 RPM	2200 RPM	2600 RPM
LVHR	75.493	82.6	125.47	125.47	125.06	125.2
LVPavg	47.392	43.411	69.497	69.497	72.296	74.671
LVPed	10.799	24.517	35.252	35.252	35.324	35.202
LVPpksys	98.073	73.654	103.66	103.66	109	114.22
LVppdPdt	1312.6	1097.7	1129.7	1129.7	1136.9	1194.2
LVpndPdt	-1626.6	-824.73	-1492.4	-1492.4	-1641.1	-1764.7
AoPavg	87.497	61.002	95.483	95.483	101.96	108.09
AoPpulse	30.042	27.357	17.27	17.27	15.016	13.162
AoPsys	100.97	74.183	104.1	104.1	109.62	114.87
AoPdia	70.926	46.826	86.83	86.83	94.605	101.71
ArtPavg	85.504	58.843	89.46	89.46	95.4	101.54
ArtPpulse	23.092	28.176	13.87	13.87	12.968	13.313
ArtPsys	100.46	76.595	101.12	101.12	106.41	111.47
ArtPdia	77.369	48.419	87.248	87.248	93.445	98.155
LVVed	57.523	59.889	50.164	50.164	50.04	49.9
LVVes	49.67	57.612	48.842	48.842	48.731	48.659
LVVSV	7.8531	2.2776	1.3225	1.3225	1.3097	1.2418
CVPavg	44.665	3.7074	8.8223	8.8223	8.797	8.6395
CVPsys	44.743	9.3911	11.969	11.969	12.211	11.971
CVPdia	44.584	0.30757	7.893	7.893	7.576	7.3222

6014-HVAD						
	Baseline	Post-Emb 60d	Treat	1800 RPM	2200 RPM	2600 RPM
LVHR	56.062	69.005	90.895	90.895	89.618	80.316
LVPavg	30.187	51.291	67.188	67.188	68.797	64.216
LVPed	17.57	23.258	18.477	18.477	18.296	21.498
LVPpksys	87.245	105.43	136.9	136.9	143.15	135.27
LVppdPdt	816.28	1152.1	2030.6	2030.6	2050.6	1543.1
LVpndPdt	-1511.2	-1871.1	-2717.8	-2717.8	-2840.3	-2489.1
AoPavg	67.752	91.592	123.24	123.24	129.11	122.92
AoPpulse	38.991	36.228	34.001	34.001	32.757	30.661
AoPsys	88.485	108.71	140	140	146.11	138.43
AoPdia	49.494	72.479	105.99	105.99	113.35	107.77
ArtPavg	69.146	94.404	105.27	105.27	111.4	105.78
ArtPpulse	39.248	32.162	16.357	16.357	17.517	15.939
ArtPsys	91.652	112.85	120.44	120.44	126.6	119.85
ArtPdia	52.404	80.684	104.09	104.09	109.09	103.91
LVVed	55.949	66.934	130.25	130.25	130.27	133.42
LVVes	44.952	62.208	122.89	122.89	123.14	123.37
LVVSV	10.998	4.7262	7.3628	7.3628	7.1319	10.045
CVPavg	2.973	8.8903	1.524	1.524	1.3932	3.2834
CVPsys	5.1242	16.104	5.1909	5.1909	5.1564	6.0274
CVPdia	1.0773	3.6656	-2.2349	-2.2349	-2.4705	1.8863

6014-HVAD			
	3200 RPM	3300RPM	3600RPM
LVHR	77.337	76.308	75.401
LVPavg	60.151	60.945	61.322
LVPed	19.095	16.919	16.402
LVPpksys	129.44	133.11	136.3
LVppdPdt	1191.5	1222.3	1317.2
LVpndPdt	-2311.8	-2417.3	-2476.8
AoPavg	119.47	123.04	126.12
AoPpulse	25.598	25.321	23.932
AoPsys	136.97	140.28	140.28
AoPdia	107.65	111.65	116.34
ArtPavg	101.52	104.78	112.69
ArtPpulse	14.251	14.705	16.024
ArtPsys	113.28	116.16	125.09
ArtPdia	99.026	101.46	109.07
LVVed	133.26	133.22	131.83
LVVes	123.27	123.31	123.41
LVVSV	9.9947	9.9133	8.4203
CVPavg	4.449	4.2378	4.2127
CVPsys	7.1967	7.3942	6.7723
CVPdia	3.4044	2.9919	3.0303

6014-HVAD			
	1800 RPM	2200 RPM	2600 RPM
LVHR	125.47	125.06	125.2
LVPavg	69.497	72.296	74.671
LVPed	35.252	35.324	35.202
LVPpksys	103.66	109	114.22
LVppdPdt	1129.7	1136.9	1194.2
LVpndPdt	-1492.4	-1641.1	-1764.7
AoPavg	95.483	101.96	108.09
AoPpulse	17.27	15.016	13.162
AoPsys	104.1	109.62	114.87
AoPdia	86.83	94.605	101.71
ArtPavg	89.46	95.4	101.54
ArtPpulse	13.87	12.968	13.313
ArtPsys	101.12	106.41	111.47
ArtPdia	87.248	93.445	98.155
LVVed	50.164	50.04	49.9
LVVes	48.842	48.731	48.659
LVVSV	1.3225	1.3097	1.2418
CVPavg	8.8223	8.797	8.6395
CVPsys	11.969	12.211	11.971
CVPdia	7.893	7.576	7.3222

6014-HVAD			
	3200 RPM	3300RPM	3600RPM
LVHR	124.44	123.62	121.51
LVPavg	76.205	76.368	76.349
LVPed	35.202	33.928	33.617
LVPpksys	118.92	119.95	121.52
LVppdPdt	1194	1192.9	1155.5
LVpndPdt	-1855.3	-1875.8	-1870.9
AoPavg	113.65	114.96	116.92
AoPpulse	10.666	10.177	8.9817
AoPsys	119.45	120.48	121.84
AoPdia	108.79	110.3	112.86
ArtPavg	108.97	110.22	112.04
ArtPpulse	11.293	10.671	8.8884
ArtPsys	116.66	117.46	117.82
ArtPdia	105.37	106.79	108.94
LVVed	49.814	49.711	49.623
LVVes	48.622	48.527	48.412
LVVSV	1.192	1.1833	1.2116
CVPavg	10.302	10.153	10.073
CVPsys	13.673	13.442	13.234
CVPdia	8.7973	8.656	8.3822

Table 21: Hemodynamic parameters for individual test subjects (cont.)

	5472-HVAD+ECM								
	Baseline	Post-Emb	60d Treat	1800 RPM	2200 RPM	2600 RPM	3200 RPM	3300RPM	3600RPM
LVHR	74.748	77.152	84.982	84.982	86.076	87.183	87.082	85.306	77.904
LVPavg	43.542	38.564	50.53	50.53	52.975	54.874	57.232	56.232	53.286
LVPed	5.2472	7.3435	19.929	19.929	19.074	17.34	16.969	16.038	16.078
LVPpksys	96.391	85.651	100.58	100.58	105.35	109.83	114.99	115.27	121.7
LVppdPdt	1242	1270.6	1114.1	1114.1	1012.4	1065.7	1108.7	1092.3	1061.9
LVpndPdt	-1690.5	-1250.7	-1435.2	-1435.2	-1483.1	-1749.8	-1832.1	-1886.4	-2729.5
AoPavg	81.699	66.115	84.692	84.692	92.187	101.96	109.14	109.83	103.95
AoPpulse	37.503	38.568	43.265	43.265	37.776	34.852	31.032	30.374	30.894
AoPsys	98.348	87.147	109.11	109.11	112.75	120.64	125.35	125.69	120.39
AoPdia	60.845	48.579	65.85	65.85	74.971	85.788	94.316	95.317	89.498
ArtPavg	83.45	66.136	74.411	74.411	80.79	87.896	94.374	95.023	89.684
ArtPpulse	39.999	61.468	39.912	39.912	30.938	26.154	23.51	23.349	27.331
ArtPsys	116.54	112.58	100.4	100.4	102.07	106.63	111.92	112.39	108.12
ArtPdia	76.546	51.112	60.493	60.493	71.136	80.48	88.406	89.045	80.792
LVVed	15.656	10.364	51.738	51.738	52.277	52.696	54.202	54.396	52.197
LVVes	13.677	10.154	49.236	49.236	47.86	47.641	52.028	52.428	47.938
LVVSV	1.9797	0.20972	2.5015	2.5015	4.4161	5.0546	2.1741	1.9677	4.2592
CVPavg	1.9154	2.0154	13.423	13.423	10.338	9.04	8.4573	23.321	17.306
CVPsys	5.2479	4.79	14.791	14.791	10.781	9.4961	8.9171	25.135	18.072
CVPdia	-1.7171	-1.1747	12.763	12.763	9.9693	8.6737	7.9907	22.416	16.598

Table 22: HE staining results showing percent fibrosis for individual test subjects

	ECM		HVAD		HVAD+ECM	
Tissue	5089	5086	5087	6014	5472	5088
LVFW	25.0%	15.0%	50.0%	20.0%	5.0%	25.0%
RVFW	10.0%	10.0%	5.0%	5.0%	5.0%	10.0%
L atrium	10.0%	15.0%	30.0%	5.0%	5.0%	10.0%
R atrium	20.0%	20.0%	50.0%	5.0%	25.0%	50.0%
IVS	10.0%	0.0%	5.0%	15.0%	10.0%	5.0%
Papillary	0.0%	25.0%	50.0%	20.0%	10.0%	10.0%

Table 23: Regional blood flow calculation (ml/min/gram tissue) for each tissue specimen in individual test subjects at various time points and HVAD settings

	Pre-embolization					Post-embolization					Chronic Treatment					VAD Failure				
	ECM		HVAD		HVAD +ECM	ECM		HVAD		HVAD +ECM	ECM		HVAD		HVAD +ECM	HVAD				
Tissue	#5086	#5089	#5087	#6014	#5088	#5472	#5086	#5089	#5087	#6014	#5088	#5472	#5086	#5089	#5087	#6014	#5088	#5472	#5087	#6014	#5088	#5472
Liver	0.083	0.092	0.099	0.167	0.040	0.084	0.242	0.043	---	0.456	0.028	0.064	0.175	0.433	0.084	0.551	0.702	1.429	0.205	0.095	0.135	0.119
Kidney	0.664	0.916	0.723	0.809	0.699	3.041	0.718	0.896	---	3.343	0.519	2.167	1.617	3.019	1.408	9.095	4.786	25.496	4.762	1.777	1.610	1.935
Spleen	0.145	0.276	0.127	0.177	0.119	0.285	0.306	0.266	---	0.286	0.187	0.112	0.256	0.238	0.133	1.523	0.668	2.800	0.669	0.175	0.122	0.202
RV	0.342	4.599	0.296	0.541	0.241	1.018	0.535	0.306	---	0.885	0.150	0.599	0.718	1.011	0.295	0.573	0.620	0.738	1.894	0.422	0.878	0.707
LV	0.432	0.233	0.340	0.640	0.328	0.783	0.359	0.178	---	0.824	0.199	0.545	0.681	0.818	0.437	0.639	0.724	0.487	2.402	0.768	0.739	0.635
Septum	0.563	0.215	0.270	0.979	0.338	1.198	0.695	0.153	---	1.378	0.257	0.837	1.214	0.818	0.509	0.999	0.728	0.852	2.840	1.043	0.928	0.972
M1	0.258	0.480	0.199	0.497	0.172	0.610	0.212	0.555	---	0.589	0.184	0.444	0.452	3.121	0.296	0.697	0.429	0.515	2.790	0.694	0.522	0.490
M2	0.492	0.222	0.624	0.936	0.403	0.703	0.323	0.118	---	0.739	0.203	0.486	0.995	0.699	0.601	0.666	0.664	0.510	3.959	0.834	0.790	0.620
M3	0.518	0.229	0.720	0.787	0.334	0.650	0.218	0.224	---	0.927	0.227	0.451	0.904	0.709	0.387	0.728	0.693	0.441	2.828	0.839	0.832	0.679
Bowel	0.133	0.407	0.291	0.235	0.199	0.832	0.166	0.259	---	0.669	0.102	0.543	0.439	0.410	0.277	1.573	1.126	4.382	1.165	0.302	0.424	0.314
Lung	1.047	0.524	0.392	0.401	0.660	0.842	1.614	0.439	---	1.185	0.518	0.648	3.742	1.735	0.800	0.862	0.588	4.835	2.431	0.315	0.230	1.936
Skin	0.035	0.000	0.014	0.043	0.011	0.052	0.012	0.023	---	0.026	0.007	1.143	0.166	0.065	0.016	0.020	0.009	1.198	0.125	0.025	0.006	0.134
Skel Mus	0.002	0.002	0.009	0.297	0.003	0.101	0.005	0.001	---	0.320	0.004	0.024	0.013	0.020	0.004	0.500	0.019	0.257	0.037	0.297	0.021	0.086
Brain Stem	0.219	0.223	0.442	0.585	0.127	0.103	0.228	0.173	---	2.046	0.147	0.142	1.054	0.341	0.489	1.804	0.954	0.296	3.689	2.511	1.351	0.394
Cerebellum	0.313	0.397	0.473	1.336	0.118	0.300	0.336	0.344	---	4.911	0.130	0.291	1.588	0.665	0.609	5.030	1.058	0.782	4.285	6.095	1.566	0.769
Frontal Lobe	0.266	0.301	---	0.650	---	---	0.279	0.316	---	3.108	---	---	1.126	0.649	---	2.351	---	---	---	3.481	---	---
Aorta	0.008	0.009	0.009	0.018	0.006	0.005	0.023	0.021	---	0.032	0.004	0.014	0.096	0.042	0.037	0.074	0.070	0.279	0.096	0.034	0.032	0.027
PA	0.045	0.047	0.012	0.027	0.009	---	0.043	0.084	---	0.057	0.004	---	0.212	0.472	0.018	0.080	0.056	---	0.099	0.046	0.041	---

Table 24: BrdU+ and BrdU+SA+ cell count (per 10,000 nuclei) in the right ventricle and lateral and anterior left ventricle for each test subject

5087 - HVAD						5089 - ECM					
RV		LV lat		LV Anter		RV		LV lat		LV Anter	
BrdU+	BrdU+SA+	BrdU+	BrdU+SA+	BrdU+	BrdU+SA+	BrdU+	BrdU+SA+	BrdU+	BrdU+SA+	BrdU+	BrdU+SA+
965	44	808	231	1176	42	1490	96	2111	167	863	60
978	88	1038	115	756	42	1346	48	1222	56	565	0
800	44	1308	77	966	42	1731	0	1111	0	655	0
1022	88	1462	115	966	42	1635	96	1333	56	625	30
1244	219	1423	154	1387	84	1490	48	1611	0	536	30
1244	88	1885	115	1008	42	1875	96	2000	56	923	30
1778	44	1231	115	756	42	1779	48	1500	0	863	60
2400	44	923	38	1303	42	1635	0	1500	56	685	0
1511	44	1538	38	1008	84	1538	48	1556	167	833	30
1244	88	1423	38	1303	42	1394	0	1667	0	893	0
5088 - HVAD+ECM						**5086 - ECM**					
RV		LV lat		LV Anter		RV		LV lat		LV Anter	
BrdU+	BrdU+SA+	BrdU+	BrdU+SA+	BrdU+	BrdU+SA+	BrdU+	BrdU+SA+	BrdU+	BrdU+SA+	BrdU+	BrdU+SA+
1860	116	2908	51	2398	0	909	0	803	109	820	0
2151	0	2449	153	1939	51	1045	45	803	73	1250	117
1686	0	2857	51	2653	51	1091	0	1095	73	703	39
2151	58	2398	102	1888	0	1227	0	1022	36	742	0
1919	58	2500	51	2500	102	1273	45	839	0	820	78
1919	0	2143	51	1633	51	1318	0	985	36	703	39
1860	58	2551	102	2041	51	1045	45	730	36	1172	78
1919	58	2194	102	1735	51	1091	45	949	0	1094	0
1977	0	1888	153	2194	102	1227	45	1131	73	1055	39
2151	58	2398	102	1888	0	1091	0	1314	109	469	78
5472 - HVAD+ECM						**6014 - HVAD**					
RV		LV lat		LV Anter		RV		LV lat		LV Anter	
BrdU+	BrdU+SA+	BrdU+	BrdU+SA+	BrdU+	BrdU+SA+	BrdU+	BrdU+SA+	BrdU+	BrdU+SA+	BrdU+	BrdU+SA+
1274	0	1306	0	1424	0	784	0	750	36	679	0
1165	0	1455	37	1424	35	821	37	643	0	643	36
1274	27	1269	37	1319	0	672	0	821	71	607	36
1463	27	1119	37	1389	0	784	0	857	0	750	0
1030	27	1455	37	1285	0	1343	75	786	36	821	0
1247	0	1567	75	1458	35	709	37	679	0	571	36
976	0	1418	37	1319	35	746	0	964	0	857	0
1111	27	1381	0	1389	0	896	37	857	36	964	36
976	0	1157	75	1285	0	970	0	821	0	857	0
1111	81	1530	37	1389	0	1007	0	1107	36	750	71

APPENDIX II: ANALYSIS OF VARIANCE

A) Weight Gain Per Day

Analysis of Variance for **Rate Weight Gain (kg/day)**, using Adjusted SS for Tests

Source	DF	Seq SS	Adj SS	Adj MS	F	P
Treatment	2	0.01769	0.01769	0.00885	0.68	0.532
Time Point	2	0.07620	0.07620	0.03810	2.91	0.106
Treatment*Time Point	4	0.05165	0.05165	0.01291	0.99	0.461
Error	9	0.11766	0.11766	0.01307		
Total	17	0.26320				

S = 0.114339 R-Sq = 55.30% R-Sq(adj) = 15.56%

Analysis of Variance for Normalized Rate Weight Gain (kg/day), using Adjusted SS for Tests

Source	DF	Seq SS	Adj SS	Adj MS	F	P
Treatment	2	0.08331	0.08331	0.04165	2.15	0.172
Time Point	2	0.11322	0.11322	0.05661	2.93	0.105
Treatment*Time Point	4	0.08625	0.08625	0.02156	1.11	0.408
Error	9	0.17419	0.17419	0.01935		
Total	17	0.45697				

S = 0.139120 R-Sq = 61.88% R-Sq(adj) = 28.00%

B) Ejection Fraction

Analysis of Variance for **EF (%)**, using Adjusted SS for Tests

Source	DF	Seq SS	Adj SS	Adj MS	F	P
Treatment	2	528.37	437.88	218.94	11.37	0.009
Time Point	2	4199.39	3816.68	1908.34	99.13	0.000
Treatment*Time Point	4	77.14	77.14	19.29	1.00	0.474
Error	6	115.50	115.50	19.25		
Total	14	4920.40				

S = 4.38748 R-Sq = 97.65% R-Sq(adj) = 94.52%

Grouping Information Using **Tukey Method and 95.0%** Confidence

Treatment	N	Mean	Grouping
2	4	67.00	A
1	5	63.67	A
0	6	54.17	B

Time Point	N	Mean	Grouping:
1	4	76.67	A
3	6	70.33	A
2	5	37.83	B

Means that do not share a letter are significantly different.

Analysis of Variance for Normalized Ejection Fraction, using Adjusted SS for Tests

Source	DF	Seq SS	Adj SS	Adj MS	F	P
Treatment	2	0.04664	0.04664	0.02332	5.53	0.099
Time Point	2	1.00323	0.92498	0.46249	109.65	0.002
Treatment*Time Point	4	0.08072	0.08072	0.02018	4.78	0.115
Error	3	0.01265	0.01265	0.00422		
Total	11	1.14325				

S = 0.0649444 R-Sq = 98.89% R-Sq(adj) = 95.94%

C) LV Volume

Analysis of Variance for **ED LVvol** (mL), using Adjusted SS for Tests

Source	DF	Seq SS	Adj SS	Adj MS	F	P
Treatment	2	14861	18446	9223	2.09	0.205
Time Point	2	68245	60198	30099	6.81	0.029
Treatment*Time Point	4	14528	14528	3632	0.82	0.556
Error	6	26527	26527	4421		
Total	14	124162				

S = 66.4925 R-Sq = 78.63% R-Sq(adj) = 50.15%

Analysis of Variance for **ES LVvol (mL)**, using Adjusted SS for Tests

Source	DF	Seq SS	Adj SS	Adj MS	F	P
Treatment	2	7053.7	8075.2	4037.6	4.47	0.065
Time Point	2	37031.6	33281.6	16640.8	18.43	0.003
Treatment*Time Point	4	3446.2	3446.2	861.5	0.95	0.495
Error	6	5417.5	5417.5	902.9		
Total	14	52948.9				

S = 30.0486 R-Sq = 89.77% R-Sq(adj) = 76.13%

Analysis of Variance for **Normalized ED LVvol (mL/kg)**, using Adjusted SS for Tests

Source	DF	Seq SS	Adj SS	Adj MS	F	P
Treatment	2	1.1497	1.2851	0.6426	1.98	0.218
Time Point	2	1.9207	2.1251	1.0625	3.28	0.109
Treatment*Time Point	4	0.4385	0.4385	0.1096	0.34	0.843
Error	6	1.9429	1.9429	0.3238		
Total	14	5.4518				

S = 0.569042 R-Sq = 64.36% R-Sq(adj) = 16.85%

Analysis of Variance for **Normalized ES LVvol (mL/kg)**, using Adjusted SS for Tests

Source	DF	Seq SS	Adj SS	Adj MS	F	P
Treatment	2	0.60836	0.64035	0.32018	6.19	0.035
Time Point	2	3.38490	3.19406	1.59703	30.90	0.001
Treatment*Time Point	4	0.27243	0.27243	0.06811	1.32	0.363
Error	6	0.31015	0.31015	0.05169		
Total	14	4.57584				

S = 0.227358 R-Sq = 93.22% R-Sq(adj) = 84.18%

Grouping Information Using **Tukey Method** and 95.0% Confidence for **N ES LVvol**

Treatment	N	Mean	Grouping:
0	6	1.018	A
2	4	0.702	A B
1	5	0.532	B

Time Point	N	Mean	Grouping
2	5	1.438	A
3	6	0.503	B
1	4	0.310	B

Means that do not share a letter are significantly different.

D) Microspheres

Analysis of Variance for **Liver**, using Adjusted SS for Tests

Source	DF	Seq SS	Adj SS	Adj MS	F	P
Treatment	2	0.02710	0.04143	0.02071	0.63	0.570
Time Point	2	0.21935	0.29056	0.14528	4.41	0.079
Treatment*Time Point	4	0.20597	0.20597	0.05149	1.56	0.314
Error	5	0.16459	0.16459	0.03292		
Total	13	0.61701				

S = 0.181434 R-Sq = 73.32% R-Sq(adj) = 30.64%

Analysis of Variance for **Kidney**, using Adjusted SS for Tests

Source	DF	Seq SS	Adj SS	Adj MS	F	P
Treatment	2	8.575	8.485	4.243	0.69	0.542
Time Point	2	27.715	27.493	13.747	2.25	0.201
Treatment*Time Point	4	7.221	7.221	1.805	0.30	0.870
Error	5	30.577	30.577	6.115		
Total	13	74.089				

S = 2.47295 R-Sq = 58.73% R-Sq(adj) = 0.00%

Analysis of Variance for **Spleen**, using Adjusted SS for Tests

Source	DF	Seq SS	Adj SS	Adj MS	F	P
Treatment	2	0.1109	0.0778	0.0389	0.20	0.825
Time Point	2	0.4076	0.4332	0.2166	1.11	0.399
Treatment*Time Point	4	0.2676	0.2676	0.0669	0.34	0.839
Error	5	0.9762	0.9762	0.1952		
Total	13	1.7622				

S = 0.441856 R-Sq = 44.61% R-Sq(adj) = 0.00%

Analysis of Variance for **RV**, using Adjusted SS for Tests

Source	DF	Seq SS	Adj SS	Adj MS	F	P
Treatment	2	2.265	2.079	1.039	0.56	0.601
Time Point	2	1.569	0.692	0.346	0.19	0.834
Treatment*Time Point	4	3.375	3.375	0.844	0.46	0.765
Error	5	9.200	9.200	1.840		
Total	13	16.408				

S = 1.35647 R-Sq = 43.93% R-Sq(adj) = 0.00%

Analysis of Variance for **LV**, using Adjusted SS for Tests

Source	DF	Seq SS	Adj SS	Adj MS	F	P
Treatment	2	0.06253	0.09766	0.04883	2.20	0.206
Time Point	2	0.21570	0.20944	0.10472	4.72	0.070
Treatment*Time Point	4	0.28666	0.28666	0.07166	3.23	0.115
Error	5	0.11087	0.11087	0.02217		
Total	13	0.67576				

S = 0.148912 R-Sq = 83.59% R-Sq(adj) = 57.34%

Analysis of Variance for **Septum**, using Adjusted SS for Tests

Source	DF	Seq SS	Adj SS	Adj MS	F	P
Treatment	2	0.2976	0.4576	0.2288	1.74	0.267
Time Point	2	0.3623	0.3339	0.1669	1.27	0.358
Treatment*Time Point	4	0.6576	0.6576	0.1644	1.25	0.397
Error	5	0.6572	0.6572	0.1314		
Total	13	1.9748				

S = 0.362549 R-Sq = 66.72% R-Sq(adj) = 13.47%

Analysis of Variance for **M1**, using Adjusted SS for Tests

Source	DF	Seq SS	Adj SS	Adj MS	F	P
Treatment	2	0.8073	0.7745	0.3872	0.51	0.627
Time Point	2	1.4196	0.9500	0.4750	0.63	0.570
Treatment*Time Point	4	1.3194	1.3194	0.3299	0.44	0.778
Error	5	3.7692	3.7692	0.7538		
Total	13	7.3156				

S = 0.868240 R-Sq = 48.48% R-Sq(adj) = 0.00%

Analysis of Variance for **M2**, using Adjusted SS for Tests

Source	DF	Seq SS	Adj SS	Adj MS	F	P
Treatment	2	0.21536	0.20798	0.10399	3.43	0.115
Time Point	2	0.26681	0.22379	0.11189	3.69	0.104
Treatment*Time Point	4	0.29674	0.29674	0.07418	2.45	0.177
Error	5	0.15166	0.15166	0.03033		
Total	13	0.93057				

S = 0.174161 R-Sq = 83.70% R-Sq(adj) = 57.63%

Analysis of Variance for M3, using Adjusted SS for Tests

Source	DF	Seq SS	Adj SS	Adj MS	F	P
Treatment	2	0.22079	0.26653	0.13327	5.51	0.054
Time Point	2	0.14690	0.13082	0.06541	2.70	0.160
Treatment*Time Point	4	0.43824	0.43824	0.10956	4.53	0.064
Error	5	0.12098	0.12098	0.02420		
Total	13	0.92690				

S = 0.155548 R-Sq = 86.95% R-Sq(adj) = 66.07%

Analysis of Variance for **Bowel**, using Adjusted SS for Tests

Source	DF	Seq SS	Adj SS	Adj MS	F	P
Treatment	2	0.2590	0.2611	0.1305	0.74	0.524
Time Point	2	0.7426	0.8700	0.4350	2.46	0.180
Treatment*Time Point	4	0.3873	0.3873	0.0968	0.55	0.710
Error	5	0.8841	0.8841	0.1768		
Total	13	2.2731				

S = 0.420496 R-Sq = 61.11% R-Sq(adj) = 0.00%

Analysis of Variance for **Lung**, using Adjusted SS for Tests

Source	DF	Seq SS	Adj SS	Adj MS	F	P
Treatment	2	2.4616	2.2107	1.1054	1.94	0.237
Time Point	2	2.3373	1.3608	0.6804	1.20	0.376
Treatment*Time Point	4	2.6569	2.6569	0.6642	1.17	0.424
Error	5	2.8431	2.8431	0.5686		
Total	13	10.2989				

S = 0.754069 R-Sq = 72.39% R-Sq(adj) = 28.22%

Analysis of Variance for **Skin**, using Adjusted SS for Tests

Source	DF	Seq SS	Adj SS	Adj MS	F	P
Treatment	2	0.003941	0.003877	0.001939	1.56	0.298
Time Point	2	0.004487	0.002524	0.001262	1.01	0.427
Treatment*Time Point	4	0.008353	0.008353	0.002088	1.68	0.290
Error	5	0.006222	0.006222	0.001244		
Total	13	0.023004				

S = 0.0352763 R-Sq = 72.95% R-Sq(adj) = 29.68%

Analysis of Variance for Skeletal Muscle, using Adjusted SS for Tests

Source	DF	Seq SS	Adj SS	Adj MS	F	P
Treatment	2	0.15313	0.16415	0.08207	2.50	0.177
Time Point	2	0.00822	0.00727	0.00364	0.11	0.897
Treatment*Time Point	4	0.01289	0.01289	0.00322	0.10	0.979
Error	5	0.16443	0.16443	0.03289		
Total	13	0.33867				

S = 0.181347 R-Sq = 51.45% R-Sq(adj) = 0.00%

Analysis of Variance for Brain Stem, using Adjusted SS for Tests

Source	DF	Seq SS	Adj SS	Adj MS	F	P
Treatment	2	1.5243	2.1712	1.0856	4.80	0.069
Time Point	2	0.9756	1.0284	0.5142	2.27	0.199
Treatment*Time Point	4	1.3700	1.3700	0.3425	1.51	0.326
Error	5	1.1309	1.1309	0.2262		
Total	13	5.0008				

S = 0.475578 R-Sq = 77.39% R-Sq(adj) = 41.20%

Analysis of Variance for **Cerebellum**, using Adjusted SS for Tests

Source	DF	Seq SS	Adj SS	Adj MS	F	P
Treatment	2	11.930	16.321	8.160	3.86	0.097
Time Point	2	4.898	4.657	2.328	1.10	0.402
Treatment*Time Point	4	7.595	7.595	1.899	0.90	0.528
Error	5	10.576	10.576	2.115		
Total	13	34.998				

S = 1.45434 R-Sq = 69.78% R-Sq(adj) = 21.43%

Analysis of Variance for **Aorta**, using Adjusted SS for Tests

Source	DF	Seq SS	Adj SS	Adj MS	F	P
Treatment	2	0.0001161	0.0001093	0.0000547	0.13	0.884
Time Point	2	0.0079922	0.0076947	0.0038474	8.89	0.023
Treatment*Time Point	4	0.0006029	0.0006029	0.0001507	0.35	0.836
Error	5	0.0021638	0.0021638	0.0004328		
Total	13	0.0108750				

S = 0.0208027 R-Sq = 80.10% R-Sq(adj) = 48.27%

Analysis of Variance for **PA**, using Adjusted SS for Tests

Source	DF	Seq SS	Adj SS	Adj MS	F	P
Treatment	2	0.048196	0.045933	0.022966	3.13	0.131
Time Point	2	0.059793	0.040185	0.020093	2.74	0.157
Treatment*Time Point	4	0.053307	0.053307	0.013327	1.82	0.263
Error	5	0.036640	0.036640	0.007328		
Total	13	0.197936				

S = 0.0856033 R-Sq = 81.49% R-Sq(adj) = 51.87%

E) BrdU

Analysis of Variance for **BrdU+**, using Adjusted SS for Tests

Source	DF	Seq SS	Adj SS	Adj MS	F	P
Treatment	2	17039687	17039687	8519843	56.31	0.000
Tissue	2	2174346	2174346	1087173	7.19	0.001
Treatment*Tissue	4	2791537	2791537	697884	4.61	0.001
Error	171	25870951	25870951	151292		
Total	179	47876521				

S = 388.963 R-Sq = 45.96% R-Sq(adj) = 43.44%

Analysis of Variance for **BrdU+SA+**, using Adjusted SS for Tests

Source	DF	Seq SS	Adj SS	Adj MS	F	P
Treatment	2	2414	2414	1207	0.67	0.515
Tissue	2	26130	26130	13065	7.21	0.001
Treatment*Tissue	4	3126	3126	781	0.43	0.786
Error	171	309818	309818	1812		
Total	179	341488				

S = 42.5653 R-Sq = 9.27% R-Sq(adj) = 5.03%

CURRICULUM VITAE

Erin F. Smith
Graduate Student
Department of Bioengineering
University of Louisville
Louisville, Kentucky, USA
efsmit05@louisville.edu

Education

Future (*Fall 2013*)	University of Louisville School of Medicine Class of 2017
2012 – Present	University of Louisville JB Speed School of Engineering Master of Engineering Department: Bioengineering
2008 – 2012	University of Louisville JB Speed School of Engineering Department: Bioengineering Bachelor of Science *With Highest Honors*
2007 – 2008	St. Louis University Parks College of Engineering and Aviation Department: Biomedical Engineering

Research Experience

May 2012 – Present
Cardiovascular Innovation Institute (CII)
Advanced Heart Failure Rearch
Mentors: Mark Slaughter, MD; Steven Koenig, PhD; Kevin Soucy, PhD; Guruprasad Giridharan, PhD

August 2010 – December 2011
Kentucky Spinal Cord Injury Research Center (KSCIRC)
Laboratory of Locomotor Systems and Rehabilitation
Mentors: David Magnuson

Awards and Recognition

University of Louisville
Tau Beta Pi – Engineering Honors Society
Dean's Scholar, Dean's List
St. Louis University
Presidential Scholar
Pre-Medical Scholar

Extracurricular Activities

1. Biomedical Engineering Society
    - President 2010 - 2011
    - Treasurer 2011 - 2012
2. Community Service – Baptist Hospital East - 2008
    - Phase II Recovery
    - Post Anesthesia Care Unit